University of Piraeus

Department of Digital Systems

Postgraduate Programme “Digital Communications & Networks”

MSc Research Project

WIRELESS COMMUNICATIONS VIA CASCADED-RIS AIDED SYSTEMS

GEORGIOU ARGYRIOS

Submitted for partial fulfilment of the

requirements for acquiring M.Sc.

2022

Acknowledgements

"I am indebted to my father for living, but to my teacher for living well"

Only these words of Alexander the Great about his teacher, the philosopher Aristotle, can concisely and precisely reflect my respect and my gratitude about my supervisor, Angeliki Alexiou, who has constantly supported and guided me during the implementation of my project.

I would like to offer my special thanks to Sotiris Droulias for his insightful comments and help at every stage of the research project.

Lastly, I wish to convey my grateful thanks to my family for their understanding and patience throughout my studies.

Argyrios Georgiou

Dedicated to the joys of my life

my wife, Dora, and my children, Chara & Angelos

WIRELESS COMMUNICATIONS VIA CASCADED-RIS AIDED SYSTEMS

GEORGIOU ARGYRIOS

University of Piraeus, Department of Digital Systems, 2022

Supervisor: Angeliki Alexiou, Professor, University of Piraeus

Abstract

The current research project examined the contribution of Reconfigurable Intelligent Surfaces (RISs) in wireless communication networks, by applying them on a cascaded double-RIS implementation. The conducted analytical and numerical study examined the performance of the cascaded-RIS system in several use case scenarios in terms of the receiver power at the User Equipment (UE). An analytical model that captures the performance of the double-RIS aided system was proposed, while the results were also verified by following a numerical calculation (discrete model). Focus was also given on the most critical performance parameters, such as the reflection coefficient of RIS elements, the phase-related operation features of the RIS, the transmitter gain, the beam footprint at the RIS plane, the distance between the UE and the RIS. The obtained results provide reasonable support that the under-examination double-RIS aided wireless communication system can establish a multi-hop cascaded LoS link which can effectively mitigate or even eliminate the adverse NLoS effects and, in general, can improve the system's performance in terms of received power at the UE. In addition, it was found that phase-related RIS-operation features can further enhance the cascaded-RIS assisted system's performance.

Contents

List of Tables

List of Figures

ACRONYMS

ADC	Analog to Digital converters
AF	Amplify-and-Forward
AI	Artificial Intelligence
AmBC	Ambient Backscatter Communication
AP	Access Point
BCI	Brain-Computer Interface
BER	Bit Error Rate
BS	Base Station
CF-mMIMO	Cell-Free massive Multiple-Input Multiple-Output
CR	Cognitive Radio
CRAS	Connected Robotics and Autonomous Systems
CSI	Channel State Information
DAC	Digital to Analog Converter
EC	Ergodic Capacity
EE	Energy Efficiency
EM	electromagnetic
eMBB	enhanced mobile broadband
ER	Energy Receiver
ETSI	European Telecommunications Standards Institute
FD	Full-Duplex
FDMA	Frequency Division Multiple Access
FET	Field-Effect Transistor
FPGA	Field-Programmable Gate Array
FSO	Free Space Optics
HD	Half-Duplex
IIoT	Industrial Internet of Things
INR	Interference-to-Noise Ratio
IoT	Internet of Things
IR	Information Receiver
IRE	Intelligent Radio Environment
IRS	Intelligent Reflecting Surface
ITU	International Telecommunication Union
LC	Liquid Crystal
LIS	Large Intelligent Surface
LoS	Line-of-Sight
MEC	Mobile Edge Computing
MEMS	Micro-Electro-Mechanical System
MIMO	Multiple-Input Multiple-Output
MISO	Multiple-Input Single-Output
ML	Machine Learning
mMIMO	massive Multiple-Input Multiple-Output
mMTIC	massive Machine-Type IoT Communication
mmWave	millimeter Wave
NLoS	Non-Line-Of-Sight

NOMA	Non-Orthogonal Multiple Access
OAM	Orbital Angular Momentum
OMA	Orthogonal Multiple Access
OP	Outage Probability
PA	Power Amplifier
PLS	Physical Layer Security
PU	Primary User
QC	Quantum Communication
QoE	Quality of Experience
QoS	Quality of Service
RB	Resource Block
RF	Radio Frequency
RIS	Reconfigurable Intelligent Surface
RX	Receiver
SDS	Software-Defined Surface
SE	Spectral Efficiency
SER	Symbol Error Rate
SINR	Signal-to-Interference-plus-Noise Ratio
SL	Spectrum Learning
SNDR	Signal-to-Noise-plus-Distortion Ratio
SNR	Signal-to-Noise Ratio
SRE	Smart Radio Environment
SU	Secondary User
SWIPT	Simultaneous Wireless Information and Power Transfer
TDMA	Time Division Multiple Access
THz	Terahertz
TX	Transmitter
UAV	Unmanned Aerial Vehicle
UE	User equipment
UM-MIMO	Ultra-Massive Multiple-Input Multiple-Output
URLLC	Ultra-Reliable Low Latency Communications
VLC	Visible Light Communication
VR	Virtual Reality
WPT	Wireless Power Transfer
WSR	Weighted Sum Rate
5G	fifth Generation
6G	sixth Generation

INTRODUCTION: REASONING FOR RECONFIGURABLE INTELLIGENT SURFACES

The advent of fifth generation (5G) wireless networks is a reality for a growing number of users worldwide, providing enhanced mobile broadband (eMBB), ultrareliable and low-latency communications (URLLC) and massive machine type communication (mMTC) services [1] [2] [3].

Looking ahead to the 2030 horizon, the next generations of wireless communications technologies (Beyond-5G, 6G, or even 6G and Beyond) envision flexible compute-and-connect networks which will be capable to support revolutionary applications and heterogeneous services, such as Tactile Internet, Holographic Communication, Digital Replica (or Digital Twins), Connected Robotics and Autonomous Systems (CRAS), teleoperated driving and intelligent transportation systems, Wireless Brain–Computer Interfaces (BCI), Blockchain and Distributed Ledger Technologies, Industrial Internet of Things (IIoT), and more [2] [3] [4] [5].

All the aforementioned services/applications pose demanding requirements in terms of high data rate, super-connectivity, increased network capacity, ultra-high reliability, ultra-low latency, extended coverage, enhanced security, rich Quality of Service (QoS) and economically affordable implementations [6] [7] [8].

In addition to the above-mentioned stringent communication demands, it should be emphasized that according to the International Telecommunication Union Report ITU-R M.2370-0 and Ericsson Mobility Report, the total global mobile data traffic is expected to continue its high growth in the future [9] [10], especially with the advent of the 6G era [11] [12].

Thus, it becomes obvious that new enabling technologies are needed in order to support these high quality and ubiquitous wireless services and applications. In specific, the existing 5G key technologies, such as the massive multiple-input multiple-output (mMIMO) and millimeter wave (mmWave), although they can help to reach high data rates and boost spectral efficiency and network capacity, they present significant disadvantages in terms of energy efficiency, blockage sensitivity, propagation path loss and directivity [11] [13] [14] [15].

Therefore, new emerging and disruptive technologies, which are coming out of the comfort-zone of existing 5G best practices, aim to overcome the aforementioned fundamental limitations. In more detail, terahertz (THz) communication, Cell-Free mMIMO (CF-mMIMO), Ultra-Massive MIMO (UM-MIMO), Orbital Angular Momentum (OAM) multiplexing, Holographic Beamforming, Artificial Intelligence and Machine Learning (AI/ML), edge intelligence, Visible Light Communication (VLC), blockchain, Quantum Communication (QC), Ambient Backscatter Communication (AmBC) and Reconfigurable Intelligent Surfaces (RISs), new multiple access techniques and new coding techniques

have been envisioned as the most promising 6G (and Beyond)-oriented solutions [5] [6] [11] [16].

Among the above-mentioned technologies, RIS has recently attracted considerable attention as one of the key enablers of future wireless communications, which is used to model the mobile-radio environment as a controllable entity through the manipulation of electromagnetic (EM) waves [11] [17]. Targeting the 2030, RISs can be integrated to the next-generation wireless networks to transform the current adversary/uncontrollable infrastructure into a collaborative system and implement the vision of human-centered, energy-efficient and commercially viable smart radio environments (cities, homes, buildings, airports, trains, etc.) [3] [6] [13] [18] [19].

The thesis is structured as follows:

- The Background and Literature Review Section, which includes an introduction to the Smart Radio Environments and Reconfigurable Intelligent Surface technology, the advantages and disadvantages of RIS deployment, the proposed RIS applications and a comprehensive literature review both for single-RIS and cascaded-RIS systems.
- The Section of Analytical and Numerical Study, which includes the scope, the design, the concept and the implementation details of the current research project.
- The Sections of Results and Discussion, which include the representation and the interpretation of the results obtained from the simulation scenarios, as well as the discussion of their significance.
- Lastly, the conclusions drawn are presented in a bulleted-list format and the possible future work is indicated.

1. BACKGROUND INFORMATION & LITERATURE REVIEW

1.1 Smart Radio Environment (SRE)

The vision of next-generation wireless networks is the implementation of Smart Radio Environments (SREs), which transform the current environment into a software-reconfigurable space and enable end-to-end network optimization [1]. The concept of Smart Radio Environment, also known as Intelligent Radio Environment (IRE) or "Wireless 2.0" [19], refers to a distributed wireless platform capable for sensing the environment, supporting computing and information processing techniques and providing enhanced intelligent wireless communications [1].

In more detail, with regard to current wireless networks, the environment is considered an "exogenous entity" that is *"unintentional adversary"* to the communication process, and optimization capabilities are mainly limited to the network endpoints, i.e. transmitters and receivers [1] [19]. In other words, the environment is considered fixed by nature, unalterable and detrimental to the quality and effectiveness of communication [17]; consequently, the only feasible design considerations concern the adaptation to the current environment through the application of advanced transmission and reception schemes [19].

On the other hand, in the case of SREs, the wireless environment is generated by nature but is controlled by design [19] and is considered intelligent, programmable and fully customizable [1]. In fact, the environment is now one of the design parameters of the network and therefore, it can be dynamically configured and elastically optimized by appropriately steering the EM waves based on the sensing-based data received from the communication system [1] [17] [18]. In addition, the software-controlled environment can be actively engaged in data processing and transmission to support reliable and efficient communication, enhanced connectivity, accurate localization services and a guaranteed level of QoS [1] [17] [19].

The network design optimization capabilities of smart radio environment compared to the conventional radio environment are presented in Figure 1.

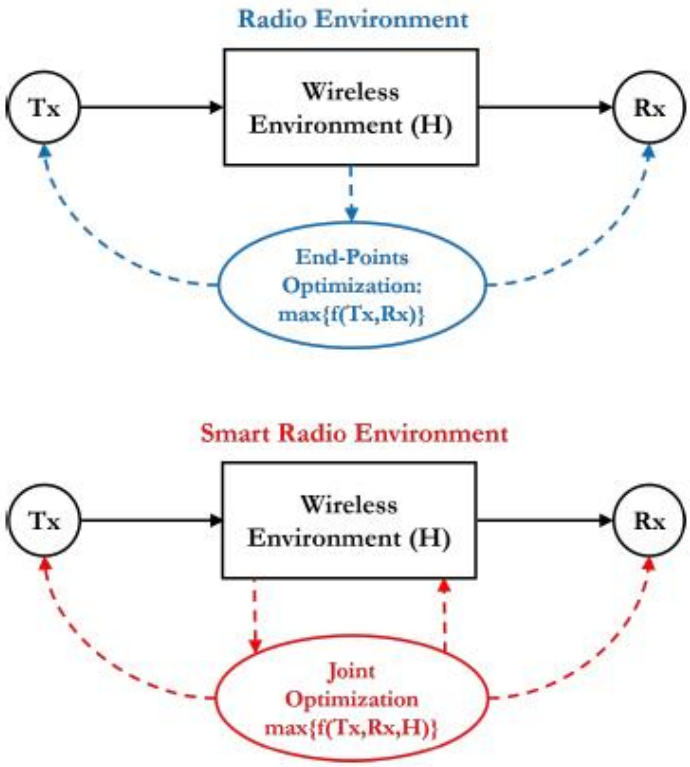

Figure 1. Optimization scheme for conventional and smart radio environment [19].

The most promising solutions for realizing the aforementioned vision of the smart radio environment include the Reconfigurable Intelligent Surfaces and Artificial Intelligence-based computational techniques [1] [18]. These novel technologies are capable to overcome the fundamental limitations (e.g. network complexity and deployment cost) arising from the currently employed communication schemes, which are mostly based on robust transmission/reception protocols, advanced signal processing algorithms, multiple antennas techniques and additional network elements (e.g. relays) [19] [20]. In particular, RISs have the potential of rendering the wireless environment controllable, configurable, programmable, and intelligent in a cost-effective, energy-efficient, low-complexity and environmental-friendly way [1] [11] [17] [19] [21], as will be further analyzed in §1.2.5.

The concept of RIS-assisted smart radio environment can support a plethora of application scenarios [1] [18]. More specifically, when the physical objects of interest are coated with reconfigurable meta-materials (to form a meta-surface), they can actively involve in information processing and transmission by manipulating (via a software controller) the electromagnetic waves as desired [1] [18]. The authors in [19] have comprehensively presented the most promising SRE use cases, including smart cities/university campuses, smart homes/buildings/factories/hospitals, smart train stations/undergrounds/airports, smart cars/trains/airplanes, smart billboards, smart glasses and clothing. A subset of potential SRE applications is shown in Figure 2.

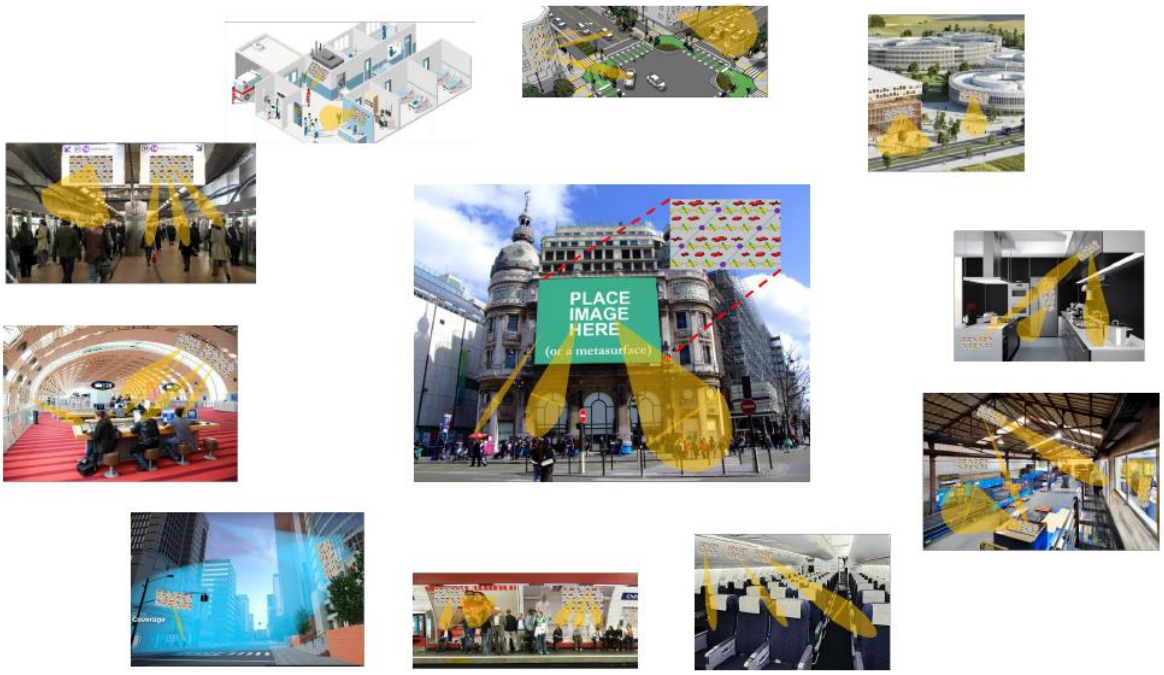

Figure 2. Potential use cases of smart radio environments [19].

1.2 Reconfigurable Intelligent Surface

1.2.1 Intro

Reconfigurable Intelligent Surfaces have been identified as the most promising technology for realizing the vision of Smart Radio Environment [6] [18]. The RISs, also known as Intelligent Reflecting Surfaces (IRSs) or Large Intelligent Surfaces (LISs) or Software-Defined Surfaces (SDSs) [2] [17], are increasingly gaining attention as key elements/components of future wireless networks due to their potential to render the propagation environment controllable, customizable and programmable [2] [6].

This material structure, designed to possess programmable macroscopic physical features beyond those found on conventional surfaces, can upgrade the current infrastructure and be used on a variety of wireless networks with the aim to achieve smart home and smart city project success [2] [6] [14] [18].

Unlike conventional wireless networks, the RIS-assisted networks enable the communication engineers to control and customize the radio environment due to the capability of unit cells (that constitute the smart surfaces) to manipulate the electromagnetic waves [2] [11] [18]. In particular, the fabrication materials of unit cells, the integrated electronic circuits/sensors, their size and their inter-distance, allow them to possess unique characteristics for tuning the electromagnetic responses (e.g. amplitude, phase) as desired, offering thus the capability for improved/optimized adaptation to the dynamically changing wireless environment, either in the far-field or in the near-field regions [2] [4] [11] [19].

In more detail, an impinging signal upon a naturally occurring material or surface will be reflected/refracted according to conventional Snell's laws and based on the wavelength of the radio wave and the permittivity, permeability and thickness of the material/surface [1] [19]). However, a smart surface exhibits unnatural and exotic properties/functions (e.g. perfect absorption, anomalous reflection, beamforming [2] [19] [22]) capable of beneficially shaping and modifying the impinging signals based on the generalized laws of reflection and refraction (i.e. beyond Snell's laws) [1] [13] [19]. Among the many functions that a RIS may be able to perform, we should focus on the following:

- Beamforming: This function consists of directing the impinging radio wave towards a targeted region (e.g. the user equipment (UE)) [2] [19].
- Anomalous reflection: this function is a form of extreme waveform manipulation based on the generalized Snell's laws, in which the incident beam can be reflected at an angle different from the angle of incidence [23] [24].
- Polarization conversion: This function consists of modifying the polarization of an incident radio wave, e.g. linear to linear, linear to circular, and circular to circular [19] [25].
- Perfect absorption: This function refers to the capability of the metasurface to fully absorb the incident plane waves and therefore, no radio waves will be reflected or refracted [19] [22].

1.2.2 Reference Structure

Although many different RIS implementations have been proposed, the key technology behind this revolutionary idea is the meta-surfaces [19]. The prefix "meta", derived from the Greek word "*μετά*" meaning "after" or "beyond", is included to indicate that these special surfaces possess exotic properties that offer unique wireless communication capabilities [17] [19]. In fact, RISs are engineered to work as reflecting/refracting surfaces between the Access Point (AP) or (Base Station (BS)) and the User Equipment (UE) in order to smartly reconfigure the wireless propagation environment [2].

Metasurfaces are generally man-made planar structures composed of thin sheets of electromagnetic material containing a large number of reconfigurable elementary elements capable of controlling the wireless propagation environment in fully customizable ways [1] [3] [6] [17] [18] [19].

The conceptual structure of a RIS is illustrated in Figure 3 [19].

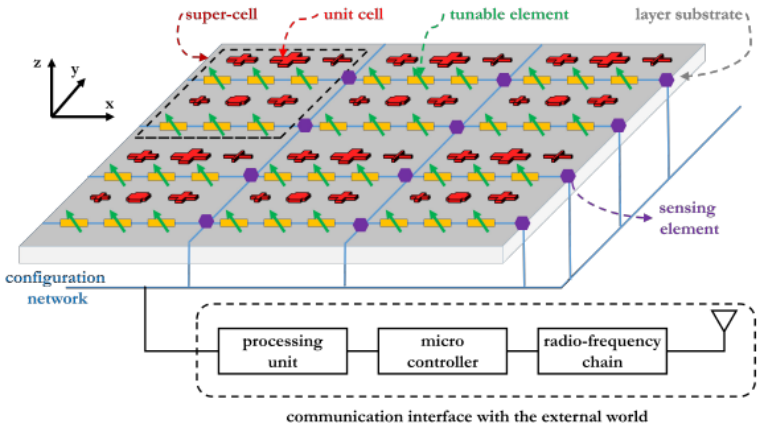

Figure 3. Reference structure of a RIS [19].

In more detail, a smart surface is modeled as zero-thickness electromagnetic structure of electrically large transverse size, i.e. the surface has a sub-wavelength thickness, while its transverse size is much larger compared to the wavelength of radio waves (and therefore the thickness of the RIS) [18] [19].

The planar structure of RIS facilitates its design, fabrication and deployment [18], although either free-form conformal two-dimensional or even three-dimensional reconfigurable intelligent surfaces are also common [19].

Furthermore, each surface generally consists of a single or multiple electromagnetic sheets/layers [4]. For example, an implementation proposed by Wu and Zhang [26] refers to a three-layer surface, in which the outer layer comprises multiple reflecting elements for directly interacting with the impinging radio waves, the middle layer (e.g. a copper backplane) acts as a structure to prevent signal/energy leakage, and the inner layer is a circuit board for controlling the reflection coefficients as desired (depending on the external stimuli) [4] [26].

In general, each sheet comprises an array of thousands of low-cost, nearly-passive, tunable reflecting elements, which are often referred to as unit cells or scattering particles or meta-atoms or even pixels [3] [6] [18] [19]. The unit cells (e.g. full or slotted patches, straight or curved strips, various types of crosses) are jointly optimized to meet the desired reconfigurability requirements and form an entity known as super-cell, as shown in Figure 3 [19]. Moreover, it should be noted that the inter-spacing distance between the unit cells is typically between $\lambda/10$ and $\lambda/5$, and therefore the coupling effect cannot be ignored when considering the design of the RIS [19] [27]. Thus, the metasurface response to the incident electromagnetic waves at macroscopic level depends on the microscopic design of the super-cells and consequently the unit-cells [19].

In addition, the scattering elements require minimal power for reconfigurability purposes and no power for signal amplification, while presenting minimal signal processing capabilities (thus denoted as “nearly-passive”) [19]. It is understandable that RIS cannot

be completely passive as it requires the integration of active components for programmability and tunability purposes [2] [27].

Considering the tuning mechanisms, it is possible to dynamically control the EM response of the RIS by adjusting the surface impedance through the application of electrical or thermal excitation, optical illumination or mechanical (physical) stretching [2] [28] (Table 1). Field-Programmable Gate Array (FPGA) chips including active elements such as PIN diodes, varactors, field-effect transistors (FETs), micro-electro-mechanical systems (MEMSs), and tunable materials, such as liquid crystals, graphene, ferrite, photoconductive semiconductors, are potential candidates for building the RIS reconfigurability concept [29] [30] [31].

Table 1. Tuning mechanisms and controllable scattering elements used in RIS implementation

Tuning Mechanisms	Electrical excitation
	Thermal excitation
	Optical illumination
	Mechanical stretching
Scattering Elements	Tunable Chips • PIN diodes • Varactors • Field Effect Transistors (FETs) • MEMS
	Tunable Materials • Liquid Crystals (LCs) • Graphene • Ferrite • Semiconductors

In addition to the metamaterial-based technologies, current practical RIS implementations include also conventional reflect-arrays [2] [17] [27]. In particular, multiple tiny discrete antenna elements act as reflectors in order to dynamically adjust their radiation patterns and, subsequently, to control the impinging signals characteristics (i.e. phase, amplitude, polarization, etc.) [17] [19]. The model structure actually consists of a large number of metallic or dielectric patches printed on a grounded dielectric substrate with an element inter-distance usually equal to the half of the wavelength of radio waves $\left(\lambda/_2\right)$ so that there is no mutual coupling between adjacent elements [19] [27]. However, it should be highlighted that the fixed structure of this implementation implies limited control over RIS [27].

The authors in [27] summarize the differences between metasurface- and reflect-array-based RIS implementations, as presented in Table 2.

Table 2. Comparison of metasurface and reflect-array based RIS [27]

Reflect-array	Metasurface
Operation well-known, relatively easy to model	Difficult to model controllable surfaces
Simple to manufacture	Potentially more advanced function
Simple control	Mutual coupling of meta-cells complicates the control
Readily available technology	Reconfigurable metasurfaces still in research phase

The MIT's RFocus prototype and the NTT DOCOMO smart glass, as illustrated Figure 4, are the best-known RIS implementations [19].

The RFocus prototype refers to a two-dimensional surface made of 3200 inexpensive passive antenna elements arranged on a 6 square-meter surface [32]. The structure reflects the impinging radio waves in a controlled way by appropriately setting the on/off states of each element and the surface does not increase the overall radiation [32]. In specific, each antenna can be between two mutually exclusive states – "ON" and "OFF": when "ON" the element is opaque to radiation and reflects the signal; otherwise (i.e. in the "OFF" state) the antenna is semi-transparent and the signal passes through [32].

The NTT DOCOMO's metasurface can manipulate radio waves by appropriately moving a glass substrate that covers a large number of sub-wavelength unit cells [33]. The smart window can be switched between reflection (full or partial) and penetration modes to achieve dynamic control of the propagation environment [33].

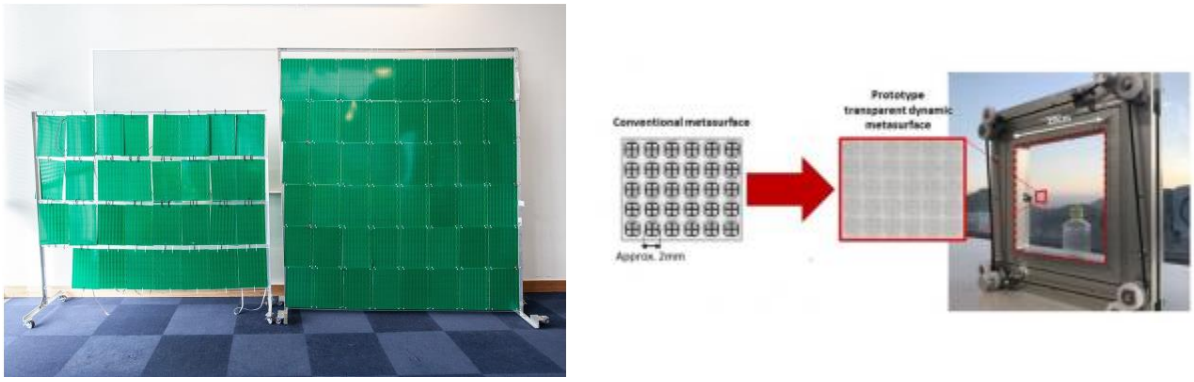

(a) (b)

Figure 4. RIS implementations: (a) MIT's RFocus prototype, and (b) NTT DOCOMO's prototype [19].

1.2.3 Communication & Control

A novel RIS-enabled communication network architecture, in addition to the smart surface, includes also an interface to enable communication with the external world, as depicted in Figure 3 [19]. In general, the system consists of an intercell communication network, which allows communication among the unit cells throughout the RIS via a transfer gateway, and a micro-controller in charge of computing and adjusting the electromagnetic behavior of the impinging radio waves as a function of the channel state information (CSI) [17] [19].

In a typical scenario of RIS deployment, the smart controller, e.g. FPGA, communicates (wireless or wired) with the AP/BS and the UE via a dedicated feedback link in order to coordinate the transmission in a real-time reconfigurable way [4] [6] [11] [19].

In addition, it should be noted that metasurfaces may be equipped with embedded low power sensors which are in charge of sensing the environment and providing the RIS of the channel state information [17] [19]. However, this extension raises the implementation cost and the power consumption of the RIS [19].

Lastly, it should be underlined that RISs are categorized as nearly-passive implementations given that their aforementioned integrated electronic circuits/sensors present minimum power requirements and signal processing requirements in order to achieve the metasurface reconfigurability and the communication with the external world [19]. Power sources, such as batteries, storage modules and energy-harvesting solutions, are usually deployed to handle the power requirements [1].

1.2.4 Dynamic Reconfigurability

Given the recent developments in metamaterials, RISs are capable of beneficially reconfiguring the wireless propagation environment by dynamically controlling the response of the incident signal [4] [14] [19]. Phase, amplitude, frequency and polarization transformations can be applied to the impinging radio waves in fully customizable ways in order to render the wireless environment programmable and controllable [1] [17] [19].

Broadly speaking, the general operation of a RIS is an iterative process that is divided into the *“Control and programming phase”* and the *“Normal operation phase”* [19]. The first phase involves the computing of the best configuration set-up and the appropriate optimization of the smart surfaces, while the second phase concerns the RIS-aided transmission of information throughout the wireless network [19]. It should be noted that the periodicity of the process depends on the changes of the channel state information, i.e. the coherence time of the environment [4] [19].

In a typical scenario of RIS operation, the micro-controller appropriately configuring the tuning mechanisms (by applying, for example, electrical voltage, thermal excitation, physical stretching (as mentioned earlier)) in order to effectively control the wavefront of the incident signal [2] [17]. In this way, the RIS can be configured by tuning/optimizing the meta-surface reflection coefficients of its elements based on the stimuli that it receives

from the external world, i.e. the channel (or, in general, the environmental) state information [1] [4] [19]. Owing to their capability to intentionally reconfiguring the end-to-end wireless channels and smartly adapting to the dynamically fluctuating propagation environment, RISs have the potential to improve the capacity and coverage of the communication networks and ultimately realize the vision of Smart Radio Environment [2] [6].

It should be highlighted that RIS can perform the channel propagation reconfigurability tasks by deploying energy-efficient technologies and low-complexity signal processing algorithms (encoding, decoding, etc.) [1] [17]. In fact, in case that the smart surfaces are equipped with sensing capabilities, nano-networking protocols can be used to enable the unit cells to be self-reconfigured; otherwise, the access point (or the base station) and the user equipment are in charge of reporting (via the feedback link) the sensed data to the micro-controller, which is responsible for computing the best wave transformations to apply (depending on the optimal configuration set-up) and for providing the appropriate control signals to the smart surface [1] [19].

1.2.5 Beneficial features

As mentioned earlier, the RIS emerging concept supports advanced wireless communication capabilities by leveraging the unique design features of the metamaterial-based arrays of massive low-cost nearly-passive reflecting elements [4] [14] [17]. In fact, these reflecting/refracting surfaces can be distributed throughout the network in order to sense the propagation environment and control the channels between the transmitters and receivers in fully customizable ways [1] [2].

Since incident-reflecting angle of the impinging signals is not anymore subject to conventional Snell's laws and given the RIS-related exotic properties (e.g. perfect absorption and anomalous reflection), the RIS-empowered networks are capable of tailoring the electromagnetic responses of the metamaterial-coated environmental objects and assist the transfer of information between the devices (Figure 5) [1] [11] [13]. In particular, the RIS reflection coefficients can be smartly programmed to properly adjust the phase, the amplitude, the frequency or even the polarization of the EM waves in order to overcome the negative effects of natural propagation environments and establish multi-hop line-of-sight (LoS) links [1] [2] [17].

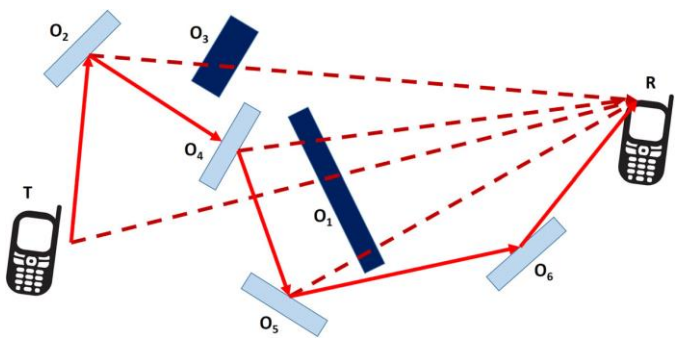

Figure 5. RIS-assisted communication in case of Non-Line-Of-Sight (NLoS) propagation [1].

Thanks to this novel approach, engineers and network designers can efficiently handle the highly probabilistic nature of EM propagation by turning it into a programmable and partially deterministic space [1] [17] [20]. Fundamental limitations of the current wireless communications (e.g. distance loss, multipath fading, shadowing, blockage) can be bypassed and new services and functionalities can be supported due to the fact that RIS approach introduces the possibility of end-to-end optimization of wireless networks instead of just managing the endpoints [1] [3] [34] [35].

First of all, from an implementation point of view the RIS-aided networks present considerable advantages and practical viability [1] [6]. More specifically, RISs can operate with improved cost efficiency, as their components, although relatively numerous, are of low-cost and require low power consumption compared to those used in existing active antenna array technologies [4] [6] [13]. Moreover, RIS-assisted communications impose only soft programming requirements, as the smart surfaces simply manipulate the incident signals without the need of complex sophisticated signal processing techniques [4] [17].

In addition, RISs can be easily and flexibly deployed in a wide range of scenarios since they are made of lightweight electromagnetic material which can easily attached to existing infrastructure elements, including but not limited to (indoor or outdoor) walls, ceilings, glasses of windows, billboards, lampposts, or even on objects such as vehicle surfaces, t-shirts and eyeglasses [6] [19] [30]. It should be highlighted that smart surfaces can also be easily removed from objects (in case needed), while neither adversely affecting the aesthetics of the surrounding environment nor reducing the visibility of people [19].

Furthermore, the passive nature of scattering elements, as they merely reflect the incident EM waves, enables them to exhibit full-band response and thus, the RIS can operate at any desired frequency ranging from microwave to optical spectrum [2] [4] [11] [17]. Additionally, RIS can support full-duplex (FD) transmission without thermal noise and self-interference effects; this renders the RIS technology a more appealing approach compared to relay-based implementations, which can either be half-duplex (HD) or require advanced self-interference cancellation techniques in case of FD mode [2] [4] [6].

Moreover, RIS can boost the signal quality at the receiver and deliver enhanced spectral efficiency[1] by improving the signal-to-interference-plus-noise ratio (SINR) and by mitigating the effects of long-distance power loss [2] [17]. In fact, RIS operation not only can improve the signal quality by buffering and/or processing the impinging radio waves in the desired way through smart reflections, but it can also enable interference-free communication either by suppressing the unwanted signals or by focusing the energy on the target UE in order to avoid creating unwanted interference in hotspot sites [17] [19]. Apart from that, RISs do not use Analog to Digital (ADCs) and Digital to Analog (DACs) converters or Power Amplifiers (PAs) and thus, they neither inject noise nor amplify the

[1] Spectral efficiency (SE) describes the ability of a communication system to accommodate data within a limited bandwidth. It reflects how efficiently the allocated bandwidth is utilised and defined as the ratio of the throughput data rate per Hertz in a given bandwidth [36]. It is usually measured in bits per second per hertz (bits/s/Hz) [36].

received noise during their operation [17]. Lastly, it should be also noted that based on Shannon's capacity formula[2] there is a substantial trade-off[3] between the energy efficiency[4] and spectral efficiency [37]; therefore, the RIS-assisted amplification of the received signal can significantly contribute to the spectral efficiency enhancement by properly selecting the optimal transmission power [37].

Furthermore, the link capacity can be improved by the increase of the SINR (based on Shannon-Hartley theorem[5]) [40], while the compatibility with existing wireless systems and emerging technologies (e.g. Non-Orthogonal Multiple Access (NOMA), massive MIMO communications in mmWave (30-300 GHz) and terahertz bands (0.3-10 THz)) apart from eliminating any hardware-related change requirements, also allows the exploitation of these communication schemes to further enrich the network features (e.g. energy efficiency, capacity/throughput[6], coverage, security) [1] [6] [14].

Additionally, the operating principle of RIS technology is based on the recyclability of existing radio waves instead of new signal emissions and therefore not only can it offer lower energy consumption but also allow for a lighter environmental footprint [19]. These nearly-passive devices add an eco-friendly approach to network design since on the one hand they do not require any dedicated power sources and on the other hand they do not contaminate the environment through the battery disposal [1] [17]. Furthermore, the living organisms can benefit from the reduced EM pollution as they are less exposed to the potential harmful effects of electromagnetic fields and/or radiation [19]. Lastly, the careful selection of environmental-friendly metamaterials that can be relatively inexpensive and easily recyclable can facilitate the design, development and implementation of sustainable wireless networks [19].

Finally, it should be emphasized the fact that RISs offer advanced focusing functionalities in the near-field[7] operating regime, which is not usual in the traditional wireless systems

---

[2] $E_e = \frac{S_e}{(2^{S_e}-1)} * N_0$, where E_e is the energy efficiency, S_e is the spectrum efficiency and N_0 is the power spectral density. Thus, E tends to zero when S tends to infinity [37].

[3] Spectrum Efficiency (SE) - EE trade-off: given a bandwidth available, to balance the achievable rate and the energy consumption of the system [38].

[4] Energy efficiency (EE) is usually defined as number of bits reliably transmitted by a unit energy and is usually quantified by bits per Joule [39].

[5] $C = B * log_2\left(1 + {}^{S}/_{N}\right)$, where C is the channel capacity, B the bandwidth of the channel, S the signal power and N the noise [40].

[6] In communication networks, throughput is the amount of digital data per time unit that is delivered over a physical or logical link, or that is passing through a certain network node. The throughput is usually measured in bits per second (bits/s or bps) and occasionally in data packets per second [41].
The transmission capacity is defined as the number of successful transmissions taking place in the network per unit area, subject to a constraint on outage probability [42].

[7] Near-field and Far-field: When a transmitter is sufficiently far away from an antenna array, the spherical wave generated by the transmitter can be approximately regarded as a plane wave at the antenna array side [11]. The distance between the transmitter/receiver and the centre of the antenna array $2 * L^2/\lambda$ (where L and λ denote the largest dimension of the antenna array and the wavelength of the signal, respectively) is a commonly used criterion to decide the boundary between the near-field and far-field regions [2]. When this distance is less than $2 * L^2/\lambda$, the transmitter/receiver are considered to be in the near-field of the RIS; otherwise, they are in the far field of the RIS [11]. In general, the essential difference between the near-field

[19]. Near-field intelligent broadcasting and beamforming (Fig.6), and improved localization accuracy both in far-field and near-field region (Fig.7) under severe blockage conditions can be achieved by deploying RIS-assisted communication setups [11] [43] [44].

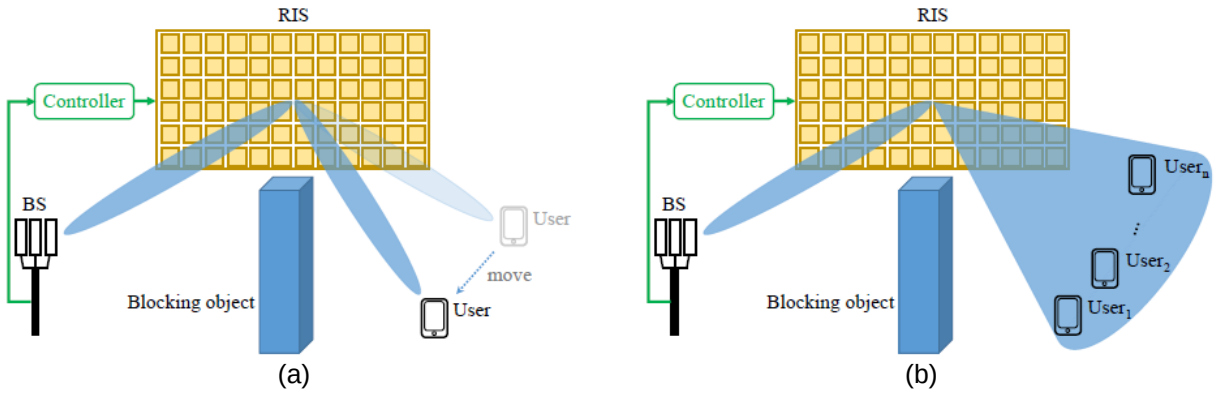

Figure 6. RIS-enabled near-field (a) beamforming, and (b) broadcasting [11].

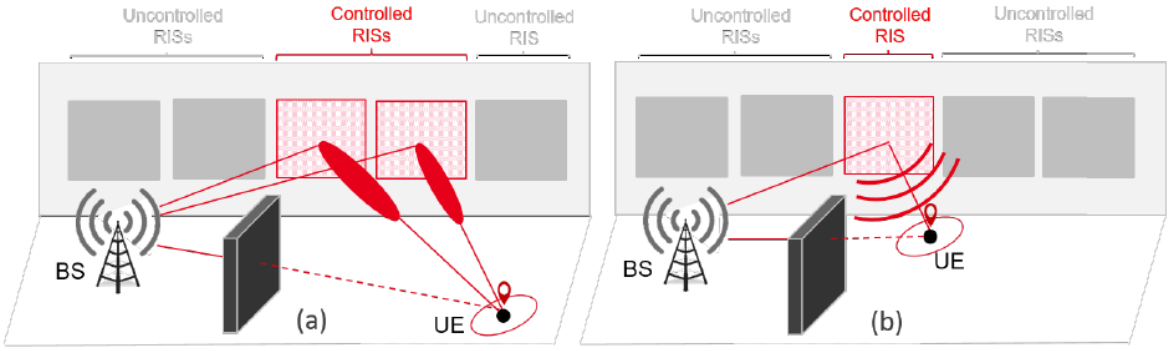

Figure 7. RIS-assisted NLoS localization in: (a) far-field, and (b) near-field regime [44].

In a nutshell, the high spectral and energy efficiency, the enhancement of capacity and coverage of wireless networks, the improvement of signal quality, the extraordinary capability of tailoring the EM waves and the possibility of overcoming fundamental limitations of the existing network designs, the compatibility with legacy technologies and the cost-effective and eco-friendly way of RIS operation, may expand the performance of wireless communications and create new opportunities both for service providers and customers [1] [2] [4] [6] [11] [17].

1.2.6 Applications

As mentioned previously, the RIS deployment is intertwined with high spectral and energy efficiency, enhanced network coverage, capacity and security, improved signal quality and radio localization precision, extraordinary capabilities of tailoring the EM waves (focusing

region and the far-field region is how the power density changes with distance; in specific, within the near-field region the power density shows significant variations [2].

enhancement and interference suppression) and overcoming fundamental limitations of the existing network designs, integration/compatibility with legacy technologies, and the cost-effective and environmental-friendly mode of operation [1] [2] [4] [6] [11] [17] [19]. In addition to the above, the ever-increasing interplay between RIS and artificial intelligence techniques in the field of wireless communications is expected to offer unprecedented performance capabilities [45].

All the aforementioned advantageous features can expand the performance of wireless communications and create new opportunities for both service providers and customers in the forthcoming 6G era. In specific, RIS can support a plethora of existing wireless network schemes and applications in the pursuit of high Quality of Experience (QoE) / Quality of Service (QoS), which will be further elaborated as follows:

a. *RIS-assisted millimeter-Wave (mmWave) and Terahertz (THz) communications*

The mmWave and THz communication systems have the capability to support high data rates by efficiently exploiting the available enormous bandwidth [4] [46]. However, mmWave/THz frequencies suffer from severe pathloss, atmospheric absorption and rainfall attenuation, blockage (e.g. foliage attenuation, material penetration losses, human body blockage) and human shadowing losses, reflection and scattering losses, and other drawbacks associated with molecular absorption noise, diffuse scattering and doppler spread [4] [46] [47] [48] [49]; hence, the long-range omnidirectional transmissions are inherently unreliable, especially in indoor and dense urban environments [46].

Fortunately, the aforementioned undesirable phenomena can be mitigated by the RIS deployment, which can introduce additional (indirect) link connections in case the direct path between the transceivers is blocked [4] [46] [47], as shown in Figure 8 [6]. In addition, RIS-aided beamforming techniques can effectively steer the impinging signal to the target UE in order to help address both the NLoS and the large free space pathloss challenges of mmWave/THz communications [46] [50].

It should be noted that simulations results verify the feasibility and effectiveness of the forementioned RIS application [43] [51] [52] [53] [54].

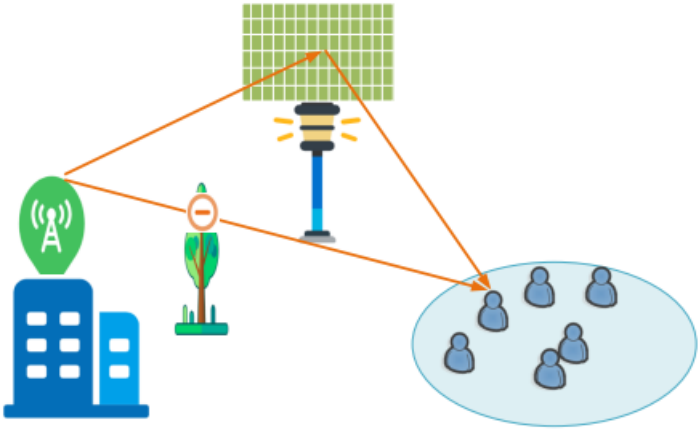

Figure 8. RIS-assisted mmWave/THz communication [6].

b. RIS-assisted multicell networks

It is common practice in multicell communication scenarios to employ dense frequency reuse schemes to maximize the spectrum efficiency [4]. However, the simultaneous usage of the same frequency resources in neighboring cells leads to inter-cell interference problems which can severely degrade the overall system performance, particularly for the edge-cell users that experience a low SINR [4] [55].

In this case, RIS can be deployed at the cell boundary, as shown in Figure 9, with a dual purpose: on the one hand, to improve the desired received signal strength and, on the other hand, to suppress the unwanted interference originating from the adjacent cells [2] [4] [56], as also explained in §1.2.5. It should be noted that simulations results verify the feasibility and effectiveness of the forementioned RIS application [4].

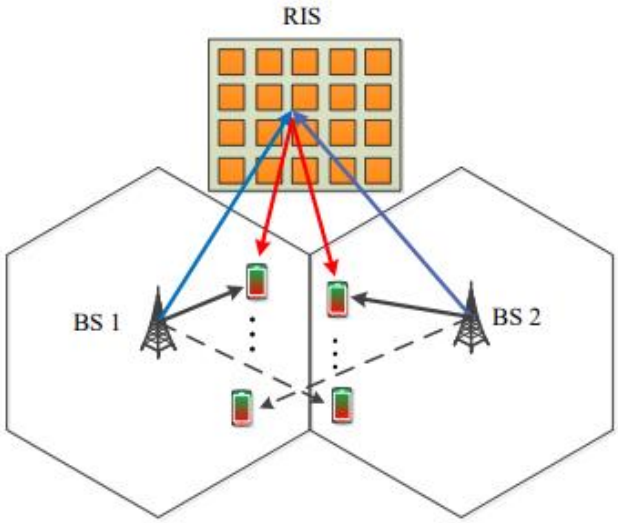

Figure 9. RIS-assisted multicell networks [4].

c. RIS-assisted Simultaneous Wireless Information and Power Transfer (SWIPT) systems

In general, SWIPT is a promising and attractive concept for the energy management of future Internet-of-Things (IoT) networks [2] [4]. SWIPT technology enables, in addition to information transmission, the energy transmission from the BS to a nearby massive number of energy-harvesting IoT devices, in order to allow them to operate and communicate simultaneously [4] [57] [58].

The main challenge to this idea is that the devices that decode the information from the received signal (known as Information Receivers (IRs)) and the devices that harvest the signal energy (known as Energy Receivers (ERs)) have different power supply requirements. In specific, the energy receivers require much higher energy and therefore their maximum link-distance is limited to areas close to the BS [4] [58]. To tackle this problem, RIS can be deployed in the vicinity of ERs to provide auxiliary transmission links which can enrich the ERs' energy harvesting capability and thus extend their operational

range [4] [58], as shown in Figure 10. It should be noted that simulations results verify the feasibility and effectiveness of the forementioned RIS application [4] [53] [59].

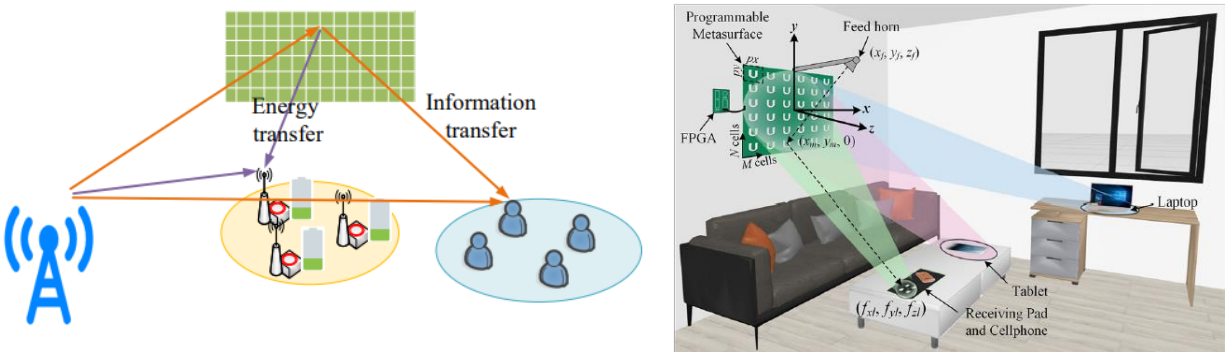

(a) (b)

Figure 10. RIS-assisted SWIPT system in: (a) Outdoor environment [6], and (b) Indoor environment [57].

d. RIS-assisted Mobile Edge Computing (MEC) networks

Mobile Edge Computing (MEC) is envisioned as a promising technique for supporting and facilitating the operation of many forthcoming novel but also resource-intensive and latency-critical applications (e.g. Virtual Reality (VR)) [4] [60] [61]. In specific, these applications place increased computation and processing requirements which cannot be supported by the resource-limited (in terms of hardware capabilities and power supply) mobile devices [4] [60]. Here come the MEC networks to migrate this load to high-performance computing servers at the edge of the network (MEC server), where AI and ML processing can be deployed in order to ensure low-latency and high-quality services [4] [60] [61].

However, MEC networks may suffer from bottleneck issues associated with the data offloading rate on edge servers due to the limited uplink capability and the severe path loss [4] [61]. Fortunately, RIS can be deployed to smartly reflect the signals in order to overcome the existing propagation-related problems and prevent the offloading delays [4] [61]. As shown in Figure 11 [60], the direct communication link (including both LoS and NLoS components) will be further enhanced by the reflected links originating from the RIS scattering elements after applying the necessary phase shifts [60].

It should be noted that simulations results verify the feasibility and effectiveness of the forementioned RIS application [4] [60] [62].

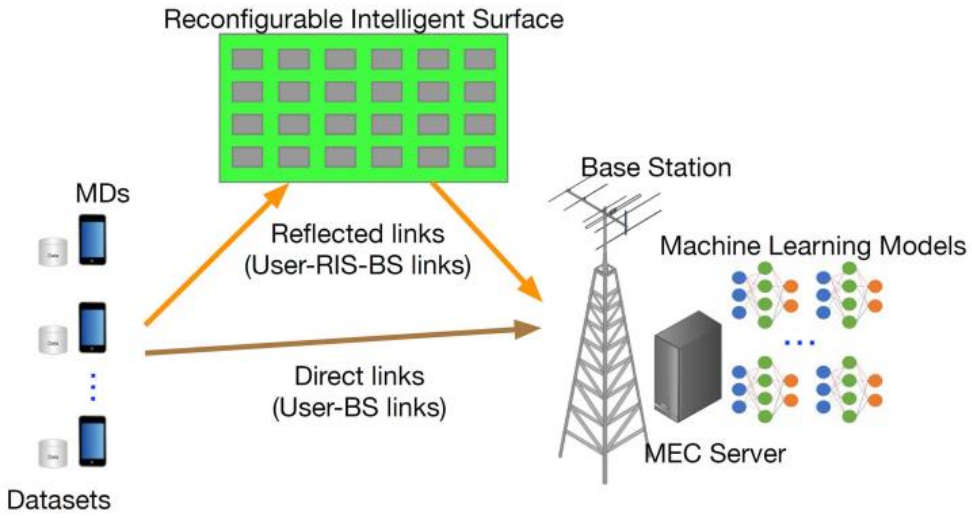

Figure 11. RIS-assisted MEC network [60].

e. RIS-assisted Non-orthogonal Multiple Access (NOMA) systems

NOMA has emerged as a promising multiple-access technique of next-generation networks, whose basic idea is to serve multiple users simultaneously and thus, enhance the spectral efficiency of the Orthogonal Multiple Access (OMA) methods (e.g. FDMA, TDMA) by allowing the users to share the same spectrum resources (i.e. resource block (RB)) (e.g. frequency/time) in a non-orthogonal way through the use of various power levels and/or different codes [4] [46] [63].

RIS technology can benefit existing NOMA networks in a variety of ways. In specific:

- ✓ The performance of NOMA can be enhanced by the RIS-empowered additional signal diversity without the need of extra time slots or energy resources [64].
- ✓ RIS technology enables smart and flexible NOMA design, as it has the ability to either improve or degrade the quality of the channel corresponding to each user by properly modifying the RIS parameters, such as the reflection coefficient and the deployment location [64].
- ✓ RIS deployment can ease the NOMA-related constraints associated with the number of antennas equipped at base station and the number of users, since it can provide additional passive array gain to support a cluster-based NOMA strategy, either with a centralized RIS-enabled design or with a distributed RIS-enhanced design, as shown in Figure 12 [64].
- ✓ RIS deployment can address the challenges of the dynamic environment, such as small-scale channel fading (i.e. random fluctuations of channel gain), blocking, and user mobility, and aims to improve the network coverage and capacity in urban environments that are severely disrupted due to high-rise buildings/constructions [2] [46].

It should be noted that simulations results verify the feasibility and effectiveness of the forementioned RIS application [64] [65] [66] [67].

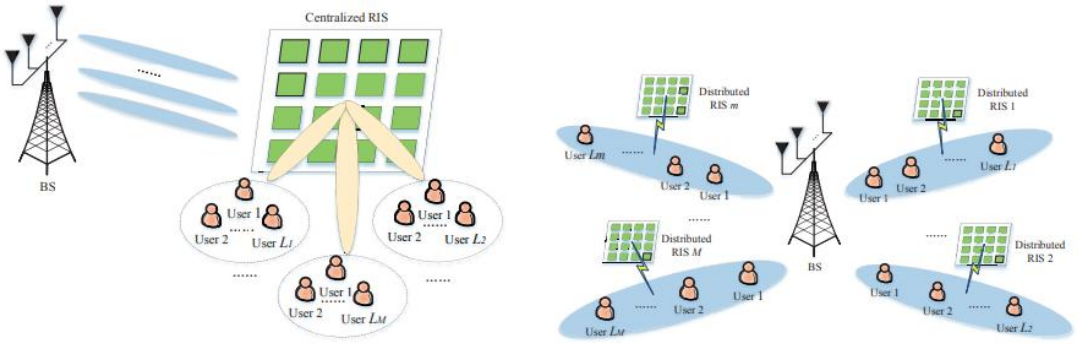

(a) (b)

Figure 12. RIS-assisted NOMA systems: (a) centralized RIS-enabled design. (b) distributed RIS-enhanced design [64].

f. RIS-assisted Multicast communications

Multicast communications are increasingly gain attention as they can apply in many popular applications, such as video conferencing, video gaming and TV and live video streaming, and can support the massive Machine-Type IoT communication (mMTIC) by simultaneously transmitting the same identical content (data stream) to multiple IoT devices [4] [68] [69].

In this case, RIS can be deployed (Fig.13) to enhance the system performance by improving the channel conditions and by maximizing the total sum rate of all multicasting groups [4] [69]. Simulations results have shown the effectiveness of the proposed method (e.g. [68], [69], [70]).

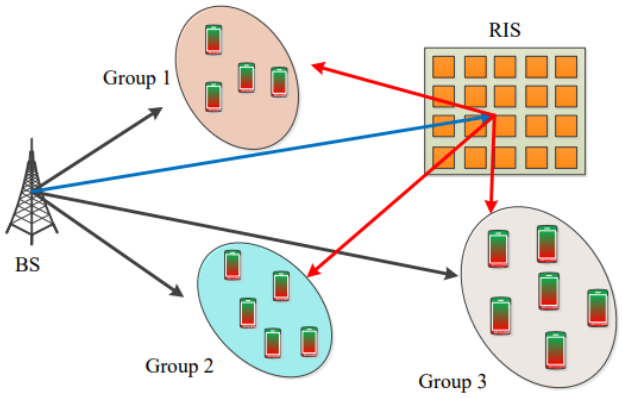

Figure 13. RIS-assisted multicast communications [4].

g. RIS-assisted Physical Layer Security (PLS) networks

Due to the broadcast characteristics of wireless communication, significant security vulnerabilities may arise, as the transmission can be exposed to eavesdropping and jamming risks [4]. In specific, wireless networks may suffer from information leakage in case of presence of malicious eavesdropper or from intentionally injected noise (by malicious jammers) which can disturb the smooth data transmission. PLS techniques

have been investigated to address such issues (instead of cryptographic approaches) by exploiting the unique wireless physical layer medium features in a low computational complex and high scalable manner [71].

RIS can be deployed in conjunction with PLS methods in order to optimize the transmit beamforming and maximize the security of the communication link by, on the one hand, boosting the signal strength to intended (legitimate) users and, on the other hand, suppressing the signal beam to other unintended users [2] [4] [46]. Figure 14 presents the RIS deployment for physical layer security purposes in a wireless network in the presence of an eavesdropper [4].

It should be noted that simulations results verify the feasibility and effectiveness of the forementioned RIS application, e.g. [2] [4].

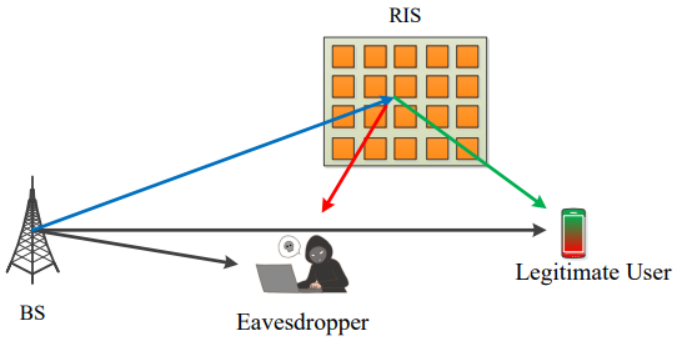

Figure 14. RIS-assisted PLS network [4].

h. RIS-assisted Cognitive Radio (CR) Networks

The spectral efficiency of wireless communications can be further enhanced by applying Cognitive Radio (CR) techniques. In cognitive radio networks, the spectrum can be shared between co-existing primary (PUs) and secondary users (SUs) by following dynamic spectrum access approach [4] [72] [73]. In particular, the network serves PUs with priority, while if there are excess resources, SUs are also served, provide that they do not interfere with the PUs [73]. The key challenge is to maximize the achievable sum-rates of the secondary system while keeping the interference originating from the SU transmitters (SU-TXs) to the PUs receivers (PU-RXs) at an acceptable level, defined by a threshold known as interference temperature constraint [4] [72] [74].

In this case, RISs can be deployed in the vicinity of PU-RXs (Figure 15) to improve the signal power to the SUs under the imposed interference temperature constraints, since RIS technology, on the one hand can redirect the incident EM waves to the desired destinations, and on the other hand, exhibits interference suppression and signal-to-interference-plus-noise ratio maximization capabilities [4] [72] [73].

It should be noted that simulations results verify the feasibility and effectiveness of the forementioned RIS application (e.g. [72], [73], [75], [76]).

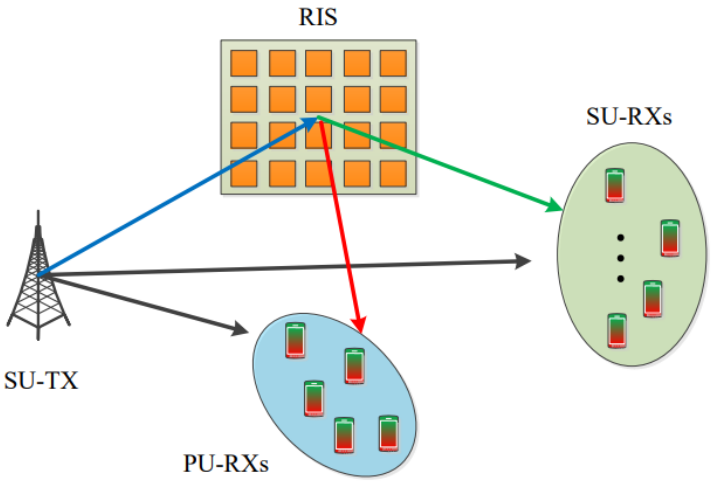

Figure 15. RIS-assisted CR networks [4].

However, apart from the deployment of Reconfigurable Intelligent Surfaces in the aforementioned emerging wireless network systems/technologies, this novel concept can provide a wide range of practical application fields in the modern world. Recent literature refers to many various application areas of wireless communications that are aligned with realizing the vision of Smart Radio Environment. In more detail, RISs can be used either in outdoor environments to establish additional communication links to the existing (direct) paths, especially when blockage conditions exist, or in indoor environments to increase the system capacity, as shown in Figure 16 [45].

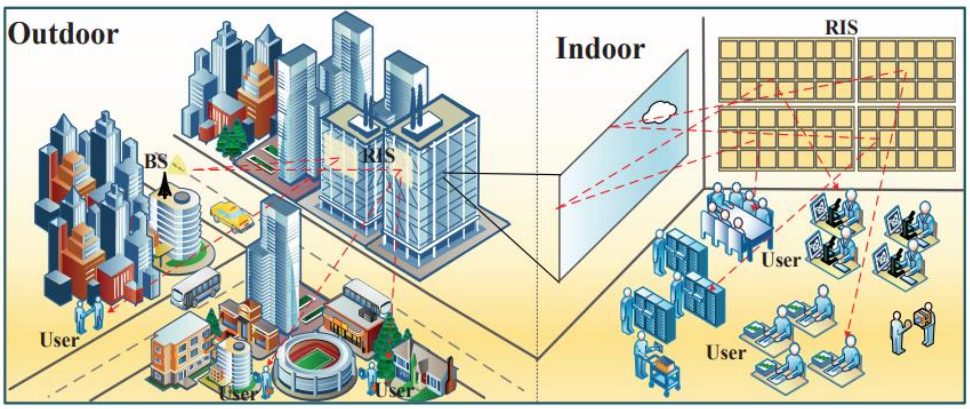

Figure 16. RIS-assisted outdoor and indoor communications [45].

In fact, RISs can be spread across a geographical area in an aesthetically friendly way to improve the propagation environment via smart signal reflections and enhance the robustness of wireless networks in order to establish high-capacity hotspots or interconnect isolated users/assets and /or IoT devices [6] [19] [45]. Article [19] includes smart cities, smart buildings (Fig.17(a) [77]), smart homes, smart university campuses, smart undergrounds, smart train stations (Fig.17(b) [3]), while [61] refers to RIS-aided IoT communications in a smart industry use case (Fig.17(c) [61]).

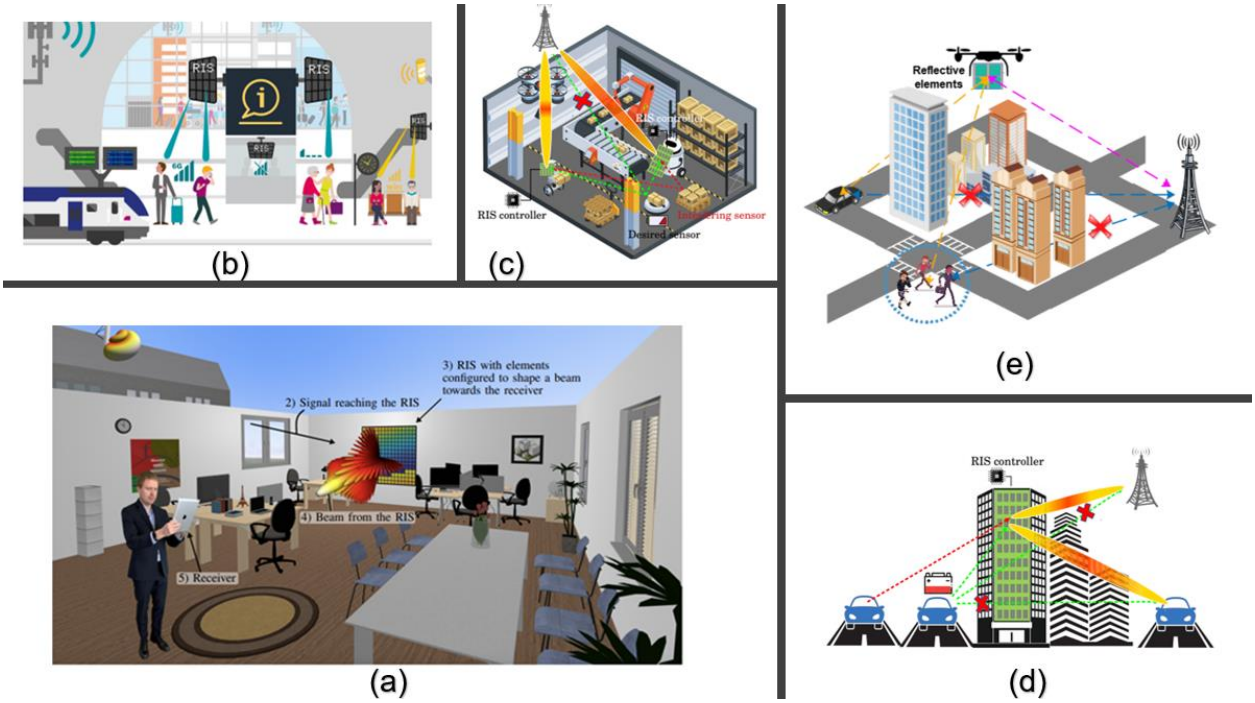

Figure 17. Envisioned RIS-empowered use cases: (a) RIS-assisted smart buildings [77], (b) RIS-assisted smart train stations [3], (c) RIS-assisted smart industry [61], (d) RIS-assisted vehicle communications [61], and RIS-assisted UAV-aided communications [78].

Additionally, RISs can be used in smart transportation systems (e.g. smart cars, smart airplanes, smart trains) to meet the stringent URLLC requirements and assist vehicle and robotic communications, given their ability to effectively compensate Doppler and delay spread effects [6] [19] [35] [61] [79] [80] [81] [82], as illustrated in Figure 17(d). From the reverse perspective, RIS can be applied to Unmanned Aerial Vehicles (UAVs) to improve cellular services and assist terrestrial communications [6] [78] [79] [80], as shown in Figure 17(e).

1.3 Literature Review

As already mentioned, Reconfigurable intelligent surfaces are considered as one of the most promising and revolutionizing techniques in the modern era of wireless communications and an increasingly important technology in the realization of future sixth-generation (6G) and beyond wireless networks. For that reason, there is a growing academic and research interest in RISs. In this paragraph, a comprehensive literature review is provided on RIS fundamental and operating principles and design considerations and on the most important application areas.

In more detail, the authors in [2] provide an overview of the state-of-the-art on RISs, with focus on their operating principles, performance evaluation, beamforming design and resource management, applications of machine learning to RIS-enhanced wireless networks, as well as the integration of RISs with other emerging technologies. In [29], a comprehensive literature review on RISs and assisted application areas is presented and

the current research activities in the evolving field of wireless networks operated by RIS are discussed thoroughly. The article [4] addresses the fundamentals, the necessity, the potential applications and the challenges of this novel technology. The authors in [21] supply a study review of RIS-assisted wireless communication with emphasis on principles, hardware architecture, control mechanisms, and analytical approaches and performance metrics of RIS-empowered systems. In [83], the authors provide insights on the application scenarios and standardization roadmap of future-oriented RISs, analyze the characteristics of RISs and summarize white papers, projects and standardization efforts related to RISs. The paper [19] introduces the emerging research field of RIS-empowered SREs, summarizes the most suitable applications, presents an electromagnetic-based communication-theoretic framework for analyzing and optimizing metamaterial-based RISs, provides a comprehensive overview of the current state of research and discusses the most important research limitations. In [50], a detailed survey of the RIS technology, design, application and research issues is provided. The authors in [26] present the fundamentals and applications of RIS technology and highlight the competitive advantages over existing technologies, while address also the key challenges in the design and implementation of RIS-aided wireless networks. Additionally, numerical results are provided to show the efficiency of RIS deployment in typical wireless networks. In [77], the authors follow a neutral approach by reviewing the fundamental and easily misinterpreted features of RIS technology.

In the context of 6G framework and Smart Radio Environments, the authors in [84] introduce the concept of RIS-assisted networks by elaborating on their advantages and limitations. In addition, the different types of RIS implementations and the available prototypes are presented from a theoretical standpoint, while a comparison with other transmission technologies is provided. The article [1] discusses how the availability of reconfigurable intelligent meta-surfaces will allow wireless network operators to redesign common and well-known network communication paradigms, while two major types of RISs are also presented. In [46], the authors supply a tutorial overview of RISs for 6G wireless networks and a comprehensive discussion on performance gains that can be achieved by integrating RISs with emerging communication technologies.

Regarding the modeling and performance of RIS-assisted wireless networks, the authors in [3] focus on the realistic modeling of RIS-assisted signal propagation, the investigation of the fundamental limits of RIS-empowered wireless communications and sensing, and the design of efficient algorithms for orchestrating networking RISs. In [11] free-space path loss models for RIS-assisted wireless communications are proposed for different scenarios by studying the physics and electromagnetic nature of RISs. In addition, three fabricated RISs are utilized to further corroborate the theoretical findings through experimental measurements conducted in a microwave anechoic chamber. The authors in [44] follow a Fisher information analysis in order to show a single-RIS system can improve localization accuracy in case of NLoS links, while they also discuss practical system approaches that could enable better LoS-to-NLoS positioning continuity in harsh environments. The paper [35] investigates the feasibility of eliminating or mitigating the multipath fading phenomenon and Doppler spread effects via RIS-empowered solutions.

In [85] the authors present an analytical model that captures the performance of the RIS-aided link in the limit of very large RIS and demonstrate numerical examples that provide insight on the interplay between the RIS size and the properties of the transmitter beam. The authors in [86] provide an accurate, open-source, and widely applicable RIS channel model for mmWave frequencies. In [87], the authors consider a nearby reconfigurable intelligent surface whose phase shifts can be adjusted in order to establish communication in an UM-MIMO THz communication system operating in a typical indoor scenario where the direct link between the transmitter and receiver is obstructed due to surrounding obstacles. The authors propose an algorithm to configure the individual phase shifts of the RIS elements, in order to maximize the achievable data rate performance. The article [88] presents a connectivity analysis of RIS-assisted THz wireless systems by accommodating the particularities of THz band links as well as the characteristics of the RIS. In [89], it is demonstrated through simulations how the RIS efficiency depends on the orientation of the RIS with respect to the transmitter and receiver, and also on the relative size of the RIS with respect to the footprint of the incident beam. The authors in [90] present an analytic framework for evaluating the ergodic capacity (EC) of the RIS-assisted systems, while the special case in which the RIS is equipped with a single reflection unit is investigated. The paper [91] evaluates the performance of RIS deployment for restoring a link between a transmitter and a receiver, operating in the D–band (110–170GHz) in terms of pathgain and capacity, as a function of the number of RIS elements, the transceiver antenna gains, the Tx/Rx–RIS distance and the elevation angles from the center of the RIS to the transceivers. In [92], the authors present a general model that accommodates the impact of transceiver hardware imperfection due to radio frequency impairments on RIS-assisted wireless systems; the systems' outage performance is evaluated based on the end-to-end signal-to-noise-plus-distortion ratio (SNDR) and system's outage probability. The article [93] proposes a model regarding the overhead that is required to estimate the channel state information and to report the optimized phase shifts to the RIS; the model is incorporated in the expressions of the system rate and energy efficiency, which are then optimized with respect to the phase shifts of the reconfigurable intelligent surface, the transmit and receive filters, the power and bandwidth used for the communication and feedback phases.

As far as the design and fabrication of RIS, the authors in [6] intend to shed some light on RISs from an industrial viewpoint and to provide a roadmap in order to make RISs feasible in industry. The paper [32] introduces the well-known two-dimensional smart surface with a rectangular array of simple RF switch elements, named as RFocus, which moves beamforming functions from the radio endpoints to the environment. The authors in [22] present the theoretical considerations and the design evolution of a proof-of-concept reconfigurable metasurface, primarily used as a tunable microwave absorber, but also as a wavefront manipulation and polarization conversion device in reflection. In [28], an intelligent metasurface with real-time self-adaptively EM manipulation capability is proposed; the self-adaptive reaction capability and practicability of the proposed metasurface have been experimentally demonstrated. The authors in [13] develop a new type of high-gain yet low-cost RIS that bears 256 elements that combines the functions of

phase shift and radiation, and show that the proposed prototype can achieve significant antenna gain and reduced power consumption for the wireless system. The article [34] describes a new RIS prototype consisting of 1100 controllable elements working at 5.8 GHz band and proposes an efficient algorithm for configuring the RIS over the air by exploiting the geometrical array properties and a practical receiver-RIS feedback link.

With regard to the performance comparison with other related technologies, the authors in [17] provide a detailed overview and historical perspective on state-of-the-art solutions, and elaborate on the fundamental differences of RIS with other technologies (e.g. relaying, MIMO beamforming, and backscatter communications), while the article [20] focuses on the key differences and similarities between RISs that are configured to operate as anomalous reflectors and relays. In addition, the authors in [94] provide the theoretical framework for the performance comparison of RISs and amplify-and-forward (AF) relaying wireless systems in terms of end-to-end signal-to-noise ratio (SNR), outage probability (OP), symbol error rate (SER) and ergodic capacity (EC). Furthermore, in [95] a performance comparison between a RIS-aided network with its relay-aided counterpart is performed in terms of achievable rate and energy efficiency.

Several research studies are proving the efficiency of Reconfigurable Intelligent Surfaces to enable energy-efficient and smart wireless communications in MIMO and massive-MIMO systems. In particular, the authors in [96] study the achievable rate optimization for multi-stream MIMO systems equipped with a RIS, and formulate a joint optimization problem of the covariance matrix of the transmitted signal and the RIS elements. In [56], the authors propose the RIS deployment at the cell boundary of multiple cells to assist the downlink transmission to cell-edge users, whilst mitigating the inter-cell interference with the goal of maximizing the weighted sum rate (WSR) of all users. In [97], the authors consider the deployment of RISs to assist multiuser MIMO uplink transmission from several multi-antenna user terminals to a multi-antenna base station; an optimization framework is proposed for jointly designing the transmit covariance matrices of the UTs and the RIS phase shift matrix to maximize the system global energy efficiency with partial CSI. The paper [98] investigates the interference-to-noise ratio (INR) at one user equipment that is caused by the signal emitted by its non-serving (interfering) RIS in a multiple-input multiple-output network where each base station serves a user equipment with the aid of a RIS. In [99], the impact of channel correlation, the number of RIS elements, and the pilot contamination on the uplink and downlink ergodic net throughput of each user is examined for RIS-assisted Cell-Free Massive MIMO systems. The authors in [100] and [101] provide insights on RIS operation of an uplink RIS-aided massive MIMO system, which is related to the asymptotic rate performance, the power scaling laws, and the impacts of various system parameters on the achievable rate. The article [102] proposes a benchmark algorithm based on the semidefinite relaxation technique to jointly optimize the beamforming vector at the transmitter and phase shift matrix of the RIS for a RIS-assisted MIMO system under spatial fading correlations, with the statistical CSI known at the transmitter and the RIS. The authors in [103] analyze the ergodic spectral efficiency of a RIS-assisted MIMO system under spatially correlated channels and propose an optimal phase shift design to maximize this efficiency. In [47], the authors

investigate the co-design of per-subcarrier power allocation matrices and multielement RIS phase shifts in downlink wideband MIMO transmission using 28 GHz frequency bands.

Furthermore, there is considerable research interest in RIS-assisted NOMA systems. In specific, the authors in [64] focus on the RIS deployment in multiuser networks employing OMA or NOMA, with an emphasis on investigating the interplay between NOMA and RIS. In [66], the authors attempt to optimize the rate performance and ensure user fairness by jointly optimizing the (active) transmit beamforming at the base station and the phase shifts (i.e., passive beamforming) at the RIS in a RIS-assisted downlink NOMA system. In [67], the authors conceive a system for serving paired power-domain NOMA users by designing the passive beamforming weights at the RISs and attempt to evaluate the network performance in terms of outage probability and ergodic rate of the prioritized user. The authors in [65] formulate a joint RIS phase shifts, hybrid beamforming, and power allocation problem with the goal of maximizing the achievable sum-rate under a minimum rate constraint for the users and a maximum transmit power constraint in a RIS-aided mmWave NOMA system.

As far as the multicast communications, the authors in [69] aim to minimize the transmit power at the sender of a secure multigroup multicast multiple-input single-output (MISO) communication system via jointly optimizing the transmit beamformer, artificial noise vector and phase shifts at the RIS subject to the secrecy rate constraints as well as the unit modulus constraints of RIS phase shifts. In [70] effort is given to maximize the sum rate of multiple multicasting groups by the joint optimization of the precoding matrix at the base station and the reflection coefficients at the RIS under both the power and unit-modulus constraint. The paper [68] assesses the bit error rate (BER) performance of a RIS-assisted dual-hop multicast wireless communication network and compare the results with those derived from conventional non-RIS channels links.

The existing literature is also focused on the field of RIS-assisted mmWave and THz communications. In more detail, the authors in [51] study the channel capacity optimization utilizing RISs in indoor mmWave environments where no LoS path is present, while simulations take place to draw conclusions. In [52], the authors use stochastic optimization methods to investigate to whether robust beamforming for RIS-aided systems can effectively compensate for the performance loss caused by the presence of random blockages, especially when the blockage probability is high. The article [104] presents a novel system model that takes into account the relationship between the transmission beam footprint at the RIS plane and the RIS size, while simulations are performed to reveal important trends regarding the optimal RIS placement according to the system parameters. The authors in [43] propose a simplified free-space path loss model for RISs, in which the impact of the antenna's directivity of the transmitter, receiver, and the unit cells of the RIS on the path loss is explicitly formulated as an angle-dependent loss factor. Additionally, two fabricated RISs operating in the mmWave band are utilized to carry out a measurement campaign. The paper [105] presents an analytical pathloss model for RIS-assisted THz wireless systems, which is validated through extensive electromagnetic

simulations, while in [106] the performance of a RIS-assisted terahertz (0.1 − 10 THz) wireless system is evaluated in terms of average SNR, EC and OP.

Regarding the CR technology, the authors in [73] investigate the concept of adopting both concepts of CRs and RISs within a network as a means of maximizing the potential benefits available and carry out Monte Carlo simulations to validate the analytical expressions for the performance metrics of the RIS-enhanced CR network. In [75], the joint application of RISs and vertical beamforming in CR networks is investigated in terms of maximizing the spectral efficiency of the secondary network. The article [72] investigates whether the spectral efficiency and energy efficiency of wireless communications can be improved by introducing multiple RISs to a downlink MISO CR system. The authors in [74] formulate an optimization problem with the objective of determining the transmit covariance matrix that maximizes the SU rate, while protecting the PU by enforcing both a PU average interference constraint and a PU outage probability constraint. In [76], the authors formulate an optimization problem with the objective to maximize the achievable WSR of SUs subject to the SU-TX total power, the PU's interference temperature and unit modulus constraints in a RIS-aided MIMO CR system. The paper [107] refers to a robust beamforming design based on the statistical CSI error model for PU-related cascaded channels in RIS-aided CR systems and jointly optimize the transmit precoding matrix and phase shifts to minimize the SU's total transmit power. In [108], the RIS technology and physical layer security (PLS) to solve the security issue of a MISO CR wiretap channel; simulations have shown that the proposed RIS-assisted design greatly enhances the secondary user’s secrecy rate compared to existing methods without RIS.

Several research studies propose to enhance MEC systems by exploiting the emerging technique of reconfigurable intelligent surfaces. The article [62] provides an overview of RIS-assisted MEC systems and highlights significant use cases as well as relevant design challenges and solutions. In [60], an infrastructure to perform machine learning tasks at an MEC server with the assistance of a reconfigurable intelligent surface is presented, while the authors in [61] develop a spectrum learning (SL)-aided RIS framework for intelligently exploiting the inherent characteristics of the radio frequency spectrum for "green" 6G networks.

As far as the simultaneous wireless information and power transfer (SWIPT) systems, the authors in [58] propose an RIS-aided SWIPT approach to maximize the WSR of RISs while guaranteeing an improved energy harvesting performance of the energy receivers. In [59], an analytical framework for the statistical analysis of the battery recharging time in RIS-assisted wireless power transfer (WPT) systems is presented, while the paper [53] proposes a new simultaneous terahertz information and power transfer (STIPT) system, which utilizes a RIS both for data and power transmission.

An increasing interest is also being shown in the contribution of RIS technology to UAV-assisted communications. In specific, the authors in [79] survey the existing literature related to RIS-aided UAV communications and highlight several emerging technologies and application scenarios for future wireless networks, while in [80], the authors discuss

the potential benefits of RIS deployment in UAV communications. In [54], UAVs and RISs are utilized to support THz communications by jointly optimizing the UAV's trajectory, the phase shift of RIS, the allocation of THz sub-bands, and the power control with the goal of maximizing the minimum average achievable rate of all users. The article [78] introduces the concept of RIS-equipped UAVs to support cellular communications networks and services of the future, while the paper [109] investigates a novel UAV secure communication system with the assistance of reconfigurable intelligent surfaces.

In addition, research interest also focuses on RIS-assisted vehicle communications. The authors in [81] investigate the spectrum sharing problem in RIS-aided vehicular networks, in which multiple vehicle-to-vehicle links reuse the spectrum already occupied by vehicle-to-infrastructure links, and through simulation attempt to unveil the benefits of introducing RISs for enhancing the QoS performance of vehicular communications. The article [82] focuses on the prospective transmission design of RIS-aided vehicle-to-everything communications with the aim to facilitate the evolution of conventional vehicular networks to autonomous driving.

The available literature also investigates the interplay between RIS and artificial AI and/or ML. In particular, the paper [18] emphasizes the fact that radio environment becomes controllable and intelligent by leveraging the emerging technologies of RIS and AI, while the article [45] explores the road to implementing the combination of RIS and AI by integrating AI-enabled technologies into RIS-based frameworks for maximizing the practicality of RIS to facilitate the realization of smart radio propagation environments. The authors in [14] present four typical RIS-aided multi-user scenarios with special emphasis on the MAC schemes and propose and elaborate on centralized, distributed, and hybrid artificial-intelligence-assisted MAC architectures in RIS-aided multi-user communications systems. In [31], the authors develop an over-the-air computation-based communication-efficient federated machine learning framework for intelligent IoT networks, in which RISs are deployed to enhance the signal strength by properly reconfiguring the wireless propagation environments.

However, the existing literature is not limited to the aforementioned application areas and use cases. For example, the authors in [110] investigate the contribution of deploying single or multiple RISs to mitigating signal blocking in case of obstructed tunnels. The paper [111] examines the URLLC-enabled communications in a factory automation scenario, in which severe blockage conditions may exist. The authors propose to deploy intelligent reflecting surface to create an alternative transmission link, which can enhance the transmission reliability and perform a performance in terms of average data rate and the average decoding error probability. The authors in [112] propose the RIS deployment in nearly all possible challenging and extreme communication environments, in order to improve the connectivity by exploiting the additional degrees of freedom associated with RISs. In [30], a comprehensive tutorial on indoor VLC systems utilizing RISs technology is provided; in addition, the authors supply an overview of optical RISs and examine the differences between optical RISs, radio frequency (RF)-RISs, and optical relays. Furthermore, the article [27] emphasizes on RIS applications related to frequencies below

10 GHz instead of focusing on the very high frequencies ranging between tens to hundreds of GHz, which are tightly intertwined with 6G networks. In [113], the authors propose a RIS-assisted multiuser full-duplex cellular network, which aims to cover dead zones and suppress user-side self-interference and co-channel interference through the RIS's phase shift tuning mechanisms. The authors in [114] study a free-space RIS-assisted MISO communication system in far-field operation under the prism of maximizing the received through optimization of transmitter beamforming, RIS phase shifts, and RIS orientation and position.

❖ Cascaded-RIS aided communication systems

Given that the current study concerns a cascaded-RIS system, special mention is made in the relevant existing literature. In specific, the authors in [115] study efficient channel estimation and passive beamforming designs for a double-intelligent reflecting surface aided single-user communication system, where a user communicates with an access point (AP) via the cascaded $user \leftrightarrow RIS\ 1 \leftrightarrow RIS\ 2 \leftrightarrow AP$ double-reflection link, as shown in Figure 18(a). The authors propose two channel estimation schemes and optimize their corresponding cooperative passive beamforming for data transmission in order to maximize the achievable rate. The simulation results shown that the double-RIS implementation approach with the proposed channel estimation and passive beamforming designs can achieve significant rate enhancement as compared to the conventional single-RIS systems. The article [116] refers also to a double-RIS aided wireless communication system, as shown in Figure 18(b), and proposes a joint passive beamforming design for the two smart surfaces. The simulation results also shown that the performance of the proposed implementation is superior to that based on a single RIS. In addition, the authors in [117] develop transmission models with multiple RISs for indoor and outdoor NLoS scenarios and their simulations results indicate that double-RIS reflected transmission can improve the performance of the communication system.

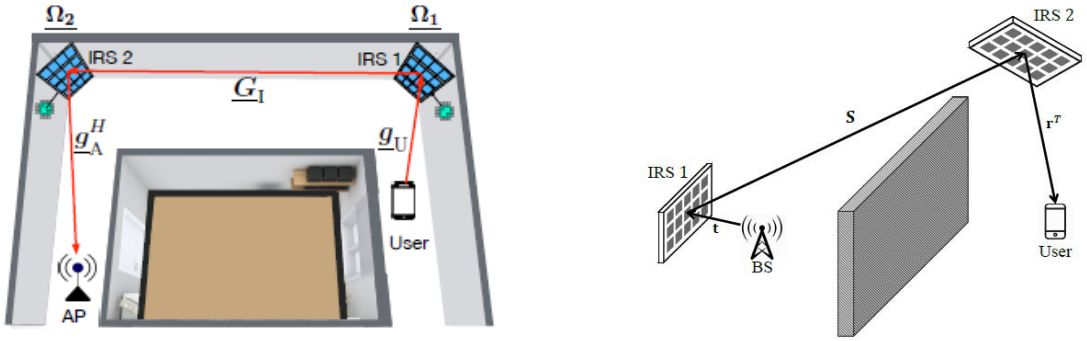

(a) (b)

Figure 18. Double-RIS cooperatively aided communication systems [115] [116].

Moving a step forward, the authors of [118] study a double-RIS assisted multi-user communication system under the co-existence of both double- and single-reflection links, as shown in Figure 19, and jointly optimize the (active) receive beamforming at the base station and the cooperative (passive) reflect beamforming at the two distributed RISs (deployed near the BS and users, respectively) to maximize the minimum SINR of all

users. Both the analytical model and the simulation results capture the superior performance of the double-RIS cooperative system over the conventional single-RIS system in terms of the maximum SNR and multi-user effective channel rank.

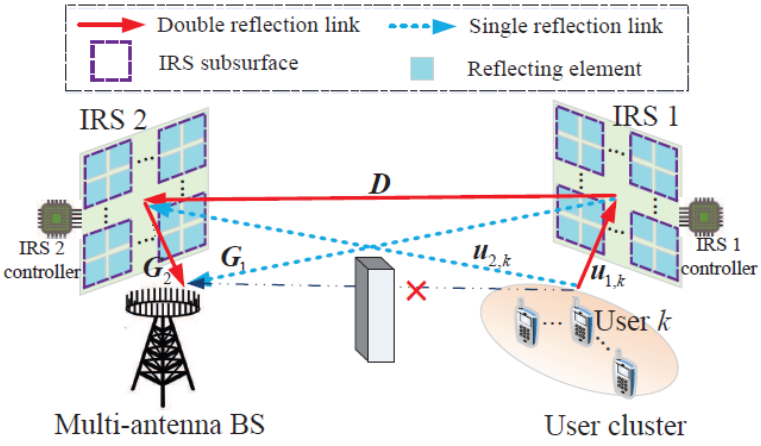

Figure 19. A double-RIS cooperatively assisted multi-user MIMO communication system [118].

The authors in [119] go even further by investigating a RIS-aided communication system, where multiple RISs assist in the communication between a multi-antenna base station and a remote single-antenna user by multi-hop signal reflection, as shown in Figure 20. This results in a multi-hop cascaded LoS link between the BS and user is established so that the received signal power at the user to be maximized. Based on this system configuration, the authors investigate the fundamental trade-off in the optimal beam routing design between maximizing the multiplicative passive beamforming gain and minimizing the multi-reflection path loss. In addition, the paper [120] proposes a multi-hop system to extend the range of THz links with the aid of multiple passive reconfigurable intelligent surfaces and an efficient method to jointly optimize the phases induced by the RISs in order to maximize the power at the receiver side.

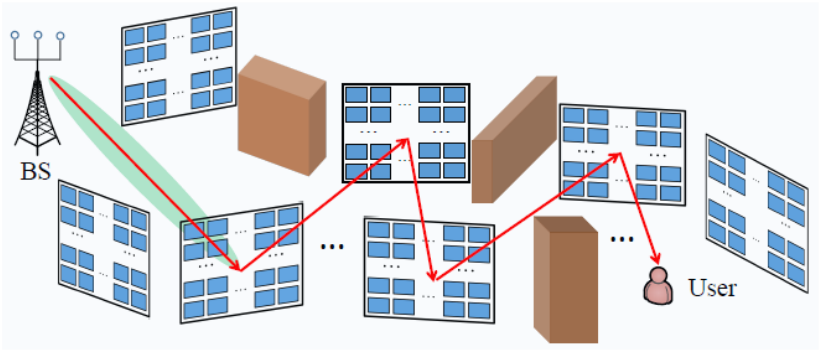

Figure 20. A multi-RIS aided communication system [119].

Furthermore, the authors in [121] and [122][8] investigate the impact of atmospheric phenomena including turbulence and stochastic beam misalignment in multi-RIS empowered free space optics (FSO) and terahertz (THz) wireless systems. The obtained results highlight the importance of accurately modeling both turbulence and misalignment when assessing the system performance when assessing the performance of multi-RIS-empowered FSO/THz wireless systems. Lastly, in [123] the performance of a cascaded RIS network affected by imperfect phase estimation is evaluated in terms of outage probability, the ergodic capacity and the average symbol error probability. The simulation results show that if the number of participating RIS is chosen appropriately, a cascaded RIS network can outperform a single-RIS system even if the phase estimation's accuracy is worse than that of a single-RIS system.

[8] Consider only the terahertz band.

2. ANALYTICAL and NUMERICAL STUDY

2.1 Scope

The project aims to examine the contribution and usefulness of Reconfigurable Intelligent Surfaces (RISs) in wireless communication networks. In particular, the study examines through simulations the efficiency of a cascaded-RIS aided communication system in several Non-Line-of-Sight (NLoS) propagation scenarios of a wireless network, in which the direct link between the Access Point (AP) (or wireless router) and the User Equipment (UE) (e.g. mobile device) is double blocked due to the presence of obstacles, such as walls or large furniture pieces. For that purpose, RIS technology has been deployed in order to effectively redirect the incident beam from the transmitter to the receiver in such a way that the adverse NLoS effects are mitigated or even eliminated. To overcome the link blockage challenges, two RISs of sufficiently large size have been deployed within the wireless propagation environment to establish a multi-hop cascaded LoS link, as will be further analyzed in §2.2.2.1 and 2.2.2.3.

It should be noted that the performance of RIS is examined in terms of the received power at the UE based on simulations results. For this purpose, different implementation approaches were followed in order to examine the overall performance of RIS deployment in the cascaded system of the current simulation study.

In more detail, the performance of the proposed cascaded-RIS aided link in terms of received power at the User Equipment is calculated using either an analytical or a discrete model, as will be analytically discussed in par 2.2.2.4. In addition, the operation of the RISs with regard to their phase shift capabilities is examined; in particular, each RIS has the opportunity either to effectively control the incident beam via appropriate phase transformations in order to flatten the wavefront of the reflected (secondary) beam or to simply reflect the beam without reconstructing the wavefront phase, as will be further described in §2.2.2.4. The aforementioned calculation approaches and RIS phase-related features are applied in all possible combinations in the case study scenarios of §2.2.2.5 in order to draw valuable conclusions about the performance of the cascaded-RIS aided communication system.

In a nutshell, the current study focuses on examining the most critical parameters that can affect the receiver power at the UE and thus, the performance of the cascaded-RIS system. Parameters such as the reflection coefficient of RIS elements, phase-related operation features of the RISs, the transmitter gain, the beam footprint at the RIS plane, the distance between UE and RIS are assumed to be key performance parameters for the cascaded-RIS aided communication system of the current study.

2.2. Design of the study

2.2.1 General

As mentioned earlier, in §1.2, the unique capabilities of RIS to manipulate the impinging electromagnetic signals in the desired way through smart reflections, render RISs a valuable design tool of wireless communication networks, especially in the case of NLoS links.

As also mentioned in §1.2, RISs can be easily attached to existing infrastructure elements (e.g. walls) in order to facilitate communication in several use case scenarios where severe blockage conditions are experienced within the wireless network. This can be a fairly common situation in an indoor environment (e.g. house, apartment), especially in the modern era of IoT, where a unique access point (or a wireless router) should be able to communicate with a plethora of user equipment devices (e.g. computer devices, wireless sensors or even refrigerators, and washing machines) that are either statically scattered (e.g. smart TV) or even moving (e.g. mobile phone) within the network space, although a direct link is not always possible/available. In more detail, the AP may be located in a different room or even on a different floor, or the transmission links towards the desired UEs to be obstructed by various structures (e.g. walls) or objects (e.g. bookcase). As a result, the signal quality at the receiver may be degraded and the link distance may be limited, and thus the Quality of Service and Quality of Experience will be poor.

As mentioned in §1.2, in general, RIS technology can be deployed in conjunction with the existing legacy technologies in a low-cost, energy-efficient, low-complexity (in terms of signal processing) and eco-friendly way in order to support NLoS communications, full-duplex transmission, enhanced spectral efficiency, improved SINR, increased link-distance and advanced functionalities both the near-field and the far-filed operating regime. This may justify the reason why several RIS-aided schemes have been proposed in the recent literature to address NLoS communications and link-distance issues (as analytically described in §1.3). Although the majority of related works is based on single-RIS implementation, cascaded-RIS networks can be deployed in order to handle more peculiar situations. In fact, there may be use cases, such as network environments with severe blockage conditions, where the deployment of a single RIS may not be sufficient to address any connectivity issues and vulnerabilities.

The current study focuses on a cascaded-RIS use case scenario of a wireless network environment with NLoS propagation conditions due to the presence of obstacles (blockage). To tackle this challenge, the deployment of a double-RIS aided system has been proposed to establish a multi-hop cascaded LoS link between the access point and user equipment and thus, restore the connectivity of the NLoS link and facilitate communication or, even, outperform the performance of the equivalent LoS link.

2.2.2 Concept

Several different scenarios (as analyzed in §2.2.2.5) have been implemented in order to theoretically test, through simulations, the efficiency of the cascaded RIS deployment in a hypothetical wireless environment suffering from severe of LoS blockage conditions between the AP and the UE. In specific, two RISs (as discussed in §2.2.2.3) are deployed to restore the hampered communication.

During the simulations performed, various design parameters were taken into account in order to holistically evaluate the impact of the cascaded RIS deployment on the link performance, as will be further analyzed in §2.2.2.4.

All the relevant design elements and parameters and the use case scenarios used for the simulations will be discussed in detail as follows:

2.2.2.1 System Model

The cascaded RIS system model used in the Simulation Section is shown in Figure 21. In particular, an AP is located at the fixed position (x_{AP}, y_{AP}, z_{AP}) at a distance d_{AP} from the origin of the local coordinate system i.e. $(0,0,0)$, along the direction defined by the angles θ_{AP} and φ_{AP}, while the UE is located at the position (x_{UE}, y_{UE}, z_{UE}). For simplifying the computational complexity, it is assumed that both items, AP and UE, are placed at the same plane ($\varphi_{AP} = 0°\ (or\ 360°)$ and $\varphi_{UE} = 180°$), defined as the coordinate plane $y = 0$ (the xz-plane) and thus, $y_{AP} = y_{UE} = 0$.

However, as previously mentioned, it is assumed that the communication between the AP and the UE is obstructed by blockage, such as walls, furniture, etc., and therefore a cascaded-RIS system made of two Reconfigurable Intelligent Surfaces is deployed. In fact, the AP beam impinges on the first RIS, named RIS1, is reflected and propagates to the second RIS, named RIS2, which in turn reflects the incident beam to the UE. It should be highlighted that in all case study scenarios of the current study it is assumed that there are not LoS links between AP-UE and RIS1-UE is always blocked, while the LoS link between RIS2-UE is never blocked. Therefore, the communication between AP-UE is achieved by the multi-hop signal reflections via the cascaded $AP - RIS1 - RIS2 - UE$ double-reflection link.

In addition, it is assumed that RIS1 is centered at the origin of the coordinate system, i.e. $x_{RIS1} = 0$, $y_{RIS1} = 0$ and $z_{RIS1} = 0$. As far as the RIS2, it is placed directly opposite from the RIS1 at a distance d_{RIS} in the position $(x_{RIS2}, y_{RIS2}, z_{RIS2})$, where $x_{RIS2} = x_{RIS1} = 0$, $y_{RIS2} = y_{RIS1} = 0$ and $z_{RIS2} = d_{RIS}$. The distance between the RIS2 and the UE is denoted as d_{UE} along the direction defined by the angles θ_{UE} and φ_{UE}.

Therefore, the exact position of the aforementioned network elements can be summarized as follows:

$$\begin{cases} AP: (x_{AP}, y_{AP}, z_{AP}) = (x_{AP}, 0, z_{AP}) \\ RIS1: (x_{RIS1}, y_{RIS1}, z_{RIS1}) = (0,0,0) \\ RIS2: (x_{RIS2}, y_{RIS2}, z_{RIS2}) = (0,0, d_{RIS}) \\ UE: (x_{UE}, y_{UE}, z_{UE}) = (x_{UE}, 0, z_{UE}) \end{cases}$$

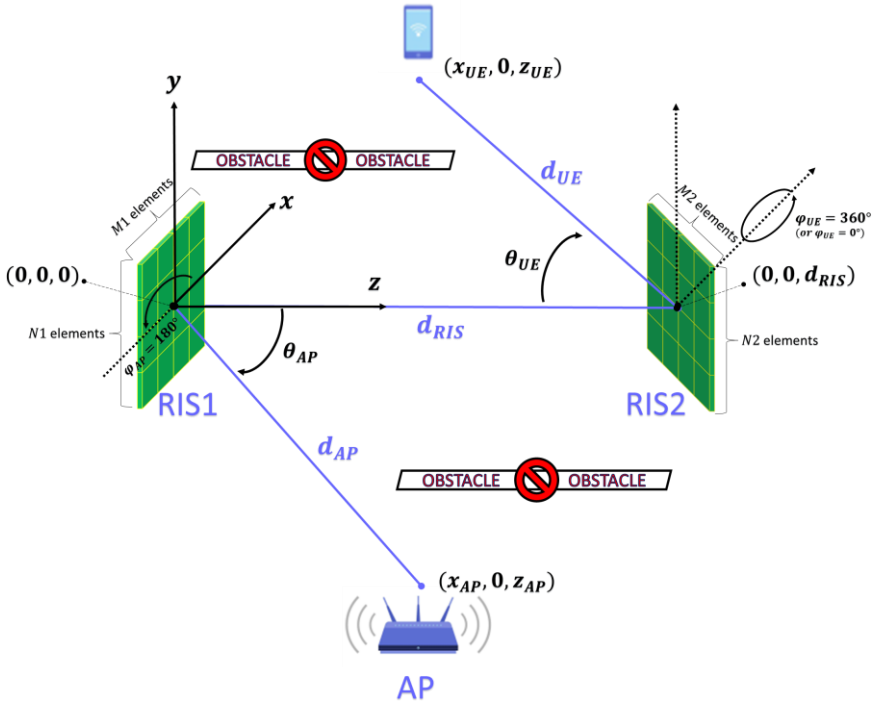

Figure 21. System model: Schematic of cascaded-RIS communication system. RIS1 and RIS2 consist of M1 × N1 and M2 × N2 elements, respectively (here shown 4 × 4 = 16 elements).

Based on the aforementioned positions of the system model elements, the remaining simulation design parameters can be calculated as follows:

$$\begin{cases} \theta_{AP} = \tan^{-1}\left(\frac{x_{AP}}{z_{AP}}\right) \\ d_{AP} = \frac{z_{AP}}{\cos\theta_{AP}} \\ \theta_{UE} = \tan^{-1}\left(\frac{x_{UE}}{d_{RIS} - z_{UE}}\right) \\ d_{UE} = \frac{d_{RIS} - z_{UE}}{\cos\theta_{UE}} \end{cases} \quad (1)$$

2.2.2.2 Access Point (AP) and User Equipment (UE)

This paragraph entails the theoretical and simulation details regarding the AP used for the purposes of current study. In specific:

- AP

The access point, or a wireless networking router, is equipped with a highly directional antenna and transmits a beam of tunable gain G_t (ranging between 30 and $60\,dB$). For the simulation purposes it is assumed that the transmitted power is $P_t = 1W$.

Given that the AP has a highly directional antenna, the main-lobe approximation can be applied for the received power [85]. In addition, it has been considered that the main lobe of the antenna pattern can be approximated by the Gaussian distribution function.

In general, the Gaussian is a radially symmetrical distribution and the corresponding intensity[9] of the beam with total power P is given by the Gaussian Function [124] [125]:

$$I(r,z) = \frac{2P}{\pi w(z)^2} exp\left(-2\frac{r^2}{w(z)^2}\right) \quad (2)$$

where r is the radial distance from the center axis of the beam and $w(z)$ is the beam radius at which the intensity drops to $1/e^2$ (0.135) of the maximum value, at a distance z from the focal plane, also known as beam waist w_0 ($z = 0$), as shown in Figure 22 [124]. It should finally be noted that, the beam width $w(z)$ at any position z along the beam is given by [126]:

$$w(z) = w_0\sqrt{1 + \left(\frac{z}{z_R}\right)^2} \quad (3)$$

where $z_R = \pi\frac{{w_0}^2}{\lambda} \overset{k_0=\frac{2\pi}{\lambda}}{\Longrightarrow} z_R = k_0\frac{{w_0}^2}{2}$ is a parameter known as *Rayleigh range (or length)* (Note: k_0 is the free-space wavenumber) [126].

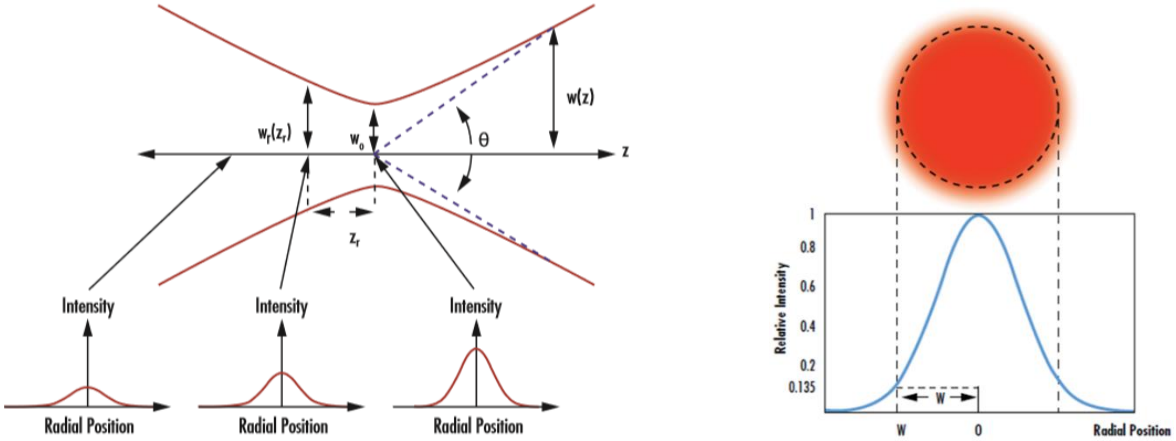

(a) (b)

Figure 22. (a) Gaussian beam radius $w(z)$ at a distance z from the beam waist w_0 [124], and (b) the beam width (diameter) $w(z)$ is defined as the radial position for which the intensity equals to $1/e^2$ (0.135) of its maximum value [124].

- UE

According to the European Telecommunications Standards Institute (ETSI), the User Equipment (UE) refers to the device (terminal) that allows an end-user to access network services [127]. The term can include devices such as mobile phones, computers/laptops/

[9] Also known as irradiance and refers to the power carried by the beam across a unit area perpendicular to the beam or, simply, the transverse energy profile of the beam.

tablets, IoT devices, etc. The UE may also have fixed, radio or, even, both network interfaces.

For the purposes of the current study, it is assumed that the UE is a mobile device (as illustrated in Figure 21) which can wirelessly communicate (via the AP) to the internet. Furthermore, in terms of device operating parameters, $G_r = 20\,dB$ has been considered as the receiver gain of the UE.

2.2.2.3 RISs used

First of all, each, each Reconfigurable intelligent Surface used in the Simulation Section consists of multiple identical unit cells. In specific, RIS1 and RIS2 consists of $M1 \times N1$ and $M2 \times N2$ elements, respectively, that are periodically arranged across the x- and y-axes, as shown in Figure 21. The fact that all unit cells are identical results in a common radiation pattern for all RIS elements.

The size of each element is $dx \times dy$, by assuming $dx = dy = {\lambda}/{5}$ (where $\lambda = 0.002$ is the free space wavelength), while the size of each RIS is considered to be sufficiently large with regard to the Access Point beam footprint. This implies that the transmitter (AP) beam can be completely captured by the RIS and therefore, the percentage of the total power collected by the RIS reaches the 100% and further increase in RIS size does not affect the propagation properties of the redirected (secondary) beam (from RIS1 to RIS2 and/or from RIS2 to UE) [85]. In this case, it is assumed that the communication link resides in an *infinite* RIS regime[10], although the surface is actually of finite size [85]. This assumption of infinitely large RIS deployment simplifies the implementation and reduces the computational complexity.

In order to practically implement the infinite RIS regime and in terms of reproducibility of simulation results, it was selected the size of the RIS to be a multiple of the ratio of beam-footprint radius on the RIS to the size of each RIS element. In particular, the number of elements in *x*- and *y*-axis, denoted as N_x and N_y, respectively, is calculated as follows, based on the simulations done in order to ensure that RIS captures 100% of the incident power:

$$\begin{cases} N_{x,1} = 5 * round\left(\frac{w_{RIS_1}}{dx}\right) \\ N_{y,1} = 5 * round\left(\frac{w_{RIS_1}}{dy}\right) \end{cases} \quad for\ RIS1 \tag{4}$$

and

[10] Finite RIS regime: the AP-beam footprint on the RIS is bigger than the actual RIS size and thus, the footprint redirected (secondary) beam (i.e. the effective aperture of the RIS) is defined by the actual RIS area [85].
Infinite RIS regime: the AP-beam footprint on the RIS is smaller than the actual RIS size and thus, the footprint redirected (secondary) beam (i.e. the effective aperture of the RIS) is determined by the AP beam footprint [85].

$$\begin{cases} N_{x,2} = 5 * round\left(\frac{w_{RIS2}}{dx}\right) \\ N_{y,2} = 5 * round\left(\frac{w_{RIS2}}{dy}\right) \end{cases} for\ RIS2 \quad (5)$$

Given that $dx = dy = {}^{\lambda}/_{5}$, it can be deduced that $N_{x,1} = N_{y,1}$ and $N_{x,2} = N_{y,2}$.

Considering the effective aperture of each RIS element A_{RIS}, i.e. the size of the element $dx \times dy$, the antenna gain of each element G_{RIS} is given by [85] [86]:

$$G_{RIS} = \frac{4\pi}{\lambda^2} A_{RIS} \quad (6)$$

With regard the reflection coefficient of the RIS, it is considered that each (m, n) RIS element has a complex reflection coefficient $R_{m,n}$, which is given by [85]:

$$R_{m,n} = \left|R_{m,n}\right| e^{-j\varphi_{m,n}} \quad (7)$$

where $\left|R_{m,n}\right| = 1$ is the amplitude of the common reflection coefficient of all RIS elements by assuming ideal phase shifters [87] and $\varphi_{m,n}$ is the phase introduced by the RIS in order to redirect the incident beam to the UE (or to the other RIS) in the desired way and is given by [85]:

$$\varphi_{m,n} = \frac{2\pi}{\lambda}[(\sin\theta_{UE}\cos\varphi_{UE} + \sin\theta_{AP}\cos\varphi_{AP})x_m + (\sin\theta_{UE}\sin\varphi_{UE} + \sin\theta_{AP}\sin\varphi_{AP})y_n] \quad (8)$$

where x_m and y_n are the coordinates of the (m, n) RIS element, as:

$$\begin{cases} x_m = m \times dx,\ m \in [1, M] \\ y_n = n \times dy, n \in [1, N] \end{cases} \quad (9)$$

It should be highlighted that for the purposes of the simulation study, $\left|R_{m,n}\right| = 1$ is selected both for RIS1 and RIS2.

2.2.2.4 RIS-assisted power path model

In general, the beam transmitted by the AP follows a cascaded RIS-aided path, firstly through RIS1 and then through RIS2, in order to reach the UE. The simulation model used in the study encompasses the following calculation approaches and RIS phase-related features:

i. the analytical and the discrete performance assessment of the efficiency of the cascaded-RIS aided communication system,
ii. the “phase-removal” and the “full-wave” operation mode of RIS. In more detail, the “phase-removal” operation refers to the tunable capacitance of RIS reflecting elements, which allows the reflection coefficients to be smartly optimized through appropriate phase shifts so that to achieve the wavefront flattening of the reflected beam either from RIS1 to RIS2 or from RIS2 to UE. On the other hand, in the “full-wave” case, no phase shifts are intended to be applied to reconstruct the wavefront

and thus, it will be less implementation demanding as it imposes relatively lower real-time processing requirements.

- Analytical Calculation and "Phase-Removed" approach

As mentioned earlier in §2.2.2.2, the AP beam used for the purposes of the simulation study is Gaussian in form. Hence, the AP footprint on RIS1 also follows the Gaussian distribution with radius w_{RIS1} and power density [given by Eq. (2)] as:

$$S_{RIS1}^{inc} = \frac{2P_t}{\pi w_{RIS1}^2} exp\left(-2\frac{{x_1}^2+{y_1}^2}{w_{RIS1}^2}\right) \quad (10)$$

Based on the approximation approach described in [85], the power density can be alternatively expressed in terms of the known parameters G_t, P_t and d_{AP} as:

$$S_{RIS1}^{inc} = \frac{G_t P_t}{4\pi {d_{AP}}^2} exp\left(-2\frac{{x_1}^2+{y_1}^2}{w_{RIS1}^2}\right) \quad (11)$$

By combining the Eq. (10) and Eq. (11), the radius w_{RIS1} of the AP beam on the RIS1 is obtained as:

$$w_{RIS1} = \sqrt{\frac{8{d_{AP}}^2}{G_t}} \quad (12)$$

Then, the AP beam is reflected by RIS1 and propagates to the second RIS along the direction defined by the angles θ_B and φ_B, as illustrated in the generic representation of Figure 23. However, in this first part of the cascaded RIS-assisted system, which includes the is perpendicular to the xy-plane of the local coordinate system, as the RIS2 is placed directly opposite from the RIS1 at a distance d_{RIS} in the position $(x_{RIS2}, y_{RIS2}, z_{RIS2})$ with $x_{RIS2} = x_{RIS1} = 0$, $y_{RIS2} = y_{RIS1} = 0$ and $z_{RIS2} = d_{RIS}$ (as mentioned in §2.2.2.1). Hence, in this case, the angle $\theta_{B,RIS1} = 0°$, while the propagation is independent of angle $\varphi_{B,IS1}$, i.e. $\varphi_{B,RIS1} \in [0°, 360°]$.

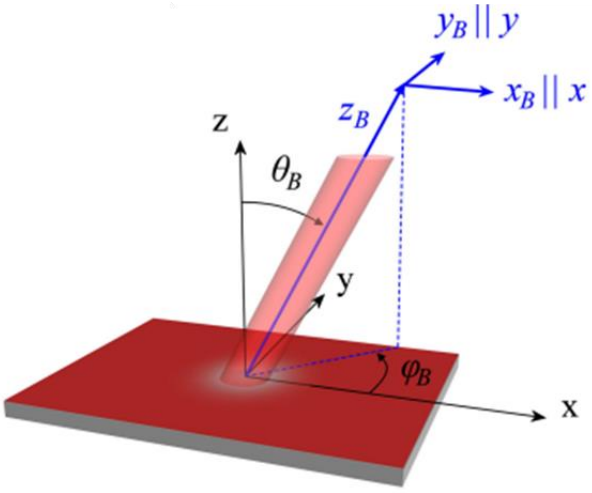

Figure 23. The incident beam propagates as a Gaussian beam along the direction defined by the angles θ_B and φ_B, after being reflected by the RIS [85].

Given the power density S_{RIS1}^{inc} of AP footprint on RIS1 (as indicated by Eq. (10)) and by following the procedure described in [85], the power density S_{RIS1}^{ref} of the secondary beam (from RIS1 to RIS2) exactly at the RIS1 plane, can be expressed as:

$$S_{RIS1}^{ref} = S_{RIS1}^{inc}|R_1|^2 \tag{13}$$

where $R_1 \equiv |R_{m,n}| = 1$, i.e. the amplitude of the common reflection coefficient of all RIS1 elements, as described in Eq. (7).

Given that:

- the intensity/irradiance I of a Gaussian beam (as expressed in Eq. (2) is related to the amplitude E of the electric field as [125]:

$$I = \frac{c_0 \varepsilon_0}{2}|E|^2 \tag{14}$$

  where c_0 is the speed of light constant in the air (or vacuum) and ε_0 is the vacuum permittivity

- the speed of light c_0 can be expressed in terms of the vacuum permittivity ε_0 and the vacuum permeability m_0 as $c_0 = 1/\sqrt{\varepsilon_0 m_0}$, while the characteristic impedance of free space z_0 can be expressed as $z_0 = \sqrt{\varepsilon_0/m_0}$ [128]
- the power density S_{RIS1}^{ref} exactly at the RIS1 plane as determined by the Eq. (13) and the complex reflection coefficient $R_{m,n}$ as described in Eq. (7)

the corresponding electric field exactly at the RIS1 plane (i.e. just before leaving the RIS1) can be calculated as follows:

$$E_{atRIS1} = |R_1|\sqrt{2z_0 S_{RIS1}^{inc}} \tag{15}$$

Next, the electric field produced by this redirected (secondary) beam (from RIS1 to RIS2) can be expressed according to [85] as:

$$E = \frac{\sqrt{2z_0 \frac{2P_t}{\pi w_{RIS1}^2}|R|^2}}{\sqrt{\left(1-i\frac{z_B}{z_R}\right)\left(1-i\frac{z_B}{z_R \cos^2\theta_B}\right)}} exp\left[-\frac{k_0}{2z_R}\left(\frac{x_B^2+y_B^2}{1-i\frac{z_B}{z_R}} - \sin^2\theta_B \frac{(x_B\cos\varphi_B + y_B \sin\varphi_B)^2}{\left(1-i\frac{z_B}{z_R}\right)\left(1+i\frac{z_R\cos^2\theta_B}{z_B}\right)}\right) - ik_0\Phi\right] \tag{16}$$

where:

- Φ is the phase advance of the redirected beam that equals to:

$$\Phi = x_B \sin\theta_B \cos\varphi_B + y_B \sin\theta_B \sin\varphi_B + z_B \tag{17}$$

- $$\begin{cases} x_B = x - z_B \sin\theta_B \cos\varphi_B \\ y_B = y - z_B \sin\theta_B \sin\varphi_B \\ z_B = z/\cos\theta_B \end{cases} \tag{18}$$

Given that $\theta_{B,RIS1} = 0°$ (as mentioned in §2.2.2.4) and Eq. (17), the Eq. (16) can be further simplified as follows:

$$E = \frac{\sqrt{2z_0 \frac{2P_t}{\pi w_{RIS1}^2}|R|^2}}{\left(1-i\frac{z_B}{z_R}\right)} exp\left(-\frac{k_0}{2z_R}\frac{x_B^2+y_B^2}{1-i\frac{z_B}{z_R}}\right) \quad (19)$$

In a cascaded way, the Gaussian beam originating from the RIS1 propagates for a distance d_{RIS} in order to impinge on RIS2 and be further reflected to the UE. The footprint on RIS2 also follows the Gaussian distribution with radius w_{RIS2} and based on Eq. (3) is given by:

$$w_{RIS2} = w_{RIS1}\sqrt{1+\left(\frac{d_{RIS}}{z_{R,new}}\right)^2} \quad (20)$$

with $z_{R,new} = k_0 \frac{w_{RIS2}^2}{2}$ the Rayleigh length of this beam (i.e. from RIS1 to RIS2).

The redirected beam from RIS2 propagates along the direction defined by the angles θ_B and φ_B, as presented in Figure 23, with $\theta_{B,RIS2} = \theta_{UE}$ and $\varphi_{B,RIS2} = 0° \ (or\ 360°)$. In addition, as mentioned in §2.2.2.3, the RIS2 elements share the common reflection coefficient presented in Eq. (7), with $R_2 \equiv |R_{m,n}|$, which is the same as the amplitude R_1 of RIS1 based on the selected design considerations of the current simulation study.

By following a procedure as in [85] and by assuming that RIS2 steers the beam at the exact UE position, i.e. $(x_{UE}, y_{UE}, z_{UE}) = (x_{UE}, 0, z_{UE})$ (as mentioned in §2.2.2.1), the power density at the UE can be expressed as:

$$S_{UE,PR} = \frac{\frac{2P_t}{\pi w_{RIS2}^2}|R_1|^2|R_2|^2}{\sqrt{\left(1+\frac{{d_{UE}}^2}{z_{R,new}^2}\right)\left(1+\frac{{d_{UE}}^2}{z_{R,new}^2 \cos^4\theta_{UE}}\right)}} \quad (21)$$

Then, the received power at the UE (in dBm), $P_{r,PR}$, can be calculated by using the power density of Eq. (21) and the effective aperture A_{UE} via the expression:

$$P_{r,PR} = 10\log_{10}(S_{UE,PR}A_{UE}) + 30\ (dBm) \quad (22)$$

where $A_{UE} = \frac{\lambda^2}{4\pi}10^{\frac{G_r}{10}}$ [129] with $G_r = 20\ dB$, as mentioned in §2.2.2.2.

- Analytical Calculation and “Full-wave” Approach

As mentioned earlier, the “full-wave” approach refers to the operation mode of the RIS with regard to the phase tuning mechanism that enables the customization of propagation through the proper manipulation of EM waves. In contrast to the “phase-removal” approach, described above, the RIS does not apply phase shifts to reconstruct the beam wavefront. In other words, in this case the RIS simply redirects the incident signal without

the reflected beam exhibiting a plane wavefront, as occurs in the “phase-removal” RIS mode.

It should be noted that this approach offers a simpler way of RIS operation without excessive processing requirements, since the RIS can literally act as a reflector with the particularity that it is no longer subject to conventional Snell’s laws, but can actually redirect the incident beam at an angle different from the angle of incidence, i.e. it goes beyond Snell’s law. It is consequently clear that a possible trade-off exists between the simplicity of implementation/operation and the optimization of RIS performance in terms of customization capability.

In this case, and by following a procedure corresponding to the one described in the “Phase-Removal” approach, the analytical expression of the received power at the UE (in dBm), $P_{r,FW}$, can be calculated as follows:

$$P_{r,FW} = 10\log_{10}(S_{UE,FW}A_{UE}) + 30\ (dBm) \tag{23}$$

where $S_{UE,FW}$ is the relative power density given by:

$$S_{UE,FW} = \frac{\frac{2P_t}{\pi w_{RIS1}^2}|R_1|^2|R_2|^2}{\sqrt{\left(1+\left(\frac{d_{RIS}-d_{UE}}{z_R}\right)^2\right)\left(1+\frac{{d_{UE}}^2}{{z_R}^2\cos^4\theta_{UE}}+\frac{{d_{RIS}}^2}{{z_R}^2}+\frac{2d_{RIS}d_{UE}}{{z_R}^2\cos^2\theta_{UE}}\right)}} \tag{24}$$

- Discrete Approach

In addition to the analytical calculation of the received power at the UE, as discussed above and expressed through the Equations (22) and (23) for the “Phase-Removal” and “Full-Wave” approaches, respectively, a discrete model is also used to numerically calculate the aforementioned performance parameter, i.e. the received power. The discrete model is used to verify the theoretical results of the analytical calculation approach.

For this purpose and based on the approach used in [85], the total electric field at the UE (or at RIS2) is the sum of the electric field of each individual RIS element. In fact, the total electric field can be given by [85] [88]:

$$E_r = \sum_{m=1}^{M}\sum_{n-1}^{N} E_{m,n} \tag{25}$$

where $E_{m,n}$ is the electrical field of the received signal from the (m,n) RIS element. In more detail and taking as an example the first part[11] of the cascaded system (i.e. the “sub-system” AP-RIS1-RIS2), the contribution of the (m,n) unit cell, based on the procedure followed in [85], can be expressed as [85] [88]:

[11] The approach for the second part of the cascaded system (i.e. RIS1-RIS2-UE) is similar.

$$E_{m,n} = \frac{|R_{m,n}|\sqrt{2z_0(dx \times dy)P_t G_t G_{RIS1} A_{RIS1} U^t U^{RIS1,t} U^{RIS1,RIS2} U^{RIS2}}}{4\pi l^t_{m,n} l^{RIS2}_{m,n}} \times exp(-j\varphi_{m,n}) exp\left(-j\frac{2\pi}{\lambda}(l^t_{m,n} + l^{RIS2}_{m,n})\right) \quad (26)$$

where:

- $R_{m,n}$ is the complex reflection coefficient of the (m,n) RIS1 element (as mentioned in §2.2.2.3),
- $(dx \times dy)$ is the effective aperture (i.e. the size) of the (m,n) RIS1 element (as mentioned in §2.2.2.3),
- G_{RIS} is the antenna gain of the (m,n) RIS1 element (as mentioned in §2.2.2.3),
- P_t is the transmitted power from the AP (as mentioned in §2.2.2.2),
- G_t is the transmitter Gain (as mentioned in §2.2.2.2),
- U^t, U^{RIS1}[12] and U^{RIS2}[13] are the radiation patterns of the AP, RIS1 and RIS2, respectively,
- $U^{RIS1,t}$ and $U^{RIS1,RIS2}$ is the value of U^{RIS1} along the direction defined by the (m,n) element and the AP and RIS2 respectively,
- $l^t_{m,n}$ and $l^{RIS2}_{m,n}$ are the distances between the (m,n) RIS1 element and the AP and RIS2, respectively.

2.2.2.5 Use cases

After describing the general configuration setup of the system model used for the simulation purposes as in §2.2.2.1, details of the deployed AP, RISs and UE as in §2.2.2.2 and 2.2.2.3, and the calculation approach and the phase-related features of the RISs (i.e. "phase-removal" and "full-wave") as in §2.2.2.4, this section contains information associated with the exact location of the aforementioned system model elements (i.e. AP, RISs and UE) and parameters such as the transmitter gain G_t and/or the distance d_{UE} between the RIS2 and the UE or the angle θ_{UE}.

For that purpose, five case studies scenarios were examined as follows:

- Scenario No1

The first case study is illustrated in Figure 24. In more detail, the AP, RIS1 and RIS2 have a fixed position, while the UE has a constant distance from RIS2 $d_{UE} = 5m$ but variable direction, defined by the angle θ_{UE} and ranging among $25°$, $50°$ and $75°$; in other words, this scenario examines the RIS-aided link of the cascaded system in case the UE is located at different fixed-distance positions from RIS2, which do not allow a LoS link of UE with RIS1 and AP due to blockage caused by obstacles.

[12] Given that the RIS elements are identical, they share a common radiation pattern given by:
$U(\theta,\varphi) = \begin{cases} \cos\theta, \theta \in \left[0,\frac{\pi}{2}\right] and\ \varphi \in [0,2\pi] \\ 0,\ otherwise \end{cases}$ [85] [88]

[13] Ibid.

It should be highlighted that all the design elements are in the same *xz*-plane (as mentioned in §2.2.2.1) and thus, it can be deduced that $\varphi_{UE} = 0°\ (or\ 360°)$ and $\varphi_{AP} = 180°$. Furthermore, the RIS1 is centered at the origin of the local coordinate system, i.e. $(x_{RIS1}, y_{RIS1}, z_{RIS1}) = (0,0,0)$, the AP is located at the position $(x_{AP}, y_{AP}, z_{AP}) = (-2,0,2.5)$, the distance between RIS1 and RIS2 is $5m$ and thus, $(x_{RIS2}, y_{RIS2}, z_{RIS2}) = (0,0,5)$. In addition, based on the trigonometric expressions of Eq. (1) the remaining simulation parameters, i.e. the distances x_{UE} and z_{UE} and the angle θ_{AP}, can be calculated. Lastly, the AP gain G_t ranges between 30 and $60\ dB$, while the UE gain G_r is constant at $20\ dB$.

Apart from the above, it should be noted that both RIS1 and RIS2 are of variable size, as defined by the Eq. (4) and (5) respectively, in order to fully capture the entire incident beam and thus, 100% of the incident power, or equivalently, the cascaded-RIS system resides in the infinite RIS regime. In particular and based on Equations (4) and (5) the size of each RIS per AP gain G_t is tabulated below:

Table 3. Number of elements in *x*- and *y*-axis ($N_{x,1}$ and $N_{y,1}$ for RIS1, and $N_{x,2}$ and $N_{y,2}$ for RIS2) for every AP gain G_t ranging between 30 and $60\ dB$.

	RIS1	RIS2		RIS1	RIS2
	$N_{x,1} = N_{y,1}$	$N_{x,2} = N_{y,2}$		$N_{x,1} = N_{y,1}$	$N_{x,2} = N_{y,2}$
$G_t = 30$	3580	3585	$G_t = 46$	570	1045
$G_t = 31$	3195	3195	$G_t = 47$	510	1110
$G_t = 32$	2845	2850	$G_t = 48$	455	1195
$G_t = 33$	2535	2545	$G_t = 49$	405	1305
$G_t = 34$	2260	2270	$G_t = 50$	360	1435
$G_t = 35$	2015	2030	$G_t = 51$	320	1595
$G_t = 36$	1795	1820	$G_t = 52$	285	1775
$G_t = 37$	1600	1630	$G_t = 53$	255	1980
$G_t = 38$	1430	1470	$G_t = 54$	230	2215
$G_t = 39$	1275	1330	$G_t = 55$	205	2480
$G_t = 40$	1135	1215	$G_t = 56$	180	2780
$G_t = 41$	1010	1125	$G_t = 57$	160	3115
$G_t = 42$	900	1060	$G_t = 58$	145	3495
$G_t = 43$	805	1015	$G_t = 59$	130	3920
$G_t = 44$	715	1000	$G_t = 60$	115	4400
$G_t = 45$	640	1010			

Through this configuration setup, the overall performance of the cascaded-RIS aided communication system is evaluated as a function of the AP gain G_t and the steering angle θ_{UE} between the RIS2 and the UE. All the possible combinations between the calculation approaches (analytical and discrete) and the RIS phase-related features ("phase-removal" and "full-wave") are used in order to assess the efficiency of the RIS-aided link. This case study scenario can be applied in the real world in an indoor wireless network environment, for example in a house/apartment or in a public place like a library, where similarities can

easily be found in the distances between the involved network elements (i.e. AP, RISs, UE) and in the presence of obstacles.

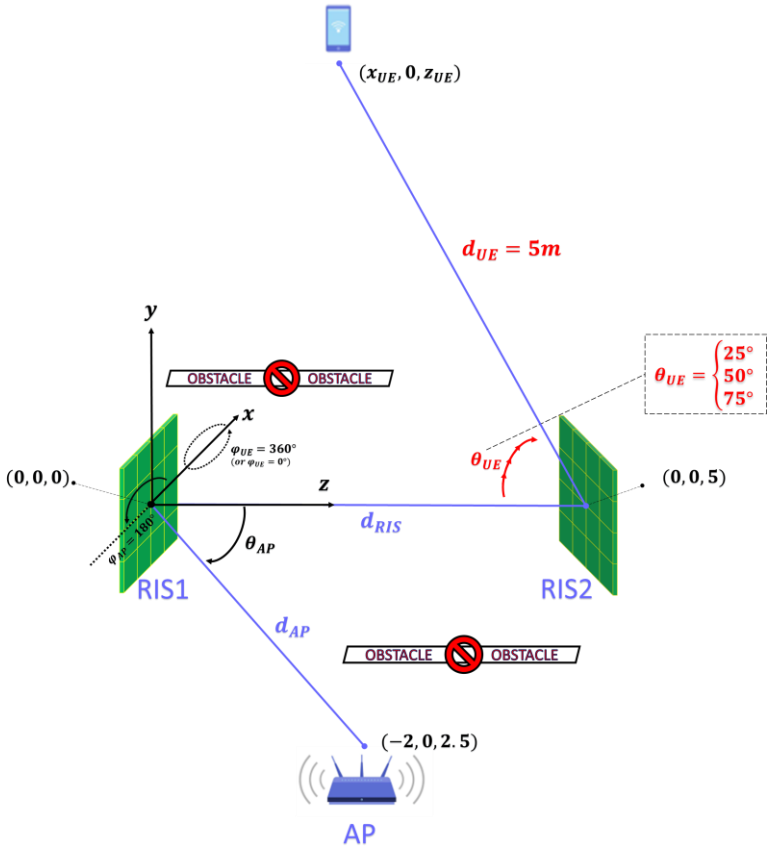

Figure 24. Case study 1: AP, RIS1 and RIS2 have a fixed position, while the UE is at a distance $d_{UE} = 5m$ along the direction $\theta_{UE} \in \{25°, 50°, 75°\}$ from RIS2.

- Scenario No2

The second case study is depicted in Figure 25. In more detail, the AP, RIS1 and RIS2 have a fixed position, while the UE moves in space in a variable distance and direction from the RIS2 ranging between 0 to 5m and among $25°$, $50°$ and $75°$, respectively. It should be highlighted that is assumed that the UE always moves behind an obstacle that blocks the LoS link of UE with RIS1 and AP.

In addition, as in the Scenario No1, all the network elements are in the same *xz*-plane and thus, it can be concluded that $\varphi_{UE} = 0° \ (or\ 360°)$ and $\varphi_{AP} = 180°$, while the RIS1, RIS2 and AP are located at the positions $(x_{RIS1}, y_{RIS1}, z_{RIS1}) = (0,0,0)$, $(x_{RIS2}, y_{RIS2}, z_{RIS2}) = (0,0,5)$ and $(x_{AP}, y_{AP}, z_{AP}) = (-2,0,2.5)$, respectively. Moreover, based on the trigonometric expressions of Eq. (1) the remaining simulation parameters, i.e. the distances x_{UE} and z_{UE} and the angle θ_{AP}, can be calculated.

Furthermore, RIS1 and RIS2 are assumed to be of variable size, as defined by the Eq. (4) and (5) respectively, in order to fully capture the entire incident beam and thus, 100% of the incident power, or equivalently, the cascaded-RIS system resides in the infinite RIS

regime. In particular, the number of elements in *x*- and *y*-axis for RIS1 and RIS2 are $N_{x,1} = N_{y,1} = 2015$ and $N_{x,2} = N_{y,2} = 2030$, respectively, based on Equations (4) and (5).

However, in this use case, the AP gain G_t is considered to have a constant value of $35\ dB$, while the UE gain G_r remains at $20\ dB$. Therefore, this case study scenario examines the RIS-aided link of the cascaded system in a *low-gain* simulation approach in case the UE moves "around" the UE (as depicted in Figure 25) at a maximum distance of $5m$. Such a use case scenario can be applied in the real world in an indoor wireless network environment, for example in a house/apartment or in a public place like a library, where similarities can easily be found in the distances between the involved network elements (i.e. AP, RISs, UE) and in the presence of obstacles.

Through this configuration setup, the overall performance of the cascaded-RIS aided communication system is evaluated as a function of the distance d_{UE} and the steering angle θ_{UE}. In addition, as in Scenario No1, all the possible combinations between the calculation approaches (analytical and discrete) and the RIS phase-related features ("phase-removal" and "full-wave") are used in order to assess the efficiency of the RIS-aided link.

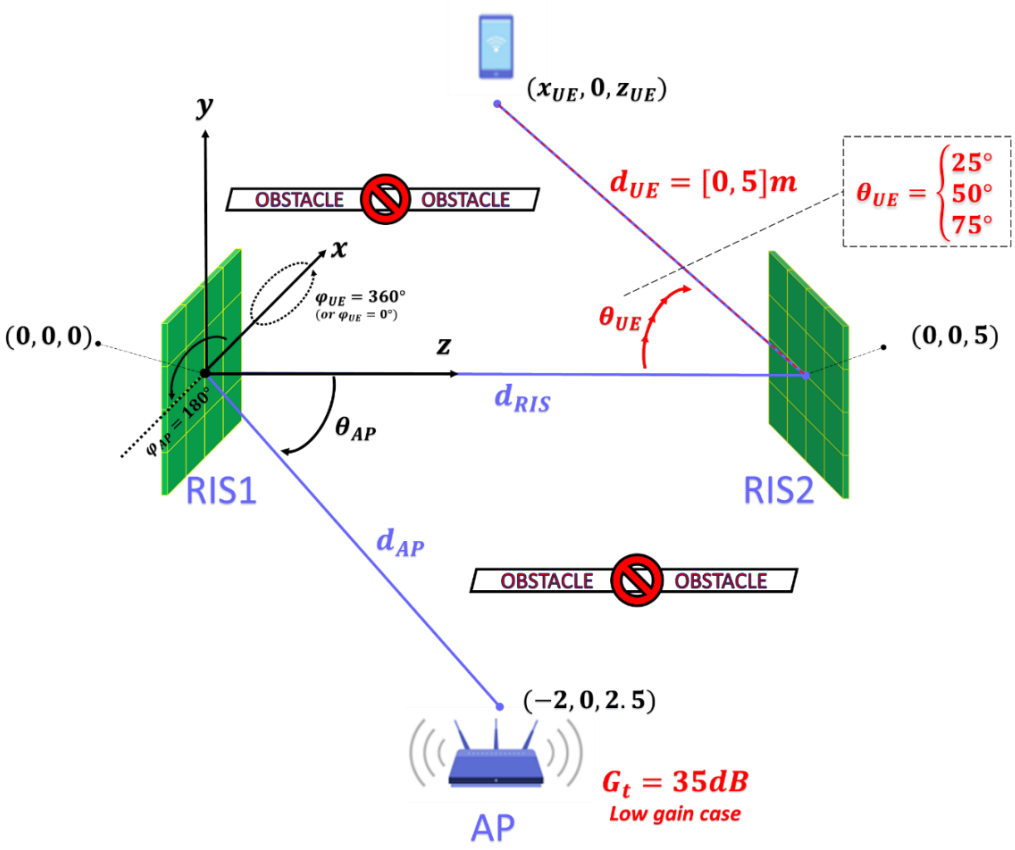

Figure 25. Case study 2: AP, RIS1 and RIS2 moves in space in a variable distance and direction from the RIS2 ranging between 0 to $5m$ and among $25°$, $50°$ and $75°$, respectively. The AP gain has a fixed value of $35dB$ (*low-gain* case).

- Scenario No3

The third case study, as shown in Figure 26, differs from the second simulation scenario only in terms of the transmitter gain used; in fact, this use case examines the performance of the cascaded-RIS aided communication system in a *high-gain* approach, in which the AP gain has a fixed value of $50\ dB$.

Hence, the design parameters can be summarized as follows:

$$\begin{cases} (x_{RIS1}, y_{RIS1}, z_{RIS1}) = (0,0,0) \\ (x_{RIS2}, y_{RIS2}, z_{RIS2}) = (0,0,5) \\ (x_{AP}, y_{AP}, z_{AP}) = (-2,0,2.5) \\ \varphi_{UE} = 0° \ (or\ 360°) \\ \varphi_{AP} = 180° \\ d_{UE} \in [0,5] \\ \theta_{UE} \in \{25°, 50°, 75°\} \\ d_{AP}, \theta_{AP}\ and\ (x_{UE}, y_{UE}, z_{UE}) \text{ are calculated by the trigonometric expressions of Eq. (1)} \\ N_{x,1} = N_{y,1} = 360 \text{ and } N_{x,2} = N_{y,2} = 1435 \text{ based on Eq. (4) and (5)} \\ G_r = 20dB \\ G_t = 50dB\ (\mathbf{high-gain\ case}) \end{cases}$$

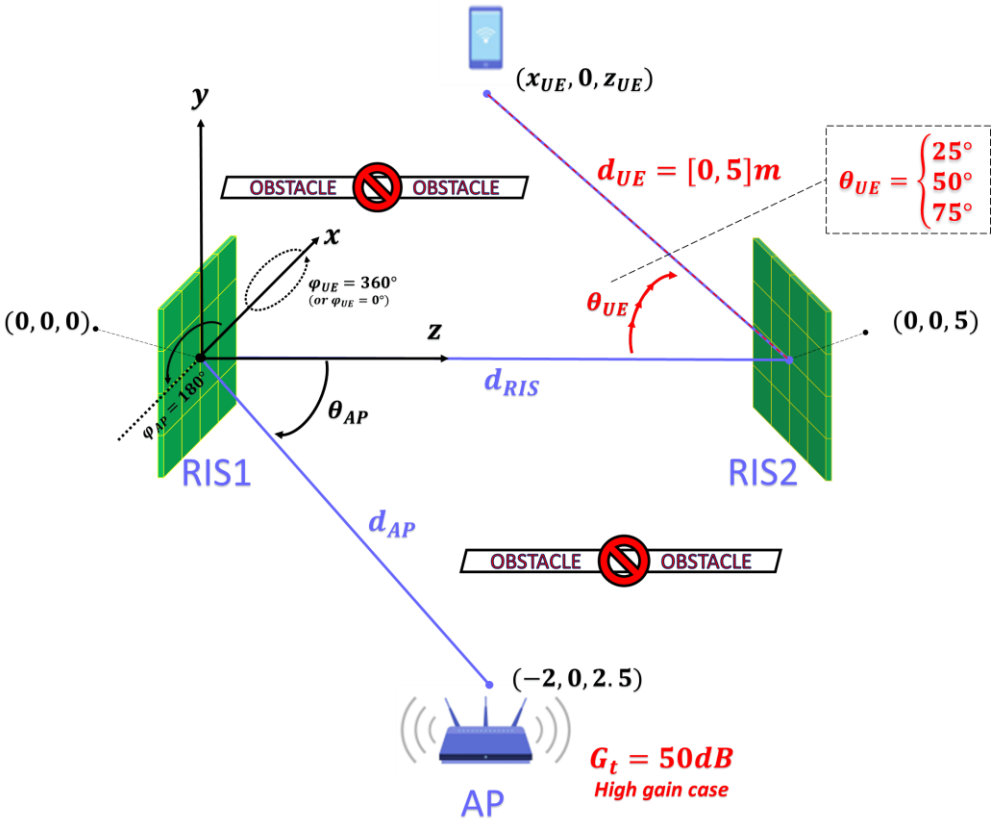

Figure 26. Case study 3: AP, RIS1 and RIS2 moves in space in a variable distance and direction from the RIS2 ranging between 0 to $5m$ and among 25°, 50° and 75°, respectively. The AP gain has a fixed value of $50dB$ (*high-gain* case).

- Scenario No4

The fourth case study is depicted in Figure 27. As in the previous use cases, the AP, RIS1 and RIS2 have a fixed position. However, in this scenario, the UE moves along the *z*-axis at three different distances across the *x*-axis, and more specifically:

$$\begin{cases} z_{UE} \in [0,5]m \\ x_{UE} \in \{5,10,15\}m \end{cases}$$

It should be highlighted that is assumed that the UE always moves behind an obstacle that blocks the LoS link of UE with RIS1 and AP.

Once again, it is assumed that all the network elements are in the same *xz*-plane and thus, it can be deduced that $\varphi_{UE} = 0°\ (or\ 360°)$ and $\varphi_{AP} = 180°$, while the RIS1, RIS2 and AP are located at the positions $(x_{RIS1}, y_{RIS1}, z_{RIS1}) = (0,0,0)$, $(x_{RIS2}, y_{RIS2}, z_{RIS2}) = (0,0,5)$ and $(x_{AP}, y_{AP}, z_{AP}) = (-2,0,2.5)$, respectively. Furthermore, the RISs are considered to be sufficiently large in order to capture 100% of the incident power; in particular, the number of elements in *x*- and *y*-axis for RIS1 and RIS2 are $N_{x,1} = N_{y,1} = 2015$ and $N_{x,2} = N_{y,2} = 2030$, respectively, based on Equations (4) and (5).

In addition, this simulation scenario corresponds to a ***low-gain*** approach in terms of AP gain, which is equal to $G_t = 35dB$ (UE gain: $G_r = 20dB$). Under this perspective, the efficiency of the cascaded-RIS aided communication system is investigated. Such a use case scenario can be applied in the real world in an indoor or outdoor wireless network environment where similarities can easily be found in the distances between the involved network elements (i.e. AP, RISs, UE) and in the presence of obstacles. For example, in case of an indoor environment, relatively long distances, similar to the x_{UE}, may apply to places such as libraries, supermarkets, office or hotel corridors, where severe blockage conditions may exist and the LoS link is almost certainly blocked by various obstacles.

Through this configuration setup, the overall performance of the cascaded-RIS system is evaluated as a function of the distances x_{UE} and z_{UE} based on AP low-gain simulation approach. Once again, all the possible combinations between the calculation methods (analytical and discrete) and the RIS phase-related features (“phase-removal” and “full-wave”) are used in order to assess the efficiency of the RIS-aided link.

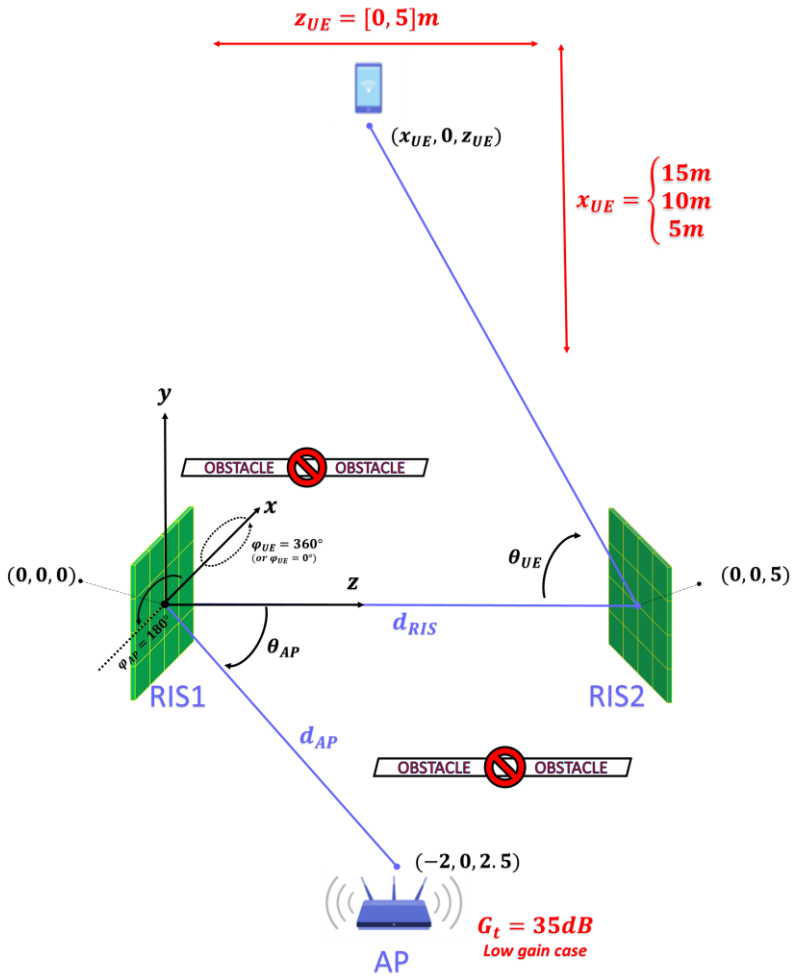

Figure 27. Case study 4: AP, RIS1 and RIS2 have a fixed position, while the UE moves along the *x*- and *z*-axis as follows: $x_{UE} = \{5,10,15\}m$ and $z_{UE} = [0,5]m$. The AP gain has a fixed value of $35dB$ (*low-gain* case).

- Scenario No5

The fifth case study, as shown in Figure 28, differs from the fourth simulation scenario only in terms of the transmitter gain used; in fact, this use case examines the performance of the cascaded-RIS aided communication system in a *high-gain* approach, in which the AP gain has a fixed value of $50\ dB$.

Hence, the design parameters can be summarized as follows:

$$\begin{cases} (x_{RIS1}, y_{RIS1}, z_{RIS1}) = (0,0,0) \\ (x_{RIS2}, y_{RIS2}, z_{RIS2}) = (0,0,5) \\ (x_{AP}, y_{AP}, z_{AP}) = (-2,0,2.5) \\ \varphi_{UE} = 0° \ (or\ 360°) \\ \varphi_{AP} = 180° \\ x_{UE} \in \{5,10,15\} \\ z_{UE} \in [0,5] \\ d_{AP}, \theta_{AP}, d_{UE}\ and\ \theta_{UE} \text{ are calculated by the trigonometric expressions of Eq. (1)} \\ N_{x,1} = N_{y,1} = 360 \text{ and } N_{x,2} = N_{y,2} = 1435 \text{ based on Eq. (4) and (5)} \\ G_r = 20dB \\ G_t = 50dB \ (\mathbf{high - gain\ case}) \end{cases}$$

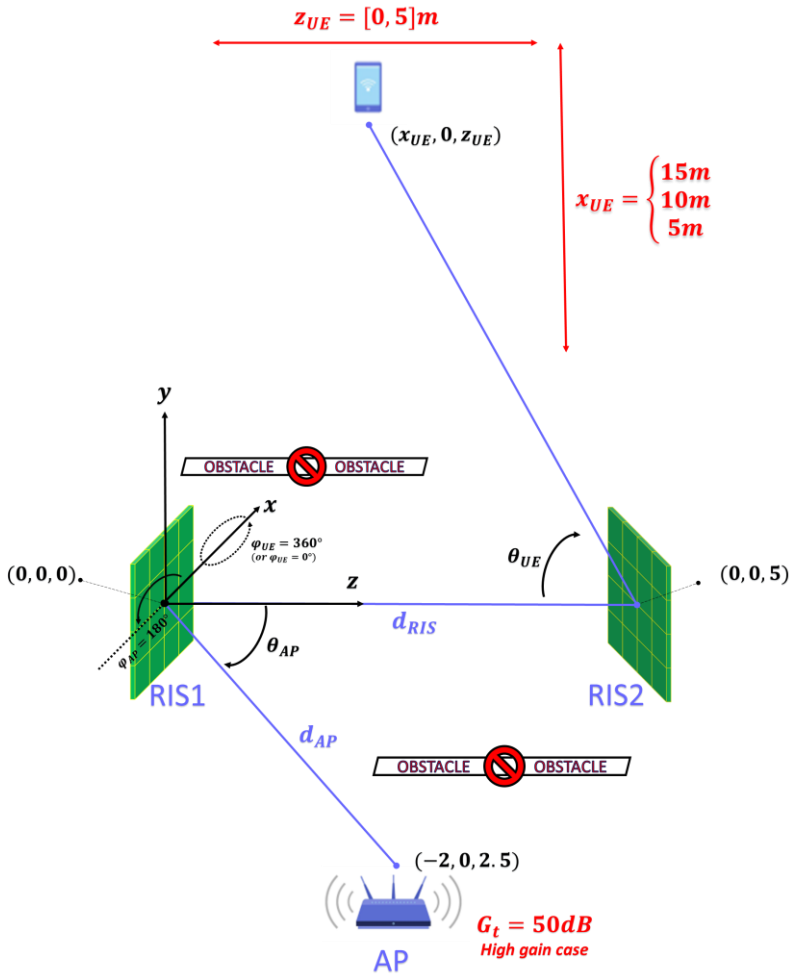

Figure 28. Case study 5: AP, RIS1 and RIS2 have a fixed position, while the UE moves along the *x*- and *z*-axis as follows: $x_{UE} = \{5,10,15\}m$ and $z_{UE} = [0,5]m$. The AP gain has a fixed value of $50dB$ (*high-gain* case).

3. RESULTS

This paragraph presents the simulation results of the case study scenarios described in §2.2.2.5. These results were obtained by using the programming and numeric computing platform MATLAB, version R2022a.

In more detail, a MATLAB code was created to introduce the simulation design parameters described in §2.2.2.1 to 2.2.2.3 and 2.2.2.5, such as the position of the network elements (i.e. the AP, RIS1, RIS2, and UE) and the RISs' reflection coefficient, and then, to implement the equations described in §2.2.2.4 in order to calculate (both analytically and numerically (i.e. discrete model)) the received power at the UE. The obtained results are graphically displayed in order to represent the selected performance indicator (i.e. the received power at the UE) as a function of the different model parameters corresponding to the use cases of §2.2.2.5.

In specific:

- Scenario No1

In this use case of the cascaded-RIS aided communication system, the power received by the UE is evaluated as a function of the tunable transmitter gain, G_t, which ranges between 30 and $60\ dB$ for different locations of the UE that are at a fixed distance from the RIS2. In specific, the UE is at a distance $d_{UE} = 5m$ along the direction defined by the angle $\theta_{UE} \in \{25°, 50°, 75°\}$.

In more detail, Figure 29 illustrates the received power $P_{r,PR}$ at the UE versus the AP gain for three different angles θ_{UE} and is calculated using both the analytical and the discrete model for the case that RIS is capable of flattening the wavefront of the incident beam by using the "phase-removal" operation approach.

It should be noted that the numerical calculation using the discrete model (solid line) verifies the theoretically expected results obtained from the analytical model (symbol 'o'). In specific, it can be observed that with increasing AP gain, the received power at the UE reaches a maximum at a transmitter gain of about $45\ dB$ and then, drops and moves to lower power levels. However, it can be concluded that there is an optimal AP gain (here: $G_t \approx 45\ dB$), independent from the steering angle θ_{UE}, in which the maximum power can be received by the UE.

In addition, as the angle of direction θ_{UE} increases, the power received by the UE decreases for the mid-range values of AP gain. However, when the angle θ_{UE} approaches 90 degrees (i.e. $\theta_{UE} = 75°$) then, the received power at the UE decreases significantly for almost the entire range of AP gain. Nevertheless, in this particular case, there is a range of AP gain (between 35 and $54\ dB$) in which the received power remains almost constant at the highest possible power level (corresponding to this angle).

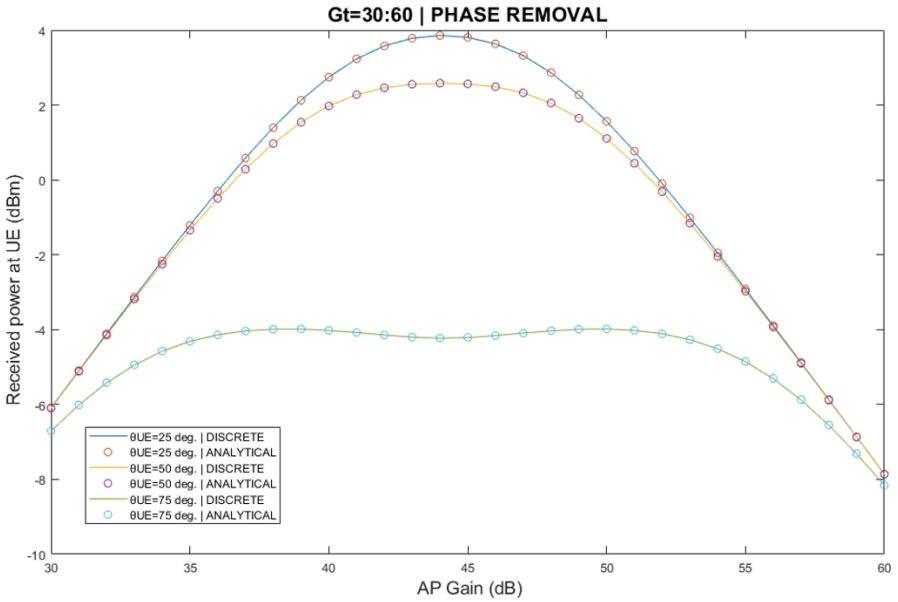

Figure 29. Received Power $P_{r,PR}$ vs AP Gain G_t with variable angle of direction θ_{UE} for a cascaded-RIS system residing in the infinite RIS regime operating in a "Phase-Removal" mode.

Relevant conclusions can be drawn from the simulation based on the "Full-Wave" RIS operation, in which they beam is simply redirected without reconstructing the wavefront. As shown in Figure 30, the discrete calculation approach (dashed line), once again, verifies the theoretically expected performance (symbol '$*$'), while it is also evident that higher power levels can be achieved with a lower steering angle θ_{UE}. Moreover, it can be seen that as the angle of direction θ_{UE} increases, the received power at the UE decreases for almost the entire range of AP gain, while this decrease is even greater in the case where the angle θ_{UE} has its maximum value, i.e. $\theta_{UE} = 75°$.

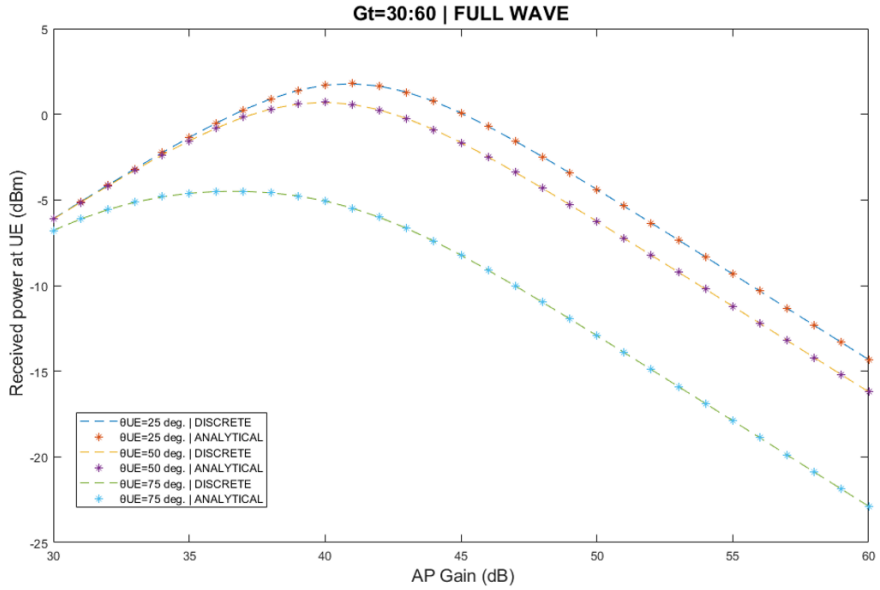

Figure 30. Received Power $P_{r,FW}$ vs AP Gain G_t with variable angle of direction θ_{UE} for a cascaded-RIS system residing in the infinite RIS regime operating in a "Full-Wave" mode.

Lastly, Figure 31 provides a combined view of the "Phase-Removal" and "Full-wave" modus operandi of the cascaded-RIS system. Using this representation, it can be deduced that the "Phase-Removal" feature can ensure better increased received power at the UE for the entire range of AP gain, especially for higher angles of direction θ_{UE}.

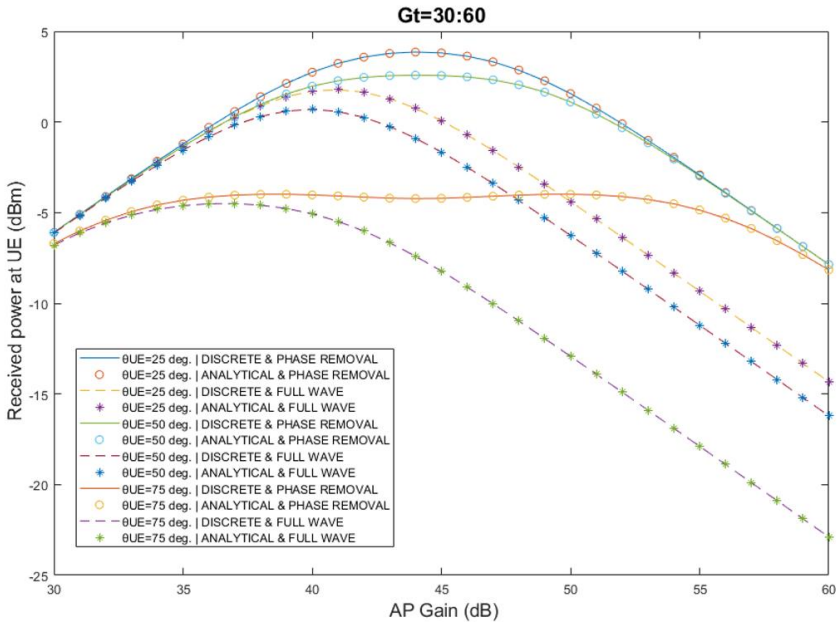

Figure 31. Combined representation of Received Power $P_{r,PR}$ and $P_{r,FW}$ vs AP Gain G_t with variable angle of direction θ_{UE} for a cascaded-RIS system residing in the infinite RIS regime operating in a "Phase-Removal" and "Full-Wave" mode, respectively.

- Scenario No2

In this use case of the cascaded-RIS aided communication system, the power received by the UE is evaluated as a function of the distance d_{UE} and the steering angle θ_{UE}, where $d_{UE} \in [0,5]m$ and $\theta_{UE} \in \{25°, 50°, 75°\}$. The AP gain G_t is considered to have a constant value of $35\ dB$, so we refer to this simulation as a *low-gain* case.

More specifically, Figure 32 presents the received power $P_{r,PR}$ at the UE versus the distance d_{UE} for three different angles θ_{UE} and is calculated both analytically and numerically for the case that RIS is capable of flattening the wavefront of the incident beam by using the "phase-removal" operation mode.

It should be noted that the numerical calculation using the discrete model (solid line) verifies the theoretically expected results obtained from the analytical model (symbol 'o'). In specific, it can be seen that for a relatively small angle of direction, i.e. $\theta_{UE} = 25°\ or\ 50°$, the received power at the UE is almost constant. Thus, it can be concluded that in this *low-angle*[14] case for the specific *short-range low-gain*[15] simulation scenario, the abovementioned network performance parameter can be considered independent of the

[14] $\theta_{UE} = 25°\ or\ 50°$
[15] $d_{UE} \in [0,5]m$ and $G_t = 35dB$

distance d_{UE} and therefore, the cascaded RIS system can ensure stable power levels at the UE.

However, when the steering angle θ_{UE} approaches 90 degrees (i.e. $\theta_{UE} = 75°$), then, the received power at the UE decreases significantly as the distance d_{UE} increases.

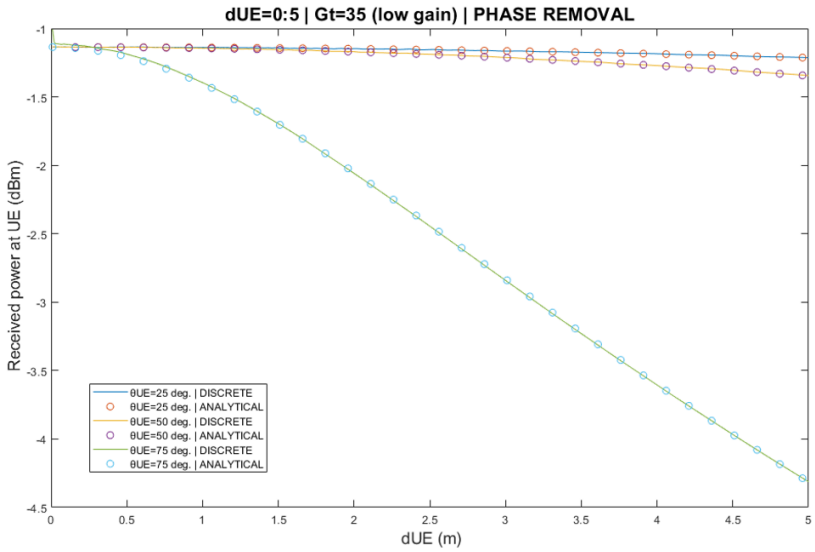

Figure 32. Received Power $P_{r,PR}$ vs distance d_{UE} with variable angle of direction θ_{UE} for a cascaded-RIS system residing in the infinite RIS regime operating in a "Phase-Removal" mode in a low-gain simulation scenario ($G_t = 35dB$).

Similar conclusions can be derived from the simulation based on the "Full-Wave" RIS operation. As shown in Figure 33, the discrete calculation approach (dashed line), once again, verifies the theoretically expected performance (symbol '$*$'), while it is obvious that the received power is almost constant over the entire range the distance d_{UE} except for the case of high angle θ_{UE} (i.e. 75°).

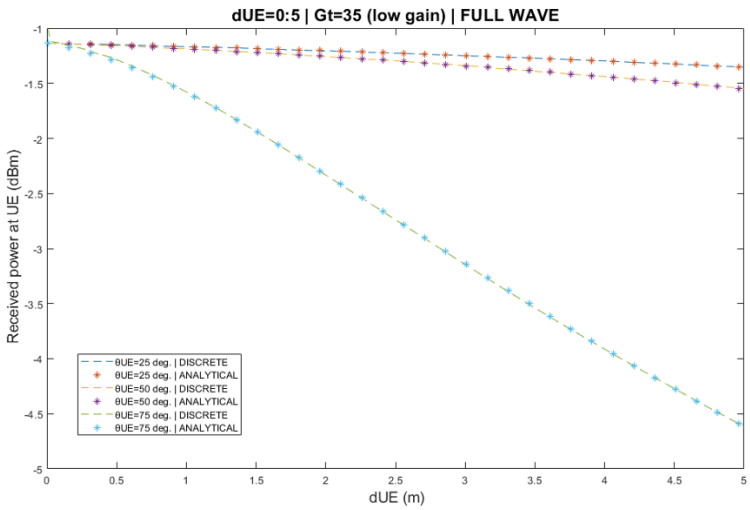

Figure 33. Received Power $P_{r,FW}$ vs distance d_{UE} with variable angle of direction θ_{UE} for a cascaded-RIS system residing in the infinite RIS regime operating in a "Full-Wave" mode in a low-gain simulation scenario ($G_t = 35dB$).

Finally, Figure 34 provides a combined view of the "Phase-Removal" and "Full-wave" mode of operation of the cascaded-RIS system. Based on the simulation results, it should be emphasized the fact that the "Phase-Removal" operation outperforms the "Full-Wave" approach on terms of the received power at the UE for the entire range of the distance d_{UE}.

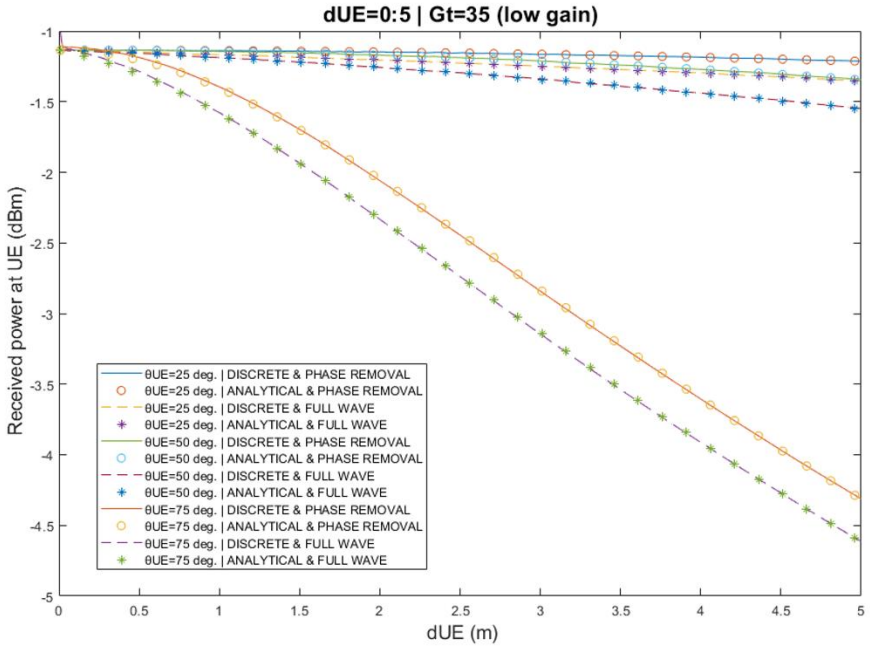

Figure 34. Combined representation of Received Power $P_{r,PR}$ and $P_{r,FW}$ vs distance d_{UE} with variable angle of direction θ_{UE} for a cascaded-RIS system residing in the infinite RIS regime operating in a "Phase-Removal" and "Full-Wave" mode, respectively, in a low-gain simulation scenario ($G_t = 35dB$).

- Scenario No3

This use case is the high-gain approach of the previously implemented simulation scenario, i.e. the AP gain is now $50dB$ instead of $35dB$. The results obtained from the simulation are depicted in Figures 35, 36 and 37.

In more detail, Figure 35 presents the received power $P_{r,PR}$ at the UE versus the distance d_{UE}, both analytically and numerically, when the cascaded-RIS system exhibits "Phase-Removal" modus operandi. Once again, the discrete model (solid line) verifies the results acquired by the analytical model (symbol 'o'). In fact, the received power curve (i.e. $P_{r,PR}$) is very similar to that of the low-gain case, as presented in Figure 32, and in this perspective the behavior of the cascaded-RIS system can be considered consistent.

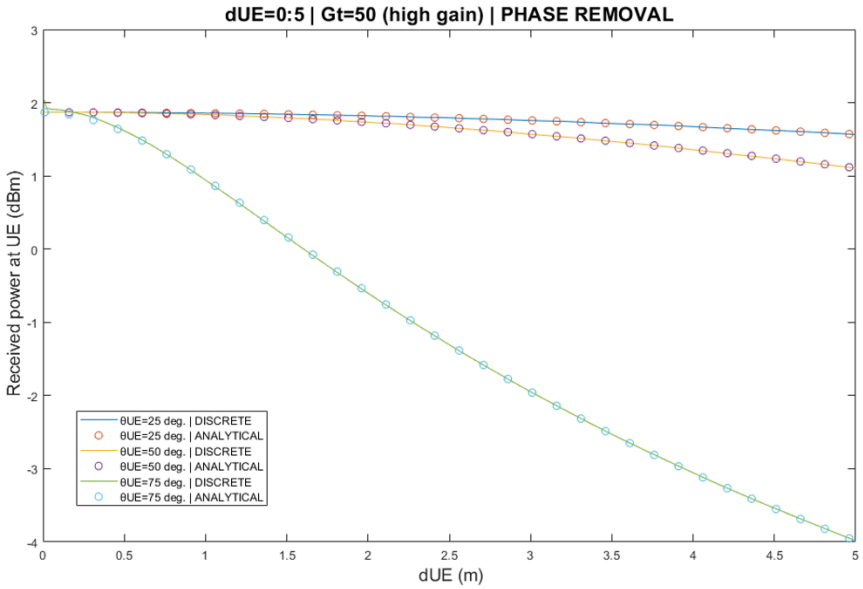

Figure 35. Received Power $P_{r,PR}$ vs distance d_{UE} with variable angle of direction θ_{UE} for a cascaded-RIS system residing in the infinite RIS regime operating in a "Phase-Removal" mode in a high-gain simulation scenario ($G_t = 50dB$).

However, the system's behavior in "Full-Wave" RIS operation (Fig.36) differs significantly from the "Phase-Removal" approach, as the received power at the UE, $P_{r,FW}$, decreases noticeably when the distance d_{UE} increases and there is no AP gain range within which a nearly constant performance can be achieved (as happened in the low-gain Scenario No2 or in the "Phase-Removal" operation of the high-gain Scenario No3).

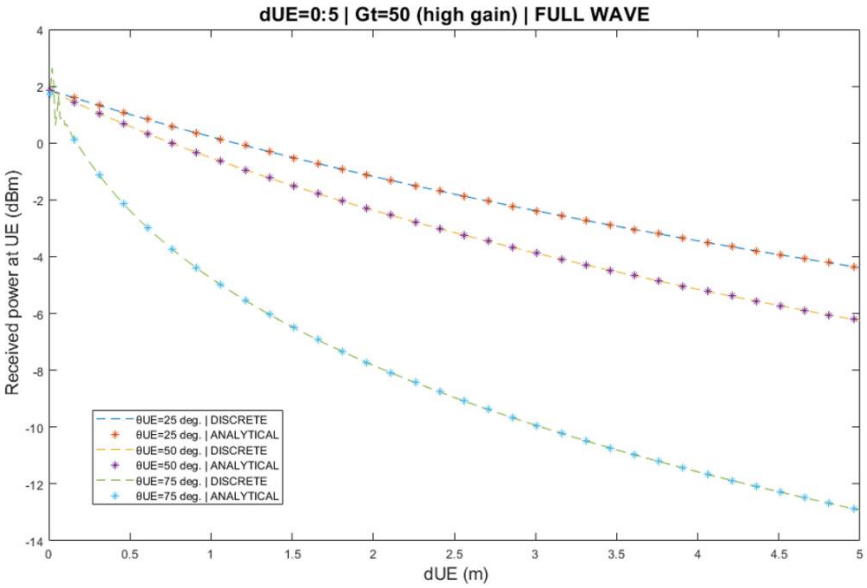

Figure 36. Received Power $P_{r,FW}$ vs distance d_{UE} with variable angle of direction θ_{UE} for a cascaded-RIS system residing in the infinite RIS regime operating in a "Full-Wave" mode in a high-gain simulation scenario ($G_t = 50dB$).

Lastly, Figure 37 provides a combined view of the "Phase-Removal" and "Full-wave" mode of operation of the cascaded-RIS system. Once again, the performance in case of "Phase-Removal" mode is overall better than the corresponding "Full-Wave" approach.

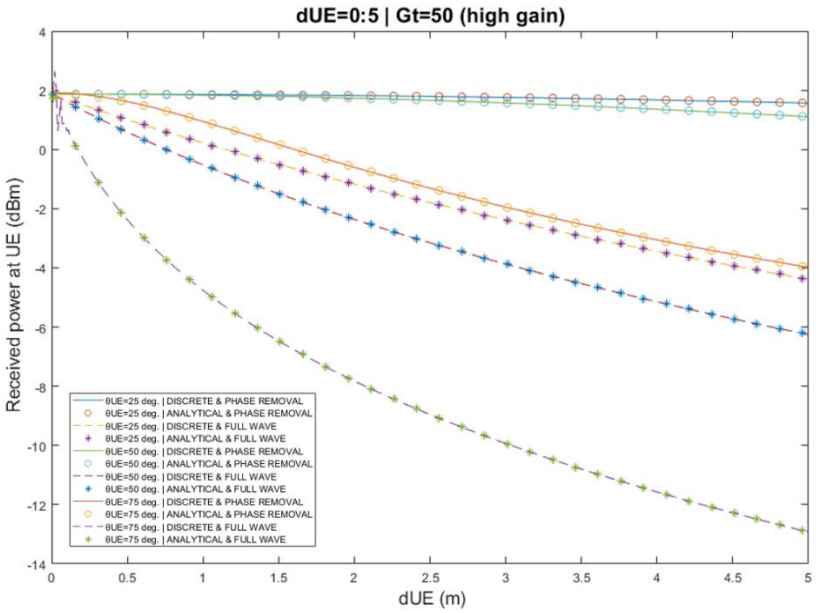

Figure 37. Combined representation of Received Power $P_{r,PR}$ and $P_{r,FW}$ vs distance d_{UE} with variable angle of direction θ_{UE} for a cascaded-RIS system residing in the infinite RIS regime operating in a "Phase-Removal" and "Full-Wave" mode, respectively, in a high-gain simulation scenario ($G_t = 50dB$).

- Scenario No4

In this use case of the cascaded-RIS aided communication system, the power received by the UE is evaluated as a function of the distances z_{UE} and x_{UE}, where $z_{UE} \in [0,5]m$ and $x_{UE} \in \{5,10,15\}m$. The AP gain G_t is considered to have a constant value of $35\ dB$, so we refer to this simulation as a *low-gain* case. The results obtained from the simulation are depicted in Figures 38, 39 and 40.

More specifically, Figure 38 shows the received power $P_{r,PR}$ at the UE versus the distance z_{UE} for three different distances x_{UE} and is calculated both analytically and numerically for the case that RIS is capable of flattening the wavefront of the incident beam by using the "phase-removal" operation mode.

First of all, it should be noted that the numerical calculation using the discrete model (solid line) verifies the theoretically expected results obtained from the analytical model (symbol 'o'). The results showed that as the distances z_{UE} and x_{UE} increase, the power received by the UE decreases, especially when the distance x_{UE} is bigger than $\approx 4.5m$ (i.e. $x_{UE} \in [4.5,5]m$). These results are also consistent with the previous low-gain case study (i.e. Scenario No2), as shown in Figure 32, where for a relatively high angle θ_{UE} (75°) (which actually corresponds to a distance z_{UE} close to $5m$) the power loss was relatively high.

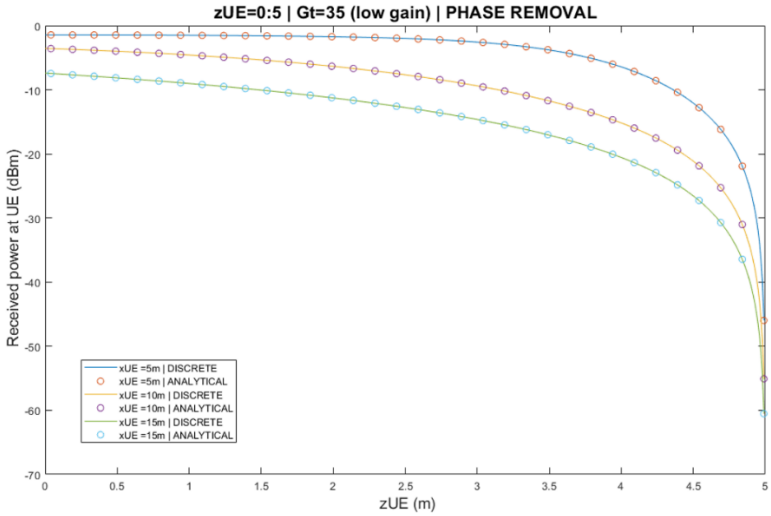

Figure 38. Received Power $P_{r,PR}$ vs distances z_{UE} and x_{UE} for a cascaded-RIS system residing in the infinite RIS regime operating in a "Phase-Removal" mode in a low-gain simulation scenario ($G_t = 35dB$).

Similar conclusions can be derived from the simulation based on the "Full-Wave" RIS operation. As shown in Figures 39 and 40, the discrete calculation approach (dashed line), once again, verifies the theoretically expected performance (symbol '$*$'), while the received power curve is almost identical with the one produced by the "Phase-Removal" approach.

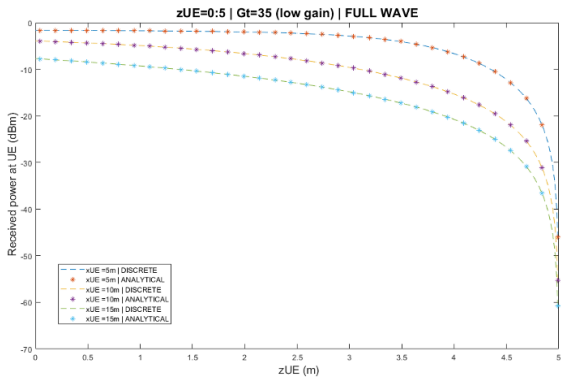

Figure 39. Received Power $P_{r,FW}$ vs distances z_{UE} and x_{UE} for a cascaded-RIS system residing in the infinite RIS regime operating in a "Full-Wave" mode in a low-gain simulation scenario ($G_t = 35dB$).

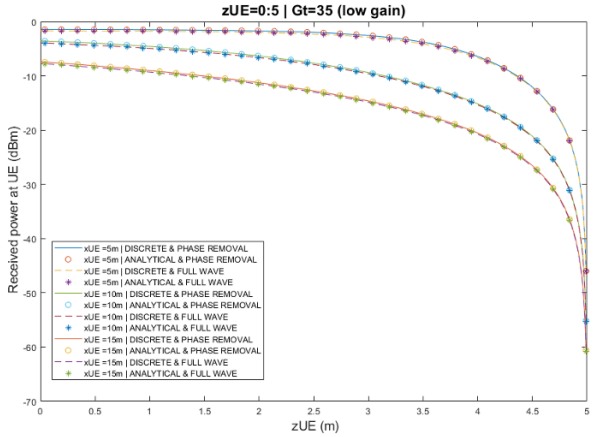

Figure 40. Combined representation of Received Power $P_{r,PR}$ and $P_{r,FW}$ vs distances z_{UE} and x_{UE} for a cascaded-RIS system residing in the infinite RIS regime operating in a "Phase-Removal" and "Full-Wave" mode, respectively, in a low-gain simulation scenario ($G_t = 35dB$).

- Scenario No5

This use case is the high-gain approach of the previously implemented simulation scenario, i.e. the AP gain is now $50dB$ instead of $35dB$. The results obtained from the simulation are illustrated in Figures 41, 42 and 43.

First of all, it should be noted that the received power curves are very similar to those produced in the above-mentioned low-gain use case. In particular, it can be observed that the received power at the UE decreases as the distances z_{UE} and x_{UE} increase, especially when $x_{UE} > 4.5m$. In fact, for the "Phase-Removal" operation, the performance of the system is relatively identical both for the low-gain Scenario No4 and the high-gain Scenario No5, as shown in Figures 37 and 41, respectively. However, this is not the case for the "Full-Wave" approach (Figure 14) in which the received power (per gain value) in each simulation subcase is always lower compared to either the "Phase-Removal" approach (Figure 43) or the corresponding low-gain RIS operation of Scenario No4 (Fig.38).

Lastly, it should be mentioned that the discrete calculation verifies the results produced by the analytical model, both for the "Phase-Removal" and "Full-Wave" approaches, as shown in Figures 41 and 42, respectively.

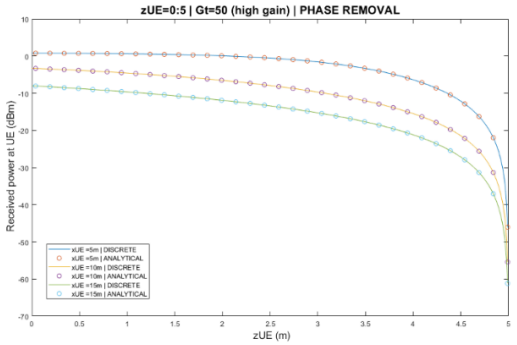

Figure 41. Received Power $P_{r,PR}$ vs distances z_{UE} and x_{UE} for a cascaded-RIS system residing in the infinite RIS regime operating in a "Phase-Removal" mode in a high-gain simulation scenario ($G_t = 50dB$).

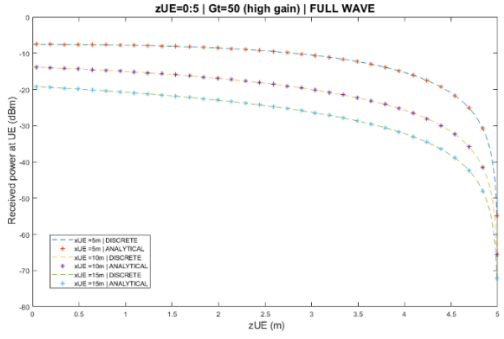

Figure 42. Received Power $P_{r,FW}$ vs distances z_{UE} and x_{UE} for a cascaded-RIS system residing in the infinite RIS regime operating in a "Full-Wave" mode in a high-gain simulation scenario ($G_t = 50dB$).

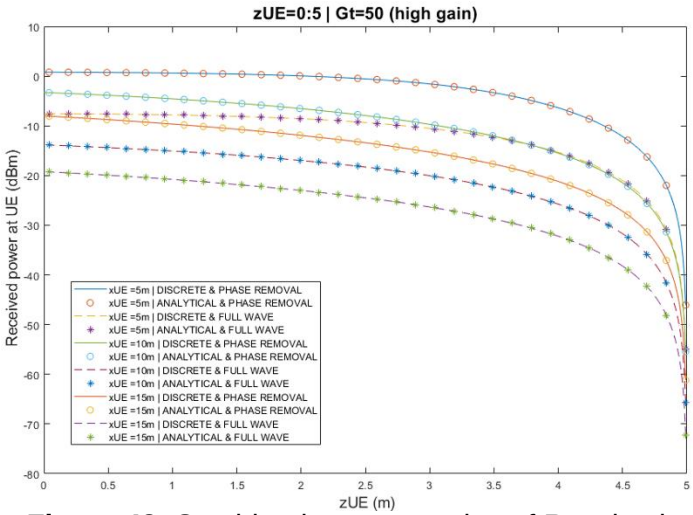

Figure 43. Combined representation of Received Power $P_{r,PR}$ and $P_{r,FW}$ vs distances z_{UE} and x_{UE} for a cascaded-RIS system residing in the infinite RIS regime operating in a "Phase-Removal" and "Full-Wave" mode, respectively, in a high-gain simulation scenario ($G_t = 50dB$).

4. DISCUSSION

Considering the results of the simulation phase (as described in §3), it should be pointed out that Reconfigurable Intelligent Surfaces can play a fundamental role in the implementation of Smart Radio Environments as they can facilitate communication by mitigating the effects of long-distance power loss and establish links even in NLoS environments, where the path between the transmitter (AP) and the receiver (UE) is blocked by various obstacles (as mentioned in §1.2.5).

In fact, RISs can be deployed in an easy, flexible, cost-effective, energy-efficient, aesthetically friendly and environmentally-safe way to transform the "unintentional adversary" environment into a collaborative system which can be controllable, customizable and programmable. As mentioned in §1.2.4, phase, amplitude, frequency and polarization transformations can be applied to the impinging radio waves in order to establish multi-hop LoS links and offer enhanced adaptation capabilities for the dynamically changing wireless environments. Nevertheless, phase shifts have been selected as the implementation approach for beamforming optimization; in specific, the RIS reflection coefficients are smartly programmed to properly adjust the phase and thereby attempt to overcome any negative effects of the natural propagation environments.

Based on the results obtained from the simulation phase (as provided in §3), it can be deduced the cascaded-RIS system allows communication between AP and UE by establishing a multi-hop LoS link for the use case scenarios described in §2.2.2.5. However, several adjustments in the system model parameters should be applied in order to maximize the received power at the UE, which has been selected as the key performance indicator of the current study; in particular, the *AP gain* and the *RIS operation in terms of phase transformation capabilities* can affect the efficiency of the cascaded-RIS aided communication system. In more detail, the selection of AP gain (specific value/range as in Scenario No1 or low-gain/high-gain approach as in Scenarios No2/No3 and No4/No5) combined with the mode of RIS operation ("Phase-Removal" or "Full-Wave") can lead to an overall stronger reception at the UE, as will be further discussed below.

First of all, the performance of the cascaded-RIS aided link residing in an infinite RIS regime in the case study scenarios of §2.2.2.5 was captured either by the analytical model or the numerical (discrete) model. The *numerical calculations verify the expected performance results obtained from the analytical model*. This finding is consistent with the behavior of the RIS-aided link in the respective single-RIS system analyzed in [85], which is subject to similar assumptions and approximations.

Moving a step further and based on the simulation results, the *"Phase-Removal" feature of RIS operation can ensure improved performance compared to the "Full-Wave" approach* in all use cases of the cascaded-RIS system of the current study. Only in the case study scenario No4 the system's performance was independent of the RIS phase-related features and hence, the RIS-aided link ensured the equal received power at the

UE either with or without reconstruction (i.e. flattening) of the wavefront of the incident beam. This means that it is generally preferable to apply appropriate phase shifts when EM waves impinge upon the RISs rather than simply reflecting the signal, although this comes at the cost of computational and implementation complexity.

Furthermore, based on the simulations results, it can be concluded that the RIS operation, especially in the "Phase-Removal" mode, has a *consistent and predictable behavior*; this means that the curve of received power follows the same pattern with respect to the variables of each simulation scenario, as shown for example in Figures 32 and 35 for the low-gain and high-gain use cases No2 and No3, respectively, or in Figures 38 and 41 for the low-gain and high-gain use cases No4 and No5, respectively. This fact can prove to be very significant as it can facilitate the design of wireless networks.

More specific observations refer to the almost constant performance of the cascaded-RIS aided communication system with "Phase-Removal" characteristics in case of relatively close distances of UE, as in Scenarios No2 and No3 where $d_{UE} \in [0,5]$ and relatively low steering angles, i.e. $\theta_{UE} = 25° \; or \; 50°$, where it can be inferred that the received power at the UE is practically independent of the distance d_{UE}. This can be important in the design of similar RIS-aided links in order to focus attention on the reflection angle θ_{UE} and not on the distance between the RIS and the UE. However, it should be highlighted that as the steering angle θ_{UE} increases and approaches 90 degrees, both with the "Full-Wave" and "Phase-Removal" approach, the system performance decreases significantly, as shown by the simulation results of Scenarios No2, No3, No4 and No5.

In addition, it is worth mentioning that in the Scenario No1 with "Phase-Removal" mode of operation and angle $\theta_{UE} = 75°$, the received power at the UE remains almost constant to the highest possible level for a wide range of AP gain (between about 35 and $54 \; dB$). This means that the cascaded-RIS performance in the specific use case can be considered almost independent of AP gain (for the selected gain range of the current study) and therefore, appropriate low-gain settings can be applied to increase the energy- and cost-efficiency and reduce the electromagnetic radiation exposure of the users. In addition, the careful selection of AP gain can on the one hand improve the system performance and on the other hand reduce the RIS size and thus, the relative computational and implementation complexity, as, for example happens, is the case with AP gain $G_t = [44,45] \; dB$, depicted in Figure 31 and Table 3.

Nevertheless, it should be emphasized that several assumptions have been made in the present study in order to simplify the simulation complexity and facilitate the derivation of conclusions. First of all, the AP beam is considered Gaussian in form, as mentioned in §2.2.2.2. However, the Gaussian beam is mostly suggested for laser applications and FSO communications. In addition, it was assumed that all the network elements, i.e. the Access Point (AP), the two Reconfigurable Intelligent Surfaces (RIS1 and RIS2) and the User Equipment (UE), are placed at the same plane defined as the coordinate plane $y = 0$ (i.e. the *ax*-plane) in order to lower the computational complexity, as mentioned in §2.2.2.1. Lastly, it was considered that the deployment of infinitely large RISs which can

capture the entire incident beam and thus, 100% of the incident power, while we are also assumed ideal phase shifters that have a common reflection coefficient of value 1, as mentioned in §2.2.2.3. However, in real life this amplitude is usually below the unity value used in the simulations [87].

Reconfigurable Intelligent surfaces can be deployed to overcome blockage conditions and establish communication between the access point and the user equipment either in indoor or outdoor wireless environments, as shown in Figure 44. The current study shows that a double-RIS aided communication system can bypass the blockage conditions through multi-hop signal reflections via the cascaded $AP - RIS1 - RIS2 - UE$ link. The obtained results are in line with relevant studies of cascaded-RIS systems ([115], [116], [118], [119], [120]), as discussed in §1.3. It remains to be seen if the proposed double-RIS system can achieve superior performance compared to a single-RIS system (as in studies [115], [116] and [118]), given also the trade-off between the multiplicative passive beamforming gain and the multi-reflection path loss, as mentioned in [119].

However, it should be mentioned that RIS-empowered networks constitute an emerging idea in the field of wireless communications and their realization is at a relatively early stage and may pose significant challenges [1] [6]. Several research studies have highlighted a number of technical challenges. However, the majority of research in the context on the practical implementation challenges of RIS-assisted networks focuses on channel estimation, passive deployment design and deployment issues [2] [4] [19] [21] [26] [46]. For this reason, research effort must be paid, in addition to addressing the above-mentioned challenges, toward the directions of path-loss and channel modeling, performance evaluation, AI/ML-driven design and optimization, beyond far-field communications, mobility management, large-scale networks and low overhead exchange algorithms [4] [19].

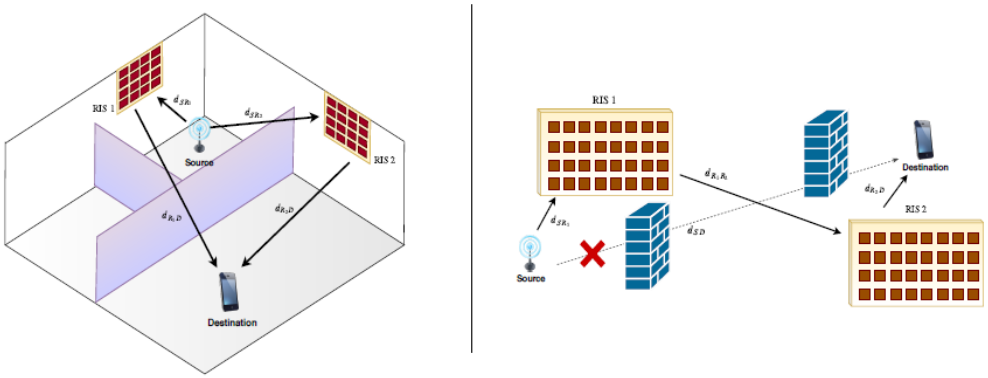

Figure 44. Cascaded-RIS aided communication systems in: (a) Indoor environment, and (b) Outdoor environment [117].

In a nutshell, the current study focuses on examining the most critical parameters that can affect the receiver power at the UE and thus, the performance of the cascaded-RIS system. In more detail, parameters such as the reflection coefficient of RIS elements, the transmitter gain G_t, the angle of beam direction θ_B (and φ_B), the beam footprint at the RIS

plane w_{RIS}, the distance d_{UE} between UE and RIS (as expressed with the use of x_B, y_B and z_B), as described in Equation (16), are the key performance parameters for the cascaded-RIS aided communication system of the current study. In addition, emphasis is given in the phase-related operation of the used reconfigurable intelligent surfaces, which is distinguished into "phase-removal" and the "full-wave" mode, as mentioned in §2.2.2.4.

Based on the obtained results, it should be emphasized that as the distance d_{UE} increases, the received power at the UE decreases; however, the aforementioned reduction is not so significant compared to other key performance parameters, as the angle of direction θ_{UE} or the operation mode of the used RISs. In particular, the angle of direction θ_{UE} can significantly impair the received power in the case that receives relatively high values, especially when approaches the 90 degrees. In addition, the simulations results show that a "Phase-Removal" approach, in which phase shifts are applied to reconstruct the beam wavefront, can ensure improved performance compared to the "Full-Wave" RIS operation.

As far as the transmitter gain G_t, it should be underlined that the footprint radius on the RIS is inversely proportional to the square root of the gain G_t, as denoted in Equation (12) and hence, these two mathematical quantities must be examined in combination. For this reason, we define a low-value range area, a mid-value range area and high-value range area and a general design guidance for the under-examination cascaded-RIS system based on an attempt to group the obtained results can be simplistically provided in the Table below:

Table 4. Design considerations based on the key performance parameters of the cascaded-RIS aided communication system of the current study.

Parameter		Received Power at the UE
Increase of d_{UE} ↗		↘ decreased power
Increase of θ_{UE} ↗		↘ decreased power
Increase Gt ↗	Low-value range (<38 dB)	↗ increased power
	Middle-value range	Depending on the other parameters
	High-value range (>48dB)	↘ decreased power
Operation mode		Phase-Removal ≥ Full-Wave

↗ : increase ↘ : decrease

5. CONCLUSIONS & FUTURE WORK

5.1 Conclusions

The current research project examined the usefulness of Reconfigurable Intelligent Surfaces (RISs) in wireless communication networks and in particular the efficiency of a cascaded-RIS aided system in Non-Line-of-Sight (NLoS) propagation scenarios. Based on the obtained results, it should be highlighted that:

- The under-examination double-RIS system can improve the system's performance in terms of received power at the UE.
- The cascaded-RIS system can establish a multi-hop cascaded LoS link which can effectively mitigate or even eliminate the adverse NLoS effects.
- Phase-related features (i.e. "Phase-Removal" RIS-operation mode) can further enhance the cascaded-RIS aided system's performance.
- Comprehensive design guidelines associated with the key performance parameters of the current research study, e.g. the reflection coefficient of RIS elements, the transmitter gain, the angle of direction of the beam, the beam footprint at the RIS plane, the distance between UE and RIS, can be provided.
- The theoretical expected results acquired by following the analytical calculation approach were verified numerically by using the discrete model.

5.2 Future Work

The following ideas could be tested to further investigate the usefulness of cascaded-RIS systems for enhancing the performance of wireless communication networks:

i. The comparison of the proposed double-RIS system to a single-RIS system for the case study scenarios of the current research project.
ii. The examination of the proposed cascaded-RIS system for smart surfaces residing in the finite regime.
iii. Practical RIS implementations should be utilized to verify the theoretical findings of the current research project through experimental measurements.

REFERENCES

[1] M. Di Renzo, M. Debbah, D.T. Phan-Huy, A. Zappone, M.S. Alouini, C. Yuen, V. Sciancalepore, G.C. Alexandropoulos, J. Hoydis, H. Gacanin, J. De Rosny, A. Bounceur, G. Lerosey, and M. Fink, "Smart radio environments empowered by reconfigurable AI meta-surfaces: an idea whose time has come," in EURASIP Journal on WirelessEURASIP Journal on Wireless Communications and Networking, vol. 129, 2019, doi: 10.1186/s13638-019-1438-9.

[2] Y. Liu, X. Liu, X. Mu, T. Hou, J. Xu, M. Di Renzo, and N. Al-Dhahir, "Reconfigurable Intelligent Surfaces: Principles and Opportunities," in IEEE Communications Surveys & Tutorials, vol. 23, no. 3, pp. 1546-1577, thirdquarter 2021, doi: 10.1109/COMST.2021.3077737.

[3] E.C. Strinati, G.C. Alexandropoulos, V. Sciancalepore, M. Di Renzo, H. Wymeersch, D.T. Phan-huyk, M. Crozzoli, R. D' Errico, E. De Carvalho, P. Popovski, P. Di Lorenzo, L. Bastianelli, M. Belouar, J.E. Mascolo, G. Gradoni, S. Phang, G. Lerosey, and B. Denis, "Wireless Environment as a Service Enabled by Reconfigurable Intelligent Surfaces: The RISE-6G Perspective," 2021 Joint European Conference on Networks and Communications & 6G Summit (EuCNC/6G Summit), Jun 2021, pp.562-567, doi: 10.1109/EuCNC/6GSummit51104.2021.9482474.

[4] C. Pan, H. Ren, K. Wang, J.F. Kolb, M. Elkashlan, M. Chen, M. Di Renzo, Y. Hao, J. Wang, A.L. Swindlehurst, X. You, and L. Hanzo, "Reconfigurable Intelligent Surfaces for 6G Systems: Principles, Applications, and Research Directions," in IEEE Communications Magazine, vol. 59, no. 6, pp. 14-20, doi: 10.1109/MCOM.001.2001076.

[5] A.L. Imoize, O. Adedeji, N. Tandiya, and S. Shetty S, "6G Enabled Smart Infrastructure for Sustainable Society: Opportunities, Challenges, and Research Roadmap," in Sensors, vol. 21, no. 5, pp. 1709, 2021, doi: 10.3390/s21051709.

[6] R. Liu, Q. Wu, M. Di Renzo and Y. Yuan, "A Path to Smart Radio Environments: An Industrial Viewpoint on Reconfigurable Intelligent Surfaces," in IEEE Wireless Communications, vol. 29, no. 1, pp. 202-208, February 2022, doi: 10.1109/MWC.111.2100258.

[7] R. Dangi, P. Lalwani, G. Choudhary, I. You, and G. Pau, "Study and Investigation on 5G Technology: A Systematic Review," in Sensors, vol. 22, no. 1, pp. 26, 2022, doi: 10.3390/s22010026.

[8] S. Dang, O. Amin, B. Shihada, and M.S. Alouini, "What should 6G be?," in Nature Electronics, vol. 3, pp. 20–29, 2020, doi: 10.1038/s41928-019-0355-6.

[9] International Telecommunication Union (ITU), "IMT traffic estimates for the years 2020 to 2030," Report ITU-R M.2370-0 (07/2015), ITU Radiocommunication Sector (ITU-R), 2015, itu.int/pub/R-REP-M.2370-2015.

[10] Ericsson, "Ericsson Mobility Report," *Report*, Ericsson, 2022, https://www.ericsson.com/en/reports-and-papers/mobility-report/reports/june-2022.

[11] W. Tang, M.M.Z. Chen, X. Chen, J.Y. Dai, Y. Han, M. Di Renzo, Y. Zeng, S. Jin, Q. Cheng, and T.J. Cui, "Wireless Communications With Reconfigurable Intelligent Surface: Path Loss Modeling and Experimental Measurement," in *IEEE Transactions on Wireless Communications*, vol. 20, no. 1, pp. 421-439, Jan. 2021, doi: 10.1109/TWC.2020.3024887.

[12] F. Tariq, M. R. A. Khandaker, K. -K. Wong, M. A. Imran, M. Bennis and M. Debbah, "A Speculative Study on 6G," in *IEEE Wireless Communications*, vol. 27, no. 4, pp. 118-125, August 2020, doi: 10.1109/MWC.001.1900488.

[13] L. Dai, B. Wang, M.Wang, X. Yang, J. Tan, S. Bi, S. Xu, F. Yang, Z. Chen, M. Di Renzo, and L. Hanzo, "Reconfigurable Intelligent Surface-Based Wireless Communications: Antenna Design, Prototyping, and Experimental Results," in *IEEE Access*, vol. 8, pp. 45913-45923, 2020, doi: 10.1109/ACCESS.2020.2977772.

[14] X. Cao, B. Yang, C. Huang, Member, C. Yuen, M. Di Renzo, Z. Han, D. Niyato, H.V. Poor, and L. Hanzo, "AI-Assisted MAC for Reconfigurable Intelligent-Surface-Aided Wireless Networks: Challenges and Opportunities," in *IEEE Communications Magazine*, vol. 59, no. 6, pp. 21-27, June 2021, doi: 10.1109/MCOM.001.2001146.

[15] Y. Niu, Y. Li, D. Jin, L. Su, and A.V. Vasilakos, "A survey of millimeter wave communications (mmWave) for 5G: opportunities and challenges," in *Wireless Networks*, vol. 21, no. 8, pp. 2657-2676, 2015, doi: 10.1007/s11276-015-0942-z.

[16] S. Alraih, I. Shayea, M. Behjati, R. Nordin, N.F. Abdullah, A. Abu-Samah, and D. Nandi, "Revolution or Evolution? Technical Requirements and Considerations towards 6G Mobile Communications," in *Sensors*, vol. 22, no. 3, 2022, doi: 10.3390/s22030762.

[17] E. Basar, M. Di Renzo, J. De Rosny, M. Debbah, M. -S. Alouini and R. Zhang, "Wireless Communications Through Reconfigurable Intelligent Surfaces," in *IEEE Access*, vol. 7, pp. 116753-116773, 2019, doi: 10.1109/ACCESS.2019.2935192.

[18] H. Gacanin and M. Di Renzo, "Wireless 2.0: Toward an Intelligent Radio Environment Empowered by Reconfigurable Meta-Surfaces and Artificial Intelligence," in I*EEE Vehicular Technology Magazine*, vol. 15, no. 4, pp. 74-82, Dec. 2020, doi: 10.1109/MVT.2020.3017927.

[19] M. Di Renzo, A. Zappone, M. Debbah, M.S. Alouini, C. Yuen, J.De Rosny, and S. Tretyakov, "Smart Radio Environments Empowered by Reconfigurable Intelligent Surfaces: How It Works, State of Research, and The Road Ahead," in *IEEE Journal on Selected Areas in Communications*, vol. 38, no. 11, pp. 2450-2525, Nov. 2020, doi: 10.1109/JSAC.2020.3007211.

[20] M. Di Renzo, K. Ntontin, J.Song, F.H. Danufane, X. Qian, F. Lazarakis, J. De Rosny, D.T. Phan-Huy, O. Simeone, R. Zhang, M. Debbah, G. Lerosey, M. Fink, S. Tretyakov, and S. Shamai, "Reconfigurable Intelligent Surfaces vs. Relaying: Differences, Similarities, and Performance Comparison," in I*EEE Open Journal of the Communications Society*, vol. 1, pp. 798-807, 2020, doi: 10.1109/OJCOMS.2020.3002955.

[21] S. Hassouna, "A Survey on Intelligent Reflecting Surfaces: Wireless Communication Perspective," *TechRxiv preprint* doi:10.36227/techrxiv.19181693.v1

[22] A. Pitilakis, O. Tsilipakos, F. Liu, K.M. Kossifos, A.C. Tasolamprou, D.H. Kwon, M.S. Mirmoosa, D. Manessis, N.V. Kantartzis, C. Liaskos, M.A. Antoniades, J. Georgiou, C.M. Soukoulis, M. Kafesaki, and S.A. Tretyakov, "A Multi-Functional Reconfigurable Metasurface: Electromagnetic Design Accounting for Fabrication Aspects," in *IEEE Transactions on Antennas and Propagation*, vol. 69, no. 3, pp. 1440-1454, March 2021, doi: 10.1109/TAP.2020.3016479.

[23] D. Pile, "Anomalous reflection," in *Nature Photonics*, vol. 9, no. 210, 2015, doi: 10.1038/nphoton.2015.48

[24] D. Sell, J. Yang, E. Wang, T. Phan, S. Doshay, and J. Fan, Jonathan, "Ultra-High-Efficiency Anomalous Refraction with Dielectric Metasurfaces," in *ACS Photonics*, vol. 5, no. 6, pp. 2402–2407, 2018, doi: 10.1021/acsphotonics.8b00183.

[25] Y. Qi, B. Zhang, C. Liu and X. Deng, "Ultra-Broadband Polarization Conversion Meta-Surface and its Application in Polarization Converter and RCS Reduction," in *IEEE Access*, vol. 8, pp. 116675-116684, 2020, doi: 10.1109/ACCESS.2020.3004127.

[26] Q. Wu and R. Zhang, "Towards Smart and Reconfigurable Environment: Intelligent Reflecting Surface Aided Wireless Network," in *IEEE Communications Magazine*, vol. 58, no. 1, pp. 106-112, January 2020, doi: 10.1109/MCOM.001.1900107.

[27] V. Tapio, I. Hemadeh, A. Mourad, A. Shojaeifard, and M. Juntti, "Survey on reconfigurable intelligent surfaces below 10 GHz.," in *EURASIP Journal on Wireless Communications and Networking*, vol. 2021, no. 1, 2021, doi: 10.1186/s13638-021-02048-5.

[28] Y. She, C. Ji, C. Huang, Z. Zhang, J. Liao, J. Wang, and X. Luo, "Intelligent reconfigurable metasurface for self-adaptively electromagnetic functionality switching," in *Photonics Research*, vol. 10, pp. 769-776, 2022, doi: 10.1364/PRJ.450297.

[29] T. Sharma, A. Chehri, and P. Fortier, "Reconfigurable Intelligent Surfaces for 5G and beyond Wireless Communications: A Comprehensive Survey,"in *Energies*, vol. 14, no. 24, 2021, doi: 10.3390/en14248219.

[30] S. Aboagye, A.R. Ndjiongue, T.M.N. Ngatched, O.A. Dobre, and H.V. Poor, "RIS-Assisted Visible Light Communication Systems: A Tutorial," *arXiv preprin*t arXiv:2204.07198 (2022).

[31] K. Yang, Y. Shi, Y. Zhou, Z. Yang, L. Fu and W. Chen, "Federated Machine Learning for Intelligent IoT via Reconfigurable Intelligent Surface," in *IEEE Network*, vol. 34, no. 5, pp. 16-22, September/October 2020, doi: 10.1109/MNET.011.2000045.

[32] V. Arun and H. Balakrishnan, "RFocus: Beamforming Using Thousands of Passive Antennas," in *Proceedings of the 17th USENIX Symposium on Networked Systems Design and Implementation*, February 2020, https://www.usenix.org/conference/nsdi20/presentation/arun

[33] NTT DOCOMO, *DOCOMO Conducts World's First Successful Trial of Transparent Dynamic Metasurface: Dynamic wave manipulation and high transparency expected to optimize 5G network construction*, 2020, https://www.docomo.ne.jp/english/info/media_center/pr/2020/0117_00.html

[34] X. Pei, H. Yin, L. Tan, L. Cao, Z. Li, K. Wang, K. Zhang, and E. Bjornson, "RIS-Aided Wireless Communications: Prototyping, Adaptive Beamforming, and Indoor/Outdoor Field Trials," in *IEEE Transactions on Communications*, vol. 69, no. 12, pp. 8627-8640, Dec. 2021, doi: 10.1109/TCOMM.2021.3116151.

[35] E. Basar, "Reconfigurable Intelligent Surfaces for Doppler Effect and Multipath Fading Mitigation," in *Frontiers Communications and Networks*, vol. 2, 2021, doi: 10.3389/frcmn.2021.672857.

[36] J. Chen, Q. Liang, B. Zhang, X. Wu, "Spectrum efficiency of nested sparse sampling and coprime sampling," in *EURASIP Journal onWireless EURASIP Journal onWireless Communications and Networking*, vol. 47, 2013, doi: 10.1186/1687-1499-2013-47.

[37] K. Ramgoolam, V. Bassoo, "Maximising energy efficiency for direct communication links in wireless body area networks," in *IET Wireless Sensor Systems*, vol. 9, pp. 32-41, 2019, doi: 10.1049/iet-wss.2018.5090.

[38] Y. Chen, S. Zhang, S. Xu and G. Y. Li, "Fundamental trade-offs on green wireless networks," in *IEEE Communications Magazine*, vol. 49, no. 6, pp. 30-37, June 2011, doi: 10.1109/MCOM.2011.5783982.

[39] K.G. Nguyen, O. Tervo, Q.D. Vu, L.N. Tran, and M. Juntti, "Energy-efficient transmission strategies for CoMP downlink—overview, extension, and numerical comparison," in *EURASIP Journal on Wireless Communications and Networking*, vol. 207, 2018, doi: 10.1186/s13638-018-1214-2.

[40] L.L. Peterson and B.S. Davie, "Chapter 2. Getting Connected," in *Computer Networks: A Systems Approach*, 5th ed, San Francisco: Morgan Kaufmann Publishers Inc., pp. 71-167, 2012.

[41] X. Li, R. Salleh, and O. Zakaria, "Wireless Spectrum Combination Protocol for 4G Networks," in *Journal of Applied Sciences*, vol. 9, no.2, pp. 334-340, 2009, doi: 10.3923/jas.2009.334.340.

[42] S. Weber, J. G. Andrews and N. Jindal, "An Overview of the Transmission Capacity of Wireless Networks," in *IEEE Transactions on Communications*, vol. 58, no. 12, pp. 3593-3604, December 2010, doi: 10.1109/TCOMM.2010.093010.090478.

[43] W. Tang, X. Chen, M.Z. Chen, J.Y. Dai, Y. Han, M. Di Renzo, S. Jin, Q. Cheng, and T.J. Cui, "Path Loss Modeling and Measurements for Reconfigurable Intelligent Surfaces in the Millimeter-Wave Frequency Band," in *IEEE Transactions on Communications*, 2022, doi: 10.1109/TCOMM.2022.3193400.

[44] M. Rahal, B. Denis, K. Keykhosravi, B. Uguen and H. Wymeersch, "RIS-Enabled Localization Continuity Under Near-Field Conditions," *2021 IEEE 22nd International Workshop on Signal Processing Advances in Wireless Communications (SPAWC)*, 2021, pp. 436-440, doi: 10.1109/SPAWC51858.2021.9593200.

[45] J. Wang, W. Tang, Y. Han, S. Jin, X Li, C.K. Wen, Q. Cheng, and T.J. Cui, "Interplay Between RIS and AI in Wireless Communications: Fundamentals, Architectures, Applications, and Open Research Problems," in *IEEE Journal on Selected Areas in Communications*, vol. 39, no. 8, pp. 2271-2288, Aug. 2021, doi: 10.1109/JSAC.2021.3087259.

[46] S. Basharat, S. A. Hassan, H. Pervaiz, A. Mahmood, Z. Ding and M. Gidlund, "Reconfigurable Intelligent Surfaces: Potentials, Applications, and Challenges for 6G Wireless Networks," in *IEEE Wireless Communications*, vol. 28, no. 6, pp. 184-191, December 2021, doi: 10.1109/MWC.011.2100016.

[47] P. Nuti, E. Balti, and B.L. Evans, "Spectral Efficiency Optimization for mmWave Wideband MIMO RIS-assisted Communication," *arXiv preprint* arXiv:2201.01739 (2021).

[48] M. Giordani, A. Zanella and M. Zorzi, "LTE and Millimeter Waves for V2I Communications: An End-to-End Performance Comparison," *2019 IEEE 89th Vehicular Technology Conference (VTC2019-Spring)*, 2019, pp. 1-7, doi: 10.1109/VTCSpring.2019.8746487.

[49] S. Tripathi, N.V. Sabu, A.K. Gupta, H.S. Dhillon, "Millimeter-Wave and Terahertz Spectrum for 6G Wireless" In: , *et al.* 6G Mobile Wireless Networks, Computer Communications and Networks, Springer, Cham., doi: 10.1007/978-3-030-72777-2_6

[50] F.C. Okogbaa, Q.Z. Ahmed, F.A. Khan, W.B. Abbas, F. Che, S.A.R Zaidi, and T. Alade, "Design and Application of Intelligent Reflecting Surface (IRS) for Beyond 5G Wireless Networks: A Review," in *Sensors*, vol. 22, no. 7, pp. 2436-2450, 2022, doi: 10.3390/s22072436.

[51] N. S. Perović, M. D. Renzo and M. F. Flanagan, "Channel Capacity Optimization Using Reconfigurable Intelligent Surfaces in Indoor mmWave Environments," *ICC 2020 - 2020 IEEE International Conference on Communications (ICC)*, 2020, pp. 1-7, doi: 10.1109/ICC40277.2020.9148781.

[52] G. Zhou, C. Pan, H. Ren, K. Wang and M. D. Renzo, "Fairness-Oriented Multiple RIS-Aided mmWave Transmission: Stochastic Optimization Methods," in *IEEE Transactions on Signal Processing*, vol. 70, pp. 1402-1417, 2022, doi: 10.1109/TSP.2022.3158026.

[53] Y. Pan, K. Wang, C. Pan, H. Zhu and J. Wang, "Self-Sustainable Reconfigurable Intelligent Surface Aided Simultaneous Terahertz Information and Power Transfer (STIPT)," in *IEEE Transactions on Wireless Communications*, vol. 21, no. 7, pp. 5420-5434, July 2022, doi: 10.1109/TWC.2022.3140268.

[54] Y. Pan, K. Wang, C. Pan, H. Zhu and J. Wang, "UAV-Assisted and Intelligent Reflecting Surfaces-Supported Terahertz Communications," in *IEEE Wireless Communications Letters*, vol. 10, no. 6, pp. 1256-1260, June 2021, doi: 10.1109/LWC.2021.3063365.

[55] F. Afroz, K. Sandrasegaran, and H. Al Kim, Haider, "Interference Management in Lte Downlink Networks," in *International Journal of Wireless & Mobile Networks*, vol. 7, no.1, pp. 91-106, 2015, doi: 10.5121/ijwmn.2015.7106.

[56] C. Pan, H. Ren, K. Wang, W. Xu, M. Elkashlan, A. Nallanathan, and L. Hanzo, "Multicell MIMO Communications Relying on Intelligent Reflecting Surfaces," in *IEEE Transactions on Wireless Communications*, vol. 19, no. 8, pp. 5218-5233, Aug. 2020, doi: 10.1109/TWC.2020.2990766.

[57] S. Tian, X. Zhang, X. Wang, J. Han, and L. Li, "Recent advances in metamaterials for simultaneous wireless information and power transmission," in *Nanophotonics*, vol. 11, no. 9, pp. 1697-1723, 2022, doi: 10.1515/nanoph-2021-0657

[58] C. Pan, H. Ren, K. Wang, M. Elkashlan, A. Nallanathan, J. Wang, and L Hanzo, "Intelligent Reflecting Surface Aided MIMO Broadcasting for Simultaneous Wireless Information and Power Transfer," in *IEEE Journal on Selected Areas in Communications*, vol. 38, no. 8, pp. 1719-1734, Aug. 2020, doi: 10.1109/JSAC.2020.3000802.

[59] L. Mohjazi, S. Muhaidat, Q. H. Abbasi, M. A. Imran, O. A. Dobre and M. D. Renzo, "Battery Recharging Time Models for Reconfigurable Intelligent Surfaces-Assisted Wireless Power Transfer Systems," in IEEE Transactions on Green Communications and Networking, vol. 6, no. 2, pp. 1173-1185, June 2022, doi: 10.1109/TGCN.2021.3120834.

[60] S. Huang, S. Wang, R. Wang, M. Wen and K. Huang, "Reconfigurable Intelligent Surface Assisted Mobile Edge Computing With Heterogeneous Learning Tasks," in *IEEE Transactions on Cognitive Communications and Networking,* vol. 7, no. 2, pp. 369-382, June 2021, doi: 10.1109/TCCN.2021.3056707.

[61] B. Yang, X. Cao, C. Huang, Y.L. Guan, C. Yuen, M. Di Renzo, D. Niyato, M. Debbah, and L. Hanzo, "Spectrum-Learning-Aided Reconfigurable Intelligent Surfaces for "Green" 6G Networks," in *IEEE Network*, vol. 35, no. 6, pp. 20-26, November/December 2021, doi: 10.1109/MNET.110.2100301.

[62] T. Bai, C. Pan, C. Han and L. Hanzo, "Reconfigurable Intelligent Surface Aided Mobile Edge Computing," in IEEE Wireless Communications, vol. 28, no. 6, pp. 80-86, December 2021, doi: 10.1109/MWC.001.2100142.

[63] Z. Qin, X. Yue, Y. Liu, Z. Ding and A. Nallanathan, "User Association and Resource Allocation in Unified NOMA Enabled Heterogeneous Ultra Dense Networks," in *IEEE Communications Magazine*, vol. 56, no. 6, pp. 86-92, June 2018, doi: 10.1109/MCOM.2018.1700497.

[64] Y. Liu, X. Mu, X. Liu, M. Di Renzo, Z. Ding and R. Schober, "Reconfigurable Intelligent Surface-Aided Multi-User Networks: Interplay Between NOMA and RIS," in *IEEE Wireless Communications*, vol. 29, no. 2, pp. 169-176, April 2022, doi: 10.1109/MWC.102.2100363.

[65] Y. Xiu, J. Zhao, W. Sun, M. Di Renzo, G. Gui, Z. Zhang, and N. Wei, "Reconfigurable Intelligent Surfaces Aided mmWave NOMA: Joint Power Allocation, Phase Shifts, and Hybrid Beamforming Optimization," in *IEEE Transactions on Wireless Communications*, vol. 20, no. 12, pp. 8393-8409, Dec. 2021, doi: 10.1109/TWC.2021.3092597.

[66] G. Yang, X. Xu, Y. -C. Liang and M. D. Renzo, "Reconfigurable Intelligent Surface-Assisted Non-Orthogonal Multiple Access," in *IEEE Transactions on Wireless Communications*, vol. 20, no. 5, pp. 3137-3151, May 2021, doi: 10.1109/TWC.2020.3047632.

[67] T. Hou, Y. Liu, Z. Song, X. Sun, Y. Chen and L. Hanzo, "Reconfigurable Intelligent Surface Aided NOMA Networks," in *IEEE Journal on Selected Areas in Communications*, vol. 38, no. 11, pp. 2575-2588, Nov. 2020, doi: 10.1109/JSAC.2020.3007039.

[68] V. C. Thirumavalavan, P. Velmurugan and S. J. Thiruvengadam, "BER Analysis of RIS Assisted Multicast Communications with Network Coding," *2020 International Conference on Signal Processing and Communications (SPCOM)*, 2020, pp. 1-5, doi: 10.1109/SPCOM50965.2020.9179528.

[69] W. Shi, J. Li, G. Xia, Y. Wang, X. Zhou, Y. Zhang, F. Shu, "Secure multigroup multicast communication systems via intelligent reflecting surface," in *China Communications*, vol. 18, no. 3, pp. 39-51, March 2021, doi: 10.23919/JCC.2021.03.004.

[70] G. Zhou, C. Pan, H. Ren, K. Wang and A. Nallanathan, "Intelligent Reflecting Surface Aided Multigroup Multicast MISO Communication Systems," in *IEEE Transactions on Signal Processing*, vol. 68, pp. 3236-3251, 2020, doi: 10.1109/TSP.2020.2990098.

[71] D. Fang, Y. Qian and R. Q. Hu, "Security for 5G Mobile Wireless Networks," in *IEEE Access*, vol. 6, pp. 4850-4874, 2018, doi: 10.1109/ACCESS.2017.2779146.

[72] J. Yuan, Y. -C. Liang, J. Joung, G. Feng and E. G. Larsson, "Intelligent Reflecting Surface-Assisted Cognitive Radio System," in *IEEE Transactions on Communications*, vol. 69, no. 1, pp. 675-687, Jan. 2021, doi: 10.1109/TCOMM.2020.3033006.

[73] A. U. Makarfi, R. Kharel, K. M. Rabie, O. Kaiwartya, X. Li and D. -T. Do, "Reconfigurable Intelligent Surfaces based Cognitive Radio Networks," *2021 IEEE Wireless Communications and Networking Conference Workshops (WCNCW)*, 2021, pp. 1-6, doi: 10.1109/WCNCW49093.2021.9419976.

[74] J. Wang, P. Cai, G. Kang, P. Zhang, "Transmission strategies with interference coordination in spectrum sharing cognitive radio networks under outage probability constraint'" in *EURASIP Journal on Wireless Communications and Networking 2012*, vol. 101, 2012, doi: 10.1186/1687-1499-2012-101.

[75] S. F. Zamanian, S. M. Razavizadeh and Q. Wu, "Vertical Beamforming in Intelligent Reflecting Surface-Aided Cognitive Radio Networks," in *IEEE Wireless Communications Letters*, vol. 10, no. 9, pp. 1919-1923, Sept. 2021, doi: 10.1109/LWC.2021.3086309.

[76] L. Zhang, Y. Wang, W. Tao, Z. Jia, T. Song and C. Pan, "Intelligent Reflecting Surface Aided MIMO Cognitive Radio Systems," in *IEEE Transactions on Vehicular Technology*, vol. 69, no. 10, pp. 11445-11457, Oct. 2020, doi: 10.1109/TVT.2020.3011308.

[77] E. Björnson, Ö. Özdogan and E. G. Larsson, "Reconfigurable Intelligent Surfaces: Three Myths and Two Critical Questions," in *IEEE Communications Magazine*, vol. 58, no. 12, pp. 90-96, December 2020, doi: 10.1109/MCOM.001.2000407.

[78] A.S. Abdalla, T.F. Rahman, and V. Marojevic, "UAVs with Reconfigurable Intelligent Surfaces: Applications, Challenges, and Opportunities", *arXiv preprint* arXiv:2012.04775 (2020).

[79] S.A.H. Mohsan, M.A. Khan, M.H. Alsharif, P. Uthansakul, and A.A.A. Solyman AAA, "Intelligent Reflecting Surfaces Assisted UAV Communications for Massive Networks: Current Trends, Challenges, and Research Directions," in *Sensors*, vol. 22, no. 14, 2022, doi: 10.3390/s22145278.

[80] G. Geraci, A. Garcia-Rodriguez, M.M. Azari, A. Lozano, M. Mezzavilla, S. Chatzinotas, Y. Chen, S. Rangan, and M. Di Renzo, "What Will the Future of UAV Cellular Communications Be? A Flight from 5G to 6G," in *IEEE Communications Surveys & Tutorials*, doi: 10.1109/COMST.2022.3171135.

[81] Y. Chen, Y. Wang, J. Zhang and M. D. Renzo, "QoS-Driven Spectrum Sharing for Reconfigurable Intelligent Surfaces (RISs) Aided Vehicular Networks," in *IEEE Transactions on Wireless Communications*, vol. 20, no. 9, pp. 5969-5985, Sept. 2021, doi: 10.1109/TWC.2021.3071332.

[82] Y. Chen, Y. Wang, J. Zhang, P. Zhang and L. Hanzo, "Reconfigurable Intelligent Surface (RIS)-Aided Vehicular Networks: Their Protocols, Resource Allocation, and Performance," in *IEEE Vehicular Technology Magazine*, vol. 17, no. 2, pp. 26-36, June 2022, doi: 10.1109/MVT.2022.3158046.

[83] M. Jian, R. Liu, and Y. Chen, "Standardization for Reconfigurable Intelligent Surfaces: Progresses, Challenges and the Road Ahead," *2021 IEEE/CIC International Conference on Communications in China (ICCC Workshops)*, 2021, pp. 337-342, doi: 10.1109/ICCCWorkshops52231.2021.9538911.

[84] M. Di Renzo, and A.I. Aravanis, "Catching the 6G Wave by Using Metamaterials," in *Shaping Future 6G Networks: Needs, Impacts, and Technologies*, IEEE, 2022, pp.69-87, doi: 10.1002/9781119765554.ch6.

[85] G. Stratidakis, S. Droulias and A. Alexiou, "Analytical Performance Assessment of Beamforming Efficiency in Reconfigurable Intelligent Surface-Aided Links," in *IEEE Access*, vol. 9, pp. 115922-115931, 2021, doi: 10.1109/ACCESS.2021.3105477.

[86] E. Basar and I. Yildirim, "SimRIS Channel Simulator for Reconfigurable Intelligent Surface-Empowered Communication Systems," *2020 IEEE Latin-American Conference on Communications (LATINCOM)*, 2020, pp. 1-6, doi: 10.1109/LATINCOM50620.2020.9282349.

[87] J. Praia, J.P. Pavia, N. Souto, M. Ribeiro, "Phase Shift Optimization Algorithm for Achievable Rate Maximization in Reconfigurable Intelligent Surface-Assisted THz Communications," in *Electronics*, vol. 11, no. 1, pp. 18-33, 2022, doi: 10.3390/electronics11010018.

[88] A. -A. A. Boulogeorgos and A. Alexiou, "Coverage Analysis of Reconfigurable Intelligent Surface Assisted THz Wireless Systems," in *IEEE Open Journal of Vehicular Technology*, vol. 2, pp. 94-110, 2021, doi: 10.1109/OJVT.2021.3051209.

[89] G. Stratidakis, S. Droulias and A. Alexiou, "Understanding the RIS efficiency: from partial to full illumination," *2022 IEEE 23rd International Workshop on Signal Processing Advances in Wireless Communication (SPAWC)*, 2022, pp. 1-5, doi: 10.1109/SPAWC51304.2022.9834003.

[90] A. -A. A. Boulogeorgos and A. Alexiou, "Ergodic capacity analysis of reconfigurable intelligent surface assisted wireless systems," 2020 IEEE 3rd 5G World Forum (5GWF), 2020, pp. 395-400, doi: 10.1109/5GWF49715.2020.9221372.

[91] E. N. Papasotiriou, A. -A. A. Boulogeorgos, A. Stratakou and A. Alexiou, "Performance Evaluation of Reconfigurable Intelligent Surface Assisted D-band Wireless Communication," *2020 IEEE 3rd 5G World Forum (5GWF)*, 2020, pp. 360-365, doi: 10.1109/5GWF49715.2020.9221316.

[92] A. -A. A. Boulogeorgos and A. Alexiou, "How Much do Hardware Imperfections Affect the Performance of Reconfigurable Intelligent Surface-Assisted Systems?," in *IEEE Open Journal of the Communications Society*, vol. 1, pp. 1185-1195, 2020, doi: 10.1109/OJCOMS.2020.3014331.

[93] A. Zappone, M. Di Renzo, F. Shams, X. Qian and M. Debbah, "Overhead-Aware Design of Reconfigurable Intelligent Surfaces in Smart Radio Environments," in *IEEE Transactions on Wireless Communications*, vol. 20, no. 1, pp. 126-141, Jan. 2021, doi: 10.1109/TWC.2020.3023578.

[94] A. -A. A. Boulogeorgos and A. Alexiou, "Performance Analysis of Reconfigurable Intelligent Surface-Assisted Wireless Systems and Comparison With Relaying," in *IEEE Access*, vol. 8, pp. 94463-94483, 2020, doi: 10.1109/ACCESS.2020.2995435.

[95] K. Ntontin, M. Di Renzo and F. Lazarakis, "On the Rate and Energy Efficiency Comparison of Reconfigurable Intelligent Surfaces with Relays," *2020 IEEE 21st International Workshop on Signal Processing Advances in Wireless Communications (SPAWC)*, 2020, pp. 1-5, doi: 10.1109/SPAWC48557.2020.9154308.

[96] N. S. Perović, L. -N. Tran, M. Di Renzo and M. F. Flanagan, "Achievable Rate Optimization for MIMO Systems With Reconfigurable Intelligent Surfaces," in *IEEE Transactions on Wireless Communications*, vol. 20, no. 6, pp. 3865-3882, June 2021, doi: 10.1109/TWC.2021.3054121.

[97] L. You, J. Xiong, Y. Huang, D.W. Kwan Ng, C. Pan, W. Wang, and X. Gao, "Reconfigurable Intelligent Surfaces-Assisted Multiuser MIMO Uplink Transmission With Partial CSI," in *IEEE Transactions on Wireless Communications*, vol. 20, no. 9, pp. 5613-5627, Sept. 2021, doi: 10.1109/TWC.2021.3068754.

[98] J. Liu, X. Qian and M. Di Renzo, "Interference Analysis in Reconfigurable Intelligent Surface-Assisted Multiple-Input Multiple-Output Systems," *ICASSP 2021 - 2021 IEEE International Conference on Acoustics, Speech and Signal Processing (ICASSP)*, 2021, pp. 8067-8071, doi: 10.1109/ICASSP39728.2021.9414684.

[99] T. Van Chien, H. Q. Ngo, S. Chatzinotas, M. Di Renzo and B. Ottersten, "Reconfigurable Intelligent Surface-Assisted Cell-Free Massive MIMO Systems Over Spatially-Correlated Channels," in *IEEE Transactions on Wireless Communications*, vol. 21, no. 7, pp. 5106-5128, July 2022, doi: 10.1109/TWC.2021.3136925.

[100] K. Zhi, C. Pan, H. Ren and K. Wang, "Power Scaling Law Analysis and Phase Shift Optimization of RIS-Aided Massive MIMO Systems With Statistical CSI," in *IEEE Transactions on Communications*, vol. 70, no. 5, pp. 3558-3574, May 2022, doi: 10.1109/TCOMM.2022.3162580.

[101] Z. Peng, T. Li, C. Pan, H. Ren, W. Xu and M. D. Renzo, "Analysis and Optimization for RIS-Aided Multi-Pair Communications Relying on Statistical CSI," in *IEEE Transactions on Vehicular Technology*, vol. 70, no. 4, pp. 3897-3901, April 2021, doi: 10.1109/TVT.2021.3062710.

[102] J. Wang, H. Wang, Y. Han, S. Jin and X. Li, "Joint Transmit Beamforming and Phase Shift Design for Reconfigurable Intelligent Surface Assisted MIMO Systems," in *IEEE Transactions on Cognitive Communications and Networking*, vol. 7, no. 2, pp. 354-368, June 2021, doi: 10.1109/TCCN.2021.3058665.

[103] J. Wang, H. Wang, Y. Han, S. Jin and X. Li, "Maximum Ergodic Spectral Efficiency of Reconfigurable Intelligent Surface Assisted MIMO Systems under Correlated Channels," *2020 International Conference on Wireless Communications and Signal Processing (WCSP)*, 2020, pp. 894-898, doi: 10.1109/WCSP49889.2020.9299731.

[104] K. Ntontin, D. Selimis, A. -A. A. Boulogeorgos, A. Alexandridis, A. Tsolis, V. Vlachodimitropoulos, and F. Lazarakis, "Optimal Reconfigurable Intelligent Surface Placement in Millimeter-Wave Communications," *2021 15th European Conference on Antennas and Propagation (EuCAP)*, 2021, pp. 1-5, doi: 10.23919/EuCAP51087.2021.9411076.

[105] A. -A. A. Boulogeorgos and A. Alexiou, "Pathloss modeling of reconfigurable intelligent surface assisted THz wireless systems," *ICC 2021 - IEEE International Conference on Communications*, 2021, pp. 1-6, doi: 10.1109/ICC42927.2021.9500473.

[106] E. N. Papasotiriou, A. -A. A. Boulogeorgos and A. Alexiou, "On the Impact of Beam Misalignment in Reconfigurable Intelligent Surface Assisted THz Systems," *2021 IEEE 22nd International Workshop on Signal Processing Advances in Wireless Communications (SPAWC)*, 2021, pp. 121-125, doi: 10.1109/SPAWC51858.2021.9593236.

[107] L. Zhang, C. Pan, Y. Wang, H. Ren and K. Wang, "Robust Beamforming Design for Intelligent Reflecting Surface Aided Cognitive Radio Systems With Imperfect Cascaded CSI," in *IEEE Transactions on Cognitive Communications and Networking*, vol. 8, no. 1, pp. 186-201, March 2022, doi: 10.1109/TCCN.2021.3107510.

[108] H. Xiao, L. Dong, W. Wang, "Intelligent Reflecting Surface-Assisted Secure Multi-Input Single-Output Cognitive Radio Transmission," in *Sensors*, vol. 20, no. 12, pp. 3480-3502, 2020, doi: 10.3390/s20123480.

[109] S. Li, B. Duo, M. D. Renzo, M. Tao and X. Yuan, "Robust Secure UAV Communications With the Aid of Reconfigurable Intelligent Surfaces," in *IEEE Transactions on Wireless Communications*, vol. 20, no. 10, pp. 6402-6417, Oct. 2021, doi: 10.1109/TWC.2021.3073746.

[110] C. Chen and C. Pan, "Blocking Probability in Obstructed Tunnels With Reconfigurable Intelligent Surface," in *IEEE Communications Letters*, vol. 26, no. 2, pp. 458-462, Feb. 2022, doi: 10.1109/LCOMM.2021.3128529.

[111] H. Ren, K. Wang and C. Pan, "Intelligent Reflecting Surface-Aided URLLC in a Factory Automation Scenario," in *IEEE Transactions on Communications*, vol. 70, no. 1, pp. 707-723, Jan. 2022, doi: 10.1109/TCOMM.2021.3125057.

[112] S. Kisseleff, S. Chatzinotas and B. Ottersten, "Reconfigurable Intelligent Surfaces in Challenging Environments: Underwater, Underground, Industrial and Disaster," in *IEEE Access*, vol. 9, pp. 150214-150233, 2021, doi: 10.1109/ACCESS.2021.3125461.

[113] Z. Peng, C. Pan, Z. Zhang, X. Chen, L. Li and A. L. Swindlehurst, "Joint Optimization for Full-Duplex Cellular Communications Via Intelligent Reflecting Surface," *ICASSP 2021 - 2021 IEEE International Conference on Acoustics, Speech and Signal Processing (ICASSP)*, 2021, pp. 7888-7892, doi: 10.1109/ICASSP39728.2021.9413615.

[114] X. Cheng, Y. Lin, W. Shi, J. Li, C. Pan, F. Shu, Y. Wu, and J. Wang, "Joint Optimization for RIS-Assisted Wireless Communications: From Physical and Electromagnetic Perspectives," in *IEEE Transactions on Communications*, vol. 70, no. 1, pp. 606-620, Jan. 2022, doi: 10.1109/TCOMM.2021.3120721.

[115] C. You, B. Zheng and R. Zhang, "Wireless Communication via Double IRS: Channel Estimation and Passive Beamforming Designs," in *IEEE Wireless Communications Letters*, vol. 10, no. 2, pp. 431-435, Feb. 2021, doi: 10.1109/LWC.2020.3034388.

[116] Y. Han, S. Zhang, L. Duan and R. Zhang, "Cooperative Double-IRS Aided Communication: Beamforming Design and Power Scaling," in *IEEE Wireless Communications Letters*, vol. 9, no. 8, pp. 1206-1210, Aug. 2020, doi: 10.1109/LWC.2020.2986290.

[117] I. Yildirim, A. Uyrus and E. Basar, "Modeling and Analysis of Reconfigurable Intelligent Surfaces for Indoor and Outdoor Applications in Future Wireless Networks," in *IEEE Transactions on Communications*, vol. 69, no. 2, pp. 1290-1301, Feb. 2021, doi: 10.1109/TCOMM.2020.3035391.

[118] B. Zheng, C. You and R. Zhang, "Double-IRS Assisted Multi-User MIMO: Cooperative Passive Beamforming Design," in *IEEE Transactions on Wireless Communications*, vol. 20, no. 7, pp. 4513-4526, July 2021, doi: 10.1109/TWC.2021.3059945.

[119] W. Mei and R. Zhang, "Cooperative Beam Routing for Multi-IRS Aided Communication," in *IEEE Wireless Communications Letters*, vol. 10, no. 2, pp. 426-430, Feb. 2021, doi: 10.1109/LWC.2020.3034370.

[120] A. Almohamad, M. Hasna, N. Zorba and T. Khattab, "Performance of THz Communications Over Cascaded RISs: A Practical Solution to the Over-Determined Formulation," in *IEEE Communications Letters*, vol. 26, no. 2, pp. 291-295, Feb. 2022, doi: 10.1109/LCOMM.2021.3132655.

[121] A. -A. A. Boulogeorgos, N. D. Chatzidiamantis, H. G. Sandalidis, A. Alexiou and M. D. Renzo, "Cascaded Composite Turbulence and Misalignment: Statistical Characterization and Applications to Reconfigurable Intelligent Surface-Empowered Wireless Systems," in *IEEE Transactions on Vehicular Technology*, vol. 71, no. 4, pp. 3821-3836, April 2022, doi: 10.1109/TVT.2021.3140084.

[122] A. -A. A. Boulogeorgos, N. Chatzidiamantis, H. G. Sandalidis, A. Alexiou and M. Di Renzo, "Performance Analysis of Multi-Reconfigurable Intelligent Surface-Empowered THz Wireless Systems," *ICC 2022 - IEEE International Conference on Communications*, 2022, pp. 1481-1487, doi: 10.1109/ICC45855.2022.9838660.

[123] D. Tyrovolas, S. A. Tegos, E. C. Dimitriadou-Panidou, P. D. Diamantoulakis, C. K. Liaskos and G. K. Karagiannidis, "Performance Analysis of Cascaded Reconfigurable Intelligent Surface Networks," in *IEEE Wireless Communications Letters*, 2022, doi: 10.1109/LWC.2022.3184635.

[124] Edmund Optics Inc., "Section 2: Gaussian Beam Propagation," in *Laser Optics Resource Guide*, 2022, https://www.edmundoptics.com/knowledge-center/application-notes/lasers/gaussian-beam-propagation/

[125] RP Photonics, "Gaussian Beams" in *RP Photonics Encyclopedia*, 2022, https://www.rp-photonics.com/gaussian_beams.html

[126] O. Svelto, "Chapter 4. Ray and Wave Propagation Through Optical Media," in *Principles of Laser*s, 5th ed, New York: Springer Science+Business Media LLC, pp. 131-162, 2010.

[127] European Telecommunications Standards Institute (ETSI), "Universal Mobile Telecommunications System (UMTS);
LTE; General UMTS Architecture (3GPP TS 23.101 version 8.0.0 Release 8)," *Technical Specification ETSI TS 123 101 V8.0.0 (2009-01)*, ETSI, 2009, http://www.etsi.org.

[128] K. Xiao, "Dimensionless Physical Constant Mysteries," *viXra preprin*t viXra:1205.0050 (2012).

[129] S.J. Orfanidis, "Chapter 16. Transmitting and Receiving Antennas," in *Electromagnetic Waves and Antennas*, Piscataway, NJ: Rutgers University, pp. 739-774, 2016.